A FREQUENCY ANALYSIS OF TEN YEARS OF SURFACE

ATMOSPHERIC DATA AT OCEAN WEATHERSHIP 'PAPA' (50 N 145W)

by

DAVID BRYAN FISSEL

B. Sc., University Of British Columbia, 1971

A THESIS SUBMITTED IN PARTIAL FULFILLMENT CF

THE REQUIREMENTS FOR THE DEGREE OF

MASTER OF SCIENCE

in the Department

of

Physics

and the Institute of Oceanography

We accept this thesis as conforming to the

required standard

THE UNIVERSITY OF BRITISH COLUMBIA

April, 1975

ABSTRACT

The standard 3-hourly meteorological observations from Ocean Weather Station 'Papa' (50N 145W) for the period 1958 to 1967 are examined. Power spectra of the wind speed, air pressure, air temperature, absolute humidity, and sea temperature are computed. The wind speed spectra from the open ocean environment are compared with those found at other ocean, coastal and land stations. The seasonal spectra of these quantities averaged over each of the ten years indicate that the character of the activity changes both with respect to the size and frequency of the variations during the course of the year. Spectra are also computed for $U \cdot U_x$, $U \cdot U_y$, $U \cdot \Delta T$ and $U \cdot \Delta q$ which through the bulk transfer formulas are representative of momentum, sensible heat and latent heat fluxes. The rotary power spectrum of the vector wind and vector wind stress show that clockwise rotations of the wind and the wind stress contain more energy than the anti-clockwise rotations.

Cross-spectral values are computed between the vector wind and scalar quantities. As well, the cross-spectra between some of the various scalar quantities were examined.

The effect of using data commonly available over the oceans on the computation of the bulk fluxes is examined. A comparison of the monthly wind stress and latent heat flux computed from the data organized into the format of the Marine Climatic Atlas with the directly calculated values show good agreement between the two methods. The sensible heat flux deviates more seriously, particularily in months of small fluxes.

The effect on computing bulk fluxes from surface weather

chart data is examined by computing these fluxes from vector averaged wind data. The use of this data format results in substantial reductions to the wind stress (magnitude reduced to one-half of the directly calculated value for an averaging period of one month). The latent heat flux is reduced by a factor of 0.53 and the sensible heat flux by a factor of 0.62 for the monthly averaging period.

TABLE OF CONTENTS

LIST OF TABLES

LIST OF FIGURES

ACKNOWLEDGEMENTS

Chapter 1

INTRODUCTION

The atmosphere and the ocean are intricately coupled by a wide variety of physical phenomena. Such interactions take place over a very large range of time and spatial scales and it is useful to classify the types of interactions according to the characteristic scale size over which each occurs. One can divide the entire time (or spatial) range into several general overlapping scale ranges (see Denman,1972 cr Fiedler and Panofsky,1970). The smallest is the microscale over which turbulent transfers of momentum, heat and water vapour occur in the surface boundary layer. This scale ranges from periods of approximately one second up to about an hour. The mesoscale ranges from several minutes to approximately two days. An intermediate scale called the synoptic scale ranges from periods of a day to several weeks. This scale is associated with movement of cyclonic and anti-cyclonic pressure systems together with their fronts. Beyond the synoptic scale, phenomena of longer periods are said to belong to the seasonal and climatic scales.

In this study, the periodicities of surface layer meteorological and oceanographic quantities at Ocean Weather Station Papa in the N.E. Pacific are examined by means of spectral analysis. This technique computes the contribution to the total variance at various frequencies. The analysis resolves periods ranging from 6 hours to two years. The cross-spectra between pairs of selected quantities were also computed. This analysis allows for the examination of the relationships

between pairs of quantities at various frequencies.

Where possible, these spectral results are compared with previous results found by other investigators. Much work has been done on the spectra of wind speed at land and coastal weather stations but similar results for an open ocean environment are very limited. The previous work on spectra of the other quantities (such as air pressure, temperature and humidity) is even less extensive at both land and sea stations.

The interactions between the atmosphere and the sea in mid-latitudes are known to vary markedly with seasons. The winds are generally lighter in summer than in winter, indicating that less momentum is transported to the sea. Computations by Tabata(1965) of the total heat transports to the atmosphere at Ocean Station 'Papa' show that this varies from about 30 cal/cm²-day during late spring to 150 cal/cm²-day in the winter. In order to study such seasonal variations, spectra for each season averaged over the ten years of available data were computed. These spectra reveal changes in both the level of fluctuations and the frequencies of identifiable spectral features with the time of year.

A recent development in spectral analysis has been the use of co-ordinate invariant rotary auto- and cross-spectra (Mooers,1973). The rotary auto-spectrum is computed from the components of a vector quantity. This analysis resolves the spectrum into separate contributions to the variance from the vectors rotating either in the clockwise or anti-clockwise directions. In a similar fashion, the rotary cross-spectrum is computed to determine coherence and phase values between a

vector time series and a time series of another quantity (either scalar or vector).

Transfers of momentum, sensible heat and water vapour take place in the turbulent boundary layers of the ocean and the atmosphere. Direct measurements of such transfers require equipment which is capable of resolving microscale quantities and is complicated and expensive. Therefore, the time and spatial distribution of direct measurements is and likely will remain very limited.

Attempts have been made to parameterize the fluxes of momentum, sensible heat and water vapour in terms of variables averaged over a period of an hour or so, that are more generally available. The momentum flux ($\vec{\tau}$) can be written as (Roll,1965)

$$\vec{\tau} = \rho\, c_D |\vec{U}| \vec{U} \qquad (1)$$

where ρ is the air density, $\vec{U}$ is the mean wind velocity over a period of about an hour measured at some reference height, and c_D is the non-dimensional drag coefficient. Determinations of the wind stress or momentum flux with fairly direct estimates, show that $c_D = (1.3$ to $1.5) \times 10^{-3}$ on average with a considerable amount of scatter and an uncertainty of the mean of 20 to 30 % (Pond et. al., 1974; Stewart, 1974). This coefficient may be a weak function of wind speed but as yet virtually no direct estimates have been made for winds greater than 15 m/sec so this dependence remains uncertain.

Similar non-dimensional bulk transfer coefficients, c_T and c_q for sensible heat (H_S) and latent heat (H_L), respectively have been defined (Roll,1965):

$$H_S = \rho\, c_p c_T U^{\Delta} T \qquad (2)$$

$$H_L = LC_q U \Delta q \qquad (3)$$

where U is the mean wind speed over an hour (this is equal to $|\vec{U}|$ within 2 to 3%), C_p is the specific heat of air at constant pressure, ΔT is the temperature difference between the sea surface and a reference height, L is the latent heat per unit mass and Δq is the absolute humidity difference between the sea surface and a reference height. Direct estimates of C_T and C_q are rather limited, but those that are available indicate that both values are around 1.5×10^{-3} with a considerable amount of scatter (Pond et. al., 1974). Using equations (1), (2), and (3), values which are representative of fluxes of momentum $(|\vec{U}|\vec{U})$, sensible heat $(U\Delta T)$ and latent heat $(U\Delta q)$ were subjected to spectral analysis.

Parameterizing the turbulent fluxes in terms of mean quantities measured over periods of an hour still leaves much to be desired when examining the large scale spatial distribution of these fluxes. This deficiency is due to the very limited availability of measurements of these mean quantities over the world's oceans. The only regular source of this kind of information comes from the ocean weatherships which are necessarily few and far between. In practice, then, one is forced to rely on data from two sources: Climatic atlases such as those published by the U. S. Navy Oceanographic Office and surface weather charts. The climatic atlases are based on meteorological measurements collected over many years from weatherships and ships-of-opportunity. The values obtained are compiled into tables for each month summarizing all observations of each quantity for various sections of the ocean surface. As

an example, the compiled wind data is displayed in the form of wind roses (which are described in Chapter 6). Meteorological weather maps issued by weather offices display the mean pressure field and reported surface observations for various periods. From the pressure distribution, the geostrophic wind can be computed and then extrapolated to the surface.

For both of these data sources, the organization of the data necessitates a considerable amount of smoothing. When the parameterization formulas are applied to this smoothed data, the resulting fluxes will differ from those computed from the direct measurements of mean quantities. The extent of the differences are examined by appropriate smoothing of the 3-hourly measurements at Ocean Weather Station 'Papa' to make them more like data that are commonly available. Using these smoothed data, the fluxes are computed by means of the bulk parameterizations and compared with the fluxes computed directly from the unsmoothed data. One can then 'correct' the parameterization coefficients to get better estimates of the fluxes from the more readily available smoothed data.

Chapter 2

DATA COLLECTION

2.1 Collection Procedures

The data used in this study were collected by the Canadian Meteorological Service(now the Atmospheric Environment Service) at Ocean Weather Station 'Papa' located at longitude 145W and latitude 50N approximately 900 miles west of Vancouver Island. The station was established in 1950 as one of a worldwide network of weatherships manned by various countries. The measurement program includes upper air soundings and routine surface meteorological readings. Since 1952, the Pacific Oceanographic Group (now Ocean and Aquatic Affairs, Pacific Region) has been making oceanographic measurements at Station 'Papa' as well. The data used in this study are from the years 1958 to 1967 inclusive.

The station is manned alternately by two ships which each spend 42 days on station. During the period over which the data were collected, the two ships were the CCGS Stonetown and the CCGS St. Catherines. While on station, the ships are normally underway. They are considered to be 'on station' if they remain inside a ten mile square centered on the station's location.

The data were obtained from the Atmospheric Environment Service on digital magnetic tape in the International Meteorological format (80 column card images). These data, after some sorting and interpretation were transferred to another tape in a more suitable form for data processing. A description of the procedure used in writing the second data

tape and time series plots of selected quantities is found in Hertzman, Miyake and Pond(1974).

The quantities taken from the data tape for use in this study (together with their original units) are wind speed, U, (in knots), wind direction, θ, (compass degrees indicating the direction from which the wind blows), air pressure, P, (in millibars), air temperature, T_a, (in ^oC), wet-bulb temperature, T_W, (in ^oC), and sea temperature, T_s, (in ^oC), all being measured at three hourly intervals. The wind is measured from one of three anemometers at 22 m above sea level. The reading, taken from the anemometer with the best exposure, is a ten minute mean. The air pressure is measured with an aneroid barometer and corrected for height and temperature. The air and wet bulb temperature are measured from a ventilated shelter at a height of 17 m above sea level. The sea temperature is determined from a surface water sample drawn with a bucket.

2.2 Missing And Erroneous Data

The data record is very nearly complete. Of the 175,296 possible samples (for 6 quantities recorded every 3 hours for ten years) only 1427, or 0.82% of the total, are missing or obviously incorrect. The worst case in the analysis that follows is for the seasonal spectra of the ten winters. Here 1.5% of the values used are missing or incorrect. Of these 1427 values, 1404 are a result of the ship leaving its station and thus missing readings. The remaining 23 are apparently erroneous values. Examples of such errors are sea temperatures that suddenly plunge to 0.0 ^oC, wet-bulb temperatures that exceed the air temperature by 0.5 C^o or more and wind directions

that are greater than 360°. A complete listing of the missing and erroneous data is given in Appendix I.

In addition to the missing or incorrect data values discussed above, examination of the sea temperature time series plots revealed regular intervals of increased diurnal variations for the first five years of the data. Because the period of the increased activity is very nearly equal to the time that one ship is on station, it is thought that this effect is due to observers on one of the weatherships inadvertantly leaving the surface water sample bucket on deck for some time before taking the temperature. A special correction for the spectra of sea surface temperature will be discussed later.

In the time series subjected to spectral analysis, the missing and erroneous data values were replaced. The replacement values were simply determined by means of linear interpolation between the last correct value before the incorrect data and the first correct value following the incorrect data. This correction procedure will have little effect on the spectral contributions of periods longer than the period of replaced data but will reduce contributions at periods less than that of the replaced data. However, since the data replaced is a very small fraction of the total data, this effect is expected to be negligible.

2.3 Derived Quantities

From the basic quantities several other surface quantities were derived and used in the analysis. The east-west and north-south components of the wind were computed taking winds directed to the east (westerly winds) and winds directed to the north (southerly winds) as being positive. The temperature difference between the sea and the air was computed taking $\Delta T = T_s - T_a$ so that positive values of ΔT should correspond to upward heat fluxes.

The absolute humidity (q_a) (with units of gm/m^3) was calculated from the values of wet-bulb temperature (T_w), air temperature (T_a) and air pressure (P). The vapour pressure of water (e) is given by

$$e = e_w - [0.00066 \, (^oC)^{-1}] P (T_a - T_w) \qquad (4)$$

where e_w is the saturation vapour pressure at T_w (CRC Handbook of Physics and Chemistry, 51st Edition, p. E-39). The absolute humidity of a saturated atmosphere (q) depends only on the absolute temperature to a very good approximation:

$$q = C_1 \exp(-C_2/T) \qquad (5)$$

where $C_1 = 6.4038 \times 10^8$ and $C_2 = -5107.4$ are determined by a least squares fit to tabulated values given in the CRC Handbook of Physics and Chemistry. Applying the equation of state of an ideal gas, ($q_a = e/(RT_a)$, where R is the gas constant) to equation (4):

$$q_a = (T_w/T_a) C_1 \exp(-C_2/T_w) - 0.148 P (T_a - T_w)/T_a \qquad (6)$$

where the temperatures are in absolute degrees, pressure is in millibars and the humidity is in gm/m^3. The atmosphere at the sea surface is taken to be saturated so that equation (5) may be applied for the absolute humidity at the sea surface (q_s):

$$q_s = 0.98 C_1 \exp(-C_2/T_s) \tag{7}$$

where the factor of 0.98 accounts for the lowering of vapour pressure due to the presence of sea salts at the surface. Equations (6) and (7) are used to compute the absolute humidity difference, $\Delta q = q_s - q_a$, so that positive values of Δq correspond to an upward water vapour flux.

Chapter 3

SPECTRAL ANALYSIS

3.1 Introduction

To study the cycles and periodicities of a time varying
quantity, some means of separating the fluctuations of various
frequencies must be employed. One can do this by elimination of
unwanted frequencies, either visually or by using analog or
digital filtering techniques. Another method is to make a least
squares fit between the original time series signal and an
oscillating signal of some well known frequency. Such methods
are useful for determining the strength of a well known
periodicity but are inadequate to provide an overview of the
periodicities that are present. Spectral analysis, rather than
eliminating frequencies, resolves the signal into its frequency
components.

A time series consisting of N equally spaced samples X(j),
j=0,1,2,...N-1 can be represented by a frequency series A(k) by
means of the discrete Fourier transform:

$$A(k) = \sum_{j=0}^{N-1} X(j) \exp(2\pi i j k/N) \qquad k=0,1,2,...N-1 \qquad (8)$$

where $i=\sqrt{-1}$ (Jenkins and Watts,1968). This expression can be
written as $A(k) = N(a(k) + i \cdot b(k))$ where $a(k)$ and $b(k)$ are the
Fourier cosine and sine coefficients:

$$a(k) = [\sum_{j=0}^{N-1} X(j) \cos(2\pi j k/N)]/N \qquad (9)$$

$$b(k) = [\sum_{j=0}^{N-1} X(j) \sin(2\pi j k/N)]/N \qquad (10)$$

These values are computed using the fast Fourier transform (FFT)

algorithm developed by Cooley and Tukey(1965). In this study, a version of the FFT algorithm devised by Singleton(1968) is used. The values of $a(k)$ and $b(k)$ are defined over frequencies ranging from the fundamental frequency of the record $\Delta f = (1/N\Delta t)$ to the Nyquist frequency $f_N = (1/2\Delta t)$ where Δt is the sampling period.

A sample power spectrum has the property that

$$\overline{X^2}(j) - (\overline{X(j)})^2 = \int_{\Delta f/2}^{f_N+\Delta f/2} \phi_{xx}(f)\,df \tag{11}$$

One can show (Jenkins and Watts,1968) that for a discrete time series of finite length

$$\phi_{xx}(f) = [a^2(f) + b^2(f)]/2\Delta f \tag{12}$$

Thus from a time series of N equally spaced points, N/2 discrete values (called harmonics) of $\phi_{xx}(f)$ will be computed. Physically, each value of $\phi_{xx}(f)$ represents the contribution to the variance per unit frequency over the frequency range from $m\Delta f - \Delta f/2$ to $m\Delta f + \Delta f/2$, for $f = m\Delta f$. It has been traditional in discussing spectral results to term the power spectral values 'energy densities' and the contribution to the variance (ϕdf), as the spectral 'energy'.

3.2 Cross-spectra

Spectral analysis can be applied to simultaneous time series of two quantities to analyse their relationship at various frequencies. For two quantities $X(j)$, $Y(j)$, $j=0,1,2,\ldots\ldots N-1$, one has a co-spectrum such that

$$\overline{XY} - \overline{X}\,\overline{Y} = \int_{\Delta f/2}^{f_N+\Delta f/2} \phi_{xy}(f)\,df \tag{13}$$

where ϕ_{xy} is computed from the Fourier coefficients $a_x(f)$, $b_x(f)$, and $a_y(f)$, $b_y(f)$, of the time series $X(t)$, $Y(t)$

respectively:

$$\phi_{xy} = (a_x a_y + b_x b_y)/2\Delta f \qquad (14)$$

Similarily, the quadrature spectrum has the property that

$$\overline{XY}^* - \overline{X}\overline{Y} = \int_{\Delta f}^{f_N + \Delta f/2} Q_{xy}(f)\,df \qquad (15)$$

where the indicates the Y time series is shifted 90 degrees in phase at all frequencies. In terms of the Fourier coefficients,

$$Q_{xy} = (a_x b_y - a_y b_x)/(2\Delta f) \qquad (16)$$

A study of the relationship between the two signals at various frequencies is made easier when some non-dimensional quantities are examined. The correlation, $\rho(f)$

$$\rho(f) = \frac{\phi_{xy}}{(\phi_{xx} \cdot \phi_{yy})^{1/2}} \qquad (17)$$

is the normalized cospectrum between the two signals. The coherence, γ_{xy} , is defined as

$$\gamma_{xy} = \left(\frac{\phi_{xy} + Q_{xy}}{\phi_{xx} \cdot \phi_{yy}} \right)^{1/2} \qquad (18)$$

This quantity ranges from 0 to 1 where a large value indicates that similar oscillations were occuring in the two signals. (γ^2_{xy} represents the fraction of the power spectrum of one signal that is related to or predictive from the power spectrum of the other signal). In the discussion of the coherence estimates, some criteria must be used to decide whether the two quantities being studied are significantly coherent. Such a criteria can be found using the probability distribution for the coherence estimates as given by Groves and Hannan(1968). The cumulative probability distribution of the coherence squared estimate γ_{xy}^2 for two randomly related signals (i.e. a true coherence of 0) is

$$P(\gamma^2) = 1 - (1 - \gamma^2)^{M-1} \qquad (19)$$

where M is the number of harmonics used in computing the estimate. That value of coherence at which there is a 95% probability that a truly random coherence value will fall below is, from (19):

$$\gamma = [\, 1 - (0.05)^{\frac{1}{M-1}} \,]^{1/2} \qquad (20)$$

This will be called the 95% significance level and is plotted on the coherence graphs. This level decreases with increasing frequency, as a result of the band averaging scheme employed which increases the amount of smoothing of spectral estimates with increasing frequency. For the purposes of our discussion of the coherence results, coherence estimates that fall below the 80% significance level are called poor, estimates that fall between the 80% and 95% significance levels are called fair, estimates between the 95% and 99% significance levels are called good and estimates above the 99% significance level are called very good.

The phase F_{xy} between the two signals at particular frequencies can be estimated by means of the formula:

$$F_{xy} = \arctan(-Q_{xy} / \phi_{xy}). \qquad (21)$$

This definition is chosen so that the phase is positive when signal Y leads signal X and negative for the opposite case.

3.3 Rotary Spectra

The spectral theory described above applies to two scalar signals. This analysis can be generalized to apply to a vector signal and a scalar signal (or indeed another vector signal although this generalization has not been required in this investigation) following the method described by Fillsbury(1972)

and Mooers(1973). This technique, known as rotary spectral analysis, offers two advantages over scalar spectral analysis. It resolves contributions to the variance and covariance from two oppositely rotating vectors at frequencies ranging from the fundamental to the Nyquist frequency. The frequencies range from $-f_N$ through $-\Delta f/2$ and from $\Delta f/2$ to f_N; the positive and negative frequencies being associated with anti-clockwise and clockwise rotations, respectively. In addition, the derived spectral quantities are independent of the coordinate system.

Let the vector time series $\vec{P}$ be represented by the time series of its two components, $X(j)$ and $Y(j)$, $j=1,2\ldots N$. The scalar time series is $S(j)$, $j=1,2\ldots N$. For each of these time series, the fast Fourier transform is used to compute their respective Fourier coefficients. These Fourier coefficients are then used to compute the power spectra of each time series ϕ_{xx}, ϕ_{yy} and ϕ_{ss}, as well as the co-spectral and quad-spectral values ϕ_{xs}, ϕ_{ys}, Q_{xs}, Q_{ys}, Q_{xy} by means equations (14) and (16). The computational formula for the rotary (vector) power spectrum is

$$\phi_{\vec{P}}(f) = (\phi_{xx} + \phi_{yy})/2 + Q_{xy}, \quad f>0 \tag{22}$$

$$\phi_{\vec{P}}(f) = (\phi_{xx} + \phi_{yy})/2 - Q_{xy}, \quad f<0 \tag{23}$$

where the factor of 2 in the denominator results from computing a two-sided rather the ordinary one-sided spectra. The rotary power spectrum has the property that

$$\int_{-f_N}^{f_N} \phi(f)\,df = \overline{X^2} + \overline{Y^2} - (\overline{X})^2 - (\overline{Y})^2 \tag{24}$$

This integral represents the total kinetic energy per unit mass if $\vec{P}$ is a velocity as is the case here. The coherence squared is computed as

$$\gamma^2_{\vec{P}s}(f) = \frac{(\phi_{xs} - Q_{ys})^2 + (\phi_{ys} + Q_{xs})^2}{(\phi_{xx} + \phi_{yy} + 2Q_{xy}) \cdot \phi_{ss}}, \quad f>0 \tag{25}$$

$$\gamma^2_{ps}(f) = \frac{(\phi_{xs}+Q_{ys})^2 + (\phi_{ys}-Q_{xs})^2}{(\phi_{xx}+\phi_{yy}-2Q_{xy})\cdot\phi_{ss}} \quad, \quad f<0 \tag{26}$$

and the phase between the two signals is given by

$$F_{ps}(f) = \arctan\left[\frac{-\phi_{ys}-Q_{xs}}{\phi_{xs}-Q_{ys}}\right], \quad f>0 \tag{27}$$

$$F_{ps}(f) = \arctan\left[\frac{-\phi_{ys}+Q_{xs}}{\phi_{xs}+Q_{ys}}\right], \quad f<0 \tag{28}$$

Both the coherence and phase values defined above, are co-ordinate independent.

3.4 Spectral Display Methods

A useful means of displaying the information in the rotary coherence squared is to use the transfer spectrum. The transfer spectrum is defined as the product of the coherence squared and the rotary power spectrum. These values indicate the amount of energy in one signal which is coherent with that of the other signal for each frequency band. Such a technique avoids misinterpreting cases of high coherence squared values at frequencies where there is very little energy in either signal.

Due to the large number of data points used for calculating the spectral values, the frequency range is correspondingly large. In some of the spectra to be discussed, the frequency range is more than three decades. This wide range makes necessary the use of a logarithmic scale for frequency in the spectral plots. In order to display the relative contributions to total variance at different frequencies, the ordinate of the spectral plots is $f\phi(f)$ using the relation

$$\int f\phi(f)d(\log f) = \int (\phi(f)/2.303)df; \tag{29}$$

The use of graphs with $f\phi(f)$ plotted against log f ensures that equal areas under the plotted curve contribute equal amounts to the variance of the quantities being analysed.

3.5 Spectral Smoothing

The random error of a spectral estimate computed from the Fourier coefficients at a single frequency (i.e. with two degrees of freedom) "is as great as the quantity being estimated" (Bendat and Piersol, 1971). In order to reduce this error, some form of smoothing must be done. Smoothing can be done over spectral estimates made from independent records (ensemble smoothing) or smoothing can be done by averaging spectral estimates over a range of frequencies from within a single record (frequency smoothing). In this study, both means of smoothing are used following a scheme described by Garrett(1970). Smoothing by frequency is done over a varying number of estimates in such a way that each smoothed estimate is nearly equally spaced on the logarithmic plots. For example, the first four estimates are computed from single frequency points (no frequency smoothing), the next estimate is averaged from 2 points, then 3 points and so on up to several hundred points per estimate. The number of points used for smoothing is chosen so that about 8 smoothed spectral estimates are produced for each decade of frequencies.

While this band averaging scheme is well suited to broad band (continuum) processes, it tends to obscure narrow band (line) processes at higher frequencies. For example, a natural forcing frequency at the ocean surface is the diurnal frequency

(period of one day) due to the daily cycle of solar radiation. The band containing the diurnal frequency in the spectral plots, is computed from 176 harmonics, just one of which is the diurnal frequency. Thus a significant peak may occur at one day, but its contribution to the band may not be large enough to raise the spectral level of the band significantly above the others. To avoid missing significant line spectral peaks, single power spectral values were examined at natural frequencies at which line spectral responses might occur: the diurnal, semi-diurnal (12 hours) and their overtones (8 hours, 6 hours) and the inertial frequency (18 hours at 50 N).

The total time series record was subdivided into N blocks and the frequency smoothed spectral estimates were computed for each block. These estimates were then ensembled averaged in order to provide further smoothing and to provide an emperical estimate of the statistical variability. The mean, $\bar{\phi}$ and the standard deviation between the estimates σ are computed for each frequency band. The spectral graphs that are presented plot $f_g \phi$ against $\log(f)$, where f_g is the geometric mean of the endpoint frequencies of the particular frequency band. The geometric mean is used rather than the arithmetic mean because then $f_g \Delta \ln \Delta f$ is more nearly equal to $\phi \Delta f$. The error bars shown on the graphs are the approximate 95% confidence intervals of the mean, computed as $\pm 2\sigma / (\sqrt{N-1})$.

3.6 Two-yearly Spectra

The basic spectra used in this study, to provide a survey of the periodicities present in each quantity, were computed from blocks of 5832 samples. Each block then covers a total period of just under two years (an ordinary two year period would contain 5840 3-hourly measurements while a two year period including one leap year contains 5848 such measurements). The number of samples, 5832, was chosen to use the fast Fourier transform algorithm efficiently. The computational time required by the fast Fourier transform increases rapidly with the size of the largest prime factor of the number of samples. 5832 was chosen since its largest prime factor is only 3 and it comes very close to providing block lengths of two years. Because the block length is not exactly two years, the strong annual spectral peak found in many of the quantities spectra will have some energy 'leakage' to adjacent frequencies. A simple calculation shows that for the rectangular window used in this study, the leakage to side lobes is extremely small, being less than 0.01% of the annual energy. The spectra produced resolve periods ranging from two years to 6 hours. The confidence intervals for each averaged spectral estimate are based on 5 individual spectral estimates. While strictly speaking, small sample statistics should be used for computing the confidence intervals, it is felt that Gaussian statistics provide representative values of the scatter about the mean.

3.7 Seasonal Spectra

A special set of spectra of the various quantities were computed for blocks of 728 samples or a period of 91 days. Each block is one 'season'. Because the available data began on Jan. 1, 1958 and ended on Dec. 31, 1967, the 'seasons' analysed were shifted from the natural seasons in order to use as much of the data as possible. For example, the first day of winter for our purposes was taken to be Jan. 1 rather than Dec. 21. In addition, the season size of 728 samples, chosen for efficient use of the FFT algorithm, makes up a year which is 8 samples less than a complete non-leap year and 16 samples less than a complete leap year. This choice also necessitates slight adjustments. In non-leap years, the first four and last four records are not used. In a leap year, the first eight and last eight data records are not used. The spectral results for each season were averaged over the ten years so that an average spectrum and its approximate 95% confidence intervals for each of the four seasons was produced.

Before the seasonal spectra were computed, the data was processed by the computer to effectively high pass filter it. This filtering was done to remove the annual cycle from the signals. Otherwise, a large trend would be present in the time series making up the seasons which could produce large, fictitious spectral values at the low frequencies. The high pass filtering was achieved by Fourier transforming each individual 'year' (2916 samples), zeroing the first three harmonics of the transform values (corresponding to periods of one year, one-half year and one-third year) and then inverse Fourier transforming

these values back into a time series. An example of the effect of this procedure is illustrated in Figure 1. As discussed previously, sideband leakage from the strong annual peak is present, but is very small (less than 0.01%) and the dominant leakage would appear in the next two harmonics which are also set to zero.
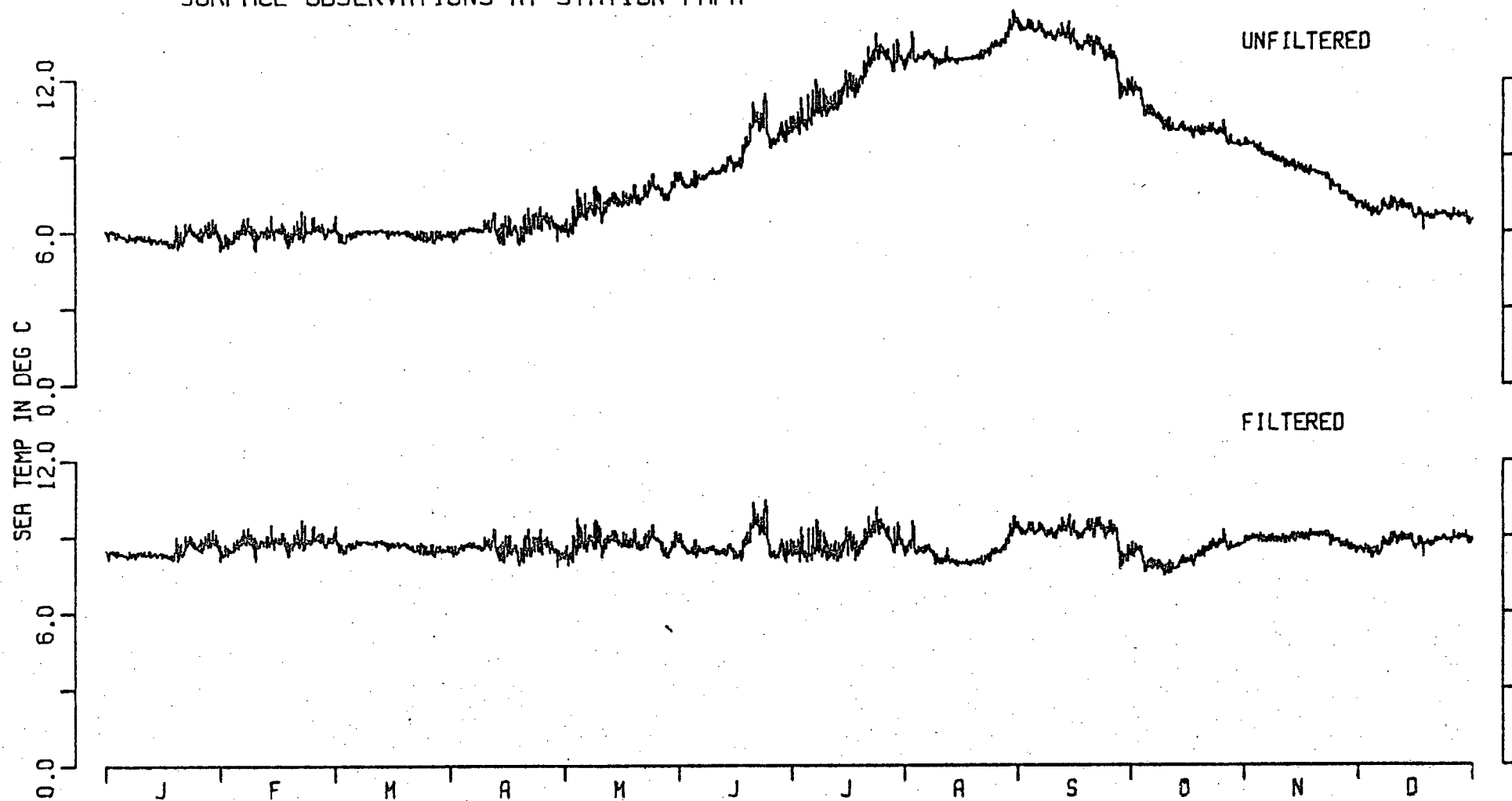
Figure 1: An example of the effect of filtering to remove the annual variation. The graph displays the sea temperature of 1962 before and after filtering.

Chapter 4

SPECTRAL RESULTS

4.1 Introduction

For each physical quantity, the power spectra are displayed and the important periodicities are described. These spectra are compared to the spectra computed by other investigators. The literature contains a sizeable number of spectra of wind speed and a smaller number of spectra of wind components, air pressure and air temperature. Spectra of absolute humidity and sea temperature are very rare. When discussing spectral results, it is often useful to know the average of the analysed quantity and the cumulative integral of the spectrum. These values are given in Appendix II for the two-yearly spectra and the seasonal spectra.

4.2 Wind

The most striking feature of the wind speed spectrum (see Figure 2) is the broad synoptic peak at 3.1 days, a result of the passage of cyclones, anti-cyclones and their frontal systems. The peak which includes contributions from a wide range of scales (having its half-power points at periods of 10 days and 1.3 days) emphasizes the irregular nature of the passage of synoptic scale scale disturbances. The synoptic peak accounts for most of the total variance of the wind speed (28.3 m^2/sec^2) for the periods resolved. The wind speed spectrum shows little variation at periods longer than one month with the exception of an important annual cycle. The annual cycle, seen as a peak at one year and a secondary peak at one-half year, due to some dis-
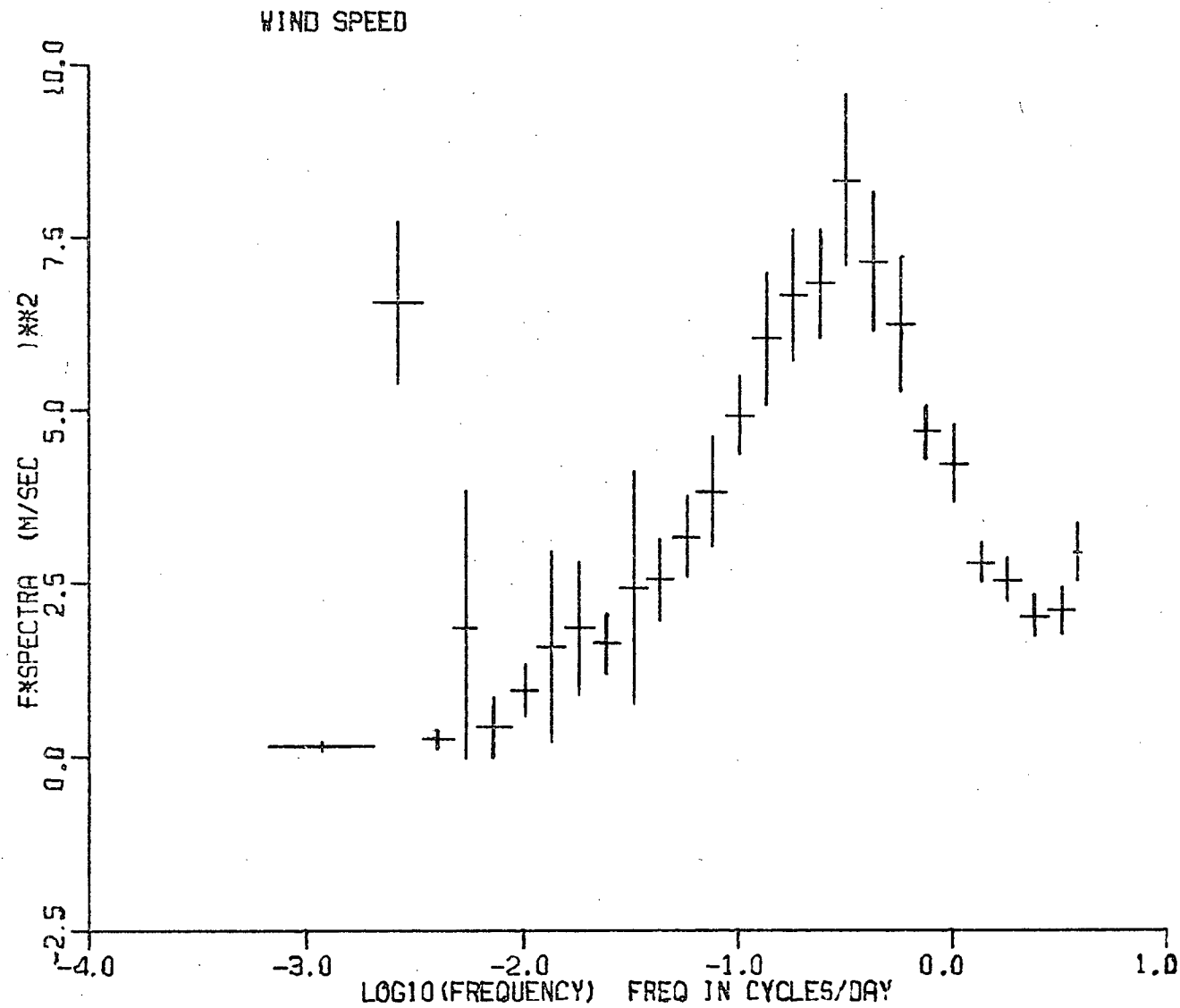
Figure 2: The two-yearly wind speed spectrum for the period 1958 to 1967. The vertical error bars represent approximate 95% confidence intervals of the mean of each spectral estimate.

tortion, has a total variance of 3.9 m²/sec². This corresponds to an average annual range $(2 \cdot \sqrt{2}[\text{variance}]^{1/2})$ of 5.7 m/sec.

At the high frequency end of the spectrum, the graph shows a steady decline to periods of about 9 hours and then an increase out to the Nyquist period of 6 hours. This upturn at the smallest periods is believed due to variance at smaller scales between 6 hours and the 10 minute averaging period being aliased back into the spectrum at lower frequencies. Because in our plots, the spectrum is multiplied by frequency, the contributions due to aliasing are more apparent at small periods than at large periods (for a discussion of this effect see Oort and Taylor,1969). In order to correct the aliased spectrum, one must assume a frequency distribution of the spectrum at higher frequencies. Because the effect of aliasing appears small, this correction was not felt to be necessary. It seems clear from inspection of the graph, that a correction for aliasing would leave the spectrum declining out to the Nyquist period. Such a decline in the spectral levels is consistent with the existence of a 'spectral gap'; a minimum of spectral levels in the mesoscale separating spectral peaks in the synoptic scale and microscale (Fiedler and Panofsky,1970).

Important changes in the wind speed spectra occur between one season and another. Figure 3 shows the wind speed spectra calculated separately for the four seasons with each season's spectrum being averaged over the ten years. Differences are found in both the level and the period of the synoptic peak. The peak is largest in the fall ($f\phi$=10.3 m²/sec²) declining through the winter (9.71 m²/sec²) and spring (6.36 m²/sec²) to
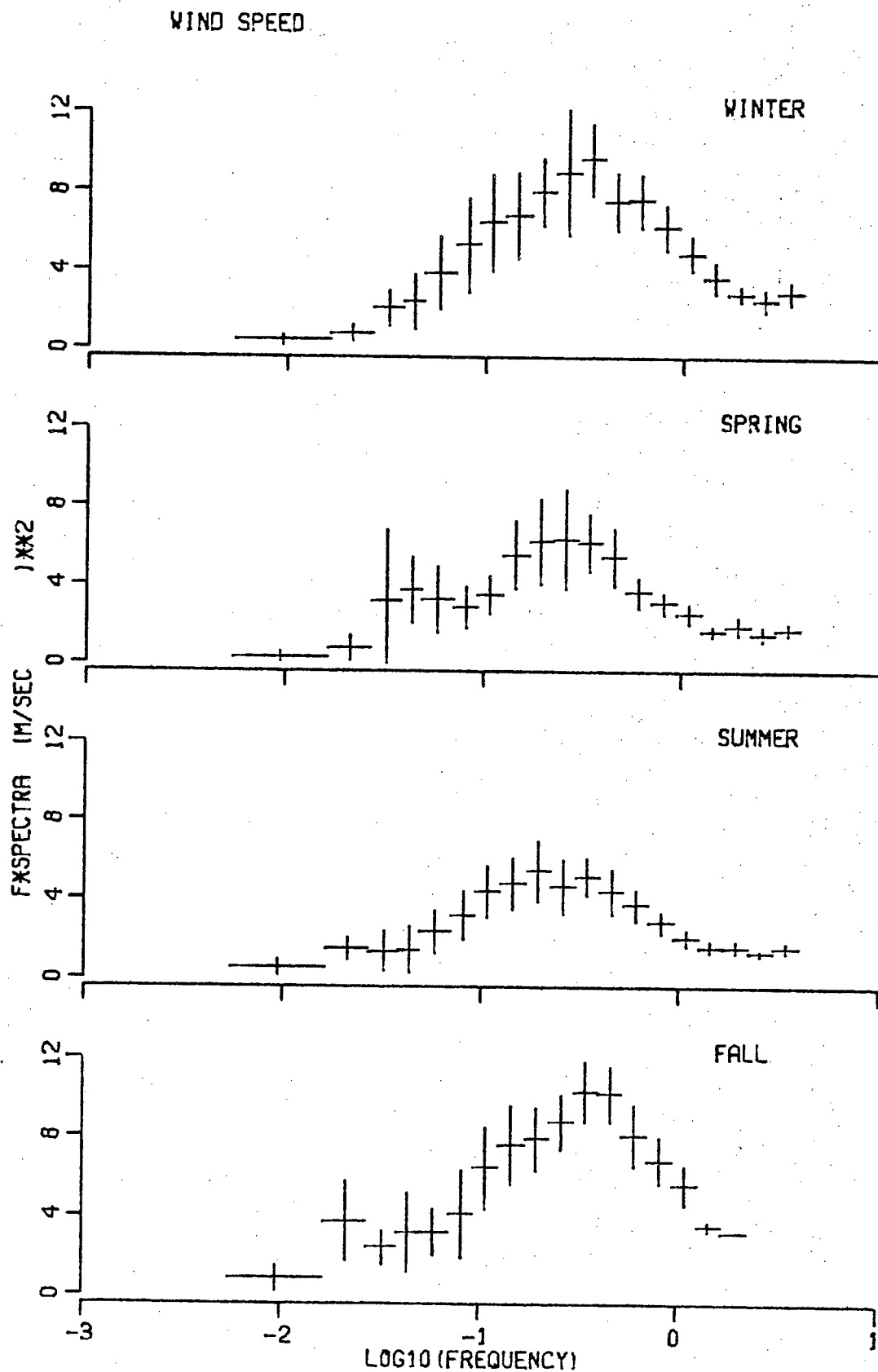
Figure 3: Wind speed spectra for each of the seasons averaged over the ten years, 1958 to 1967. The vertical error bars represent approximate 95% confidence intervals of the mean.

the lowest level in summer (5.48 m²/sec²). The period at which the peak occurs shows a similar variation being smallest in fall (2.5 days) increasing through winter and spring and being largest in summer (4.4 days). These results illustrate the general seasonal pattern of synoptic disturbances which occur more frequently and with greater intensity in the fall and winter than in the spring and summer. It is interesting to note that the largest change in the spectra is between the adjacent summer and fall seasons with more gradual changes taking place over the rest of the year. In the spring and fall, there is some evidence of activity at longer periods (20 to 45 days) but in both cases the peaks are not statistically significant.

Figure 2 shows no peak at the diurnal or semi-diurnal periods but a closer examination of single harmonics of the spectral values reveals some activity. The largest energy is found in a semi-diurnal peak with a contribution to the variance of 0.022 m²/sec² corresponding to an average range of 0.46 m/sec. At the diurnal period a small peak is found but it is not significant. A significant peak does appear at a period of one-quarter day, the first overtone of the semi-diurnal period, with a contribution to the variance of 0.016 m²/sec². No energy is found at periods of one-third of a day or the inertial period.

Examination of single harmonics of the seasonal spectra reveal similar results. No peak is found at the diurnal period for any of the seasons while each season does exhibit a semi-diurnal peak. The energy of the semi-diurnal peak, after correction for the spectral background level, is found in Table I. The background correction is made by subtracting the average of

TABLE I

The energy of single harmonic spectral peaks found at periods of one day, one-half day and one-quarter day. The annual values are computed from the spectra determined from data blocks of two years. A '-' indicates that no peak was found. Of one day, one-half day and one-quarter day. The annual values are computed 'S.D.' is the computed standard deviation of the energy estimates.

Quantity	Period	Energy				
		Annual	Winter	Spring	Summer	Fall
	(days)	(m/sec)²				
U	1.0 S.D.	0.009 ±.016	-	-	-	-
	0.5 S.D.	0.022 ±.019	0.027 ±.051	0.016 ±.029	0.024 ±.026	0.038 ±.076
	0.25 S.D.	0.016 ±.004	0.018 ±.020	-	0.006 ±.010	0.018 ±.013
Clock-wise U	1.0	-	-	-	-	-
	0.5 S.D.	0.045 ±.029	0.026 ±.043	0.048 ±.036	0.049 ±.063	0.051 ±.081
	0.25	-	-	-	-	-
Anti-clock-wise U	1.0	-	-	-	-	-
	0.5	-	-	-	-	-
	0.25 S.D.	0.004 ±.002	-	-	-	-

the spectral levels of the four adjacent harmonics. In fall, the semi-diurnal variation is the largest with an energy of 0.038 m²/sec² (an average range of 0.55 m/sec) while the spring has the lowest energy of 0.016 m²/sec² (an average range of 0.36 m/sec).

Several spectra of wind speed in the surface layer have been published. Oort and Taylor (1969) presented the wind speed spectrum for Caribou, Maine, a station with a continental climate. Van der Hoven (1957) has computed the wind speed spectrum at Brookhaven, New York on Long Island. Wind spectra at stations on the Oregon coast are found in Frye et. al. (1972) and Burt et. al. (1974) while Hwang (1970) presents a wind spectrum on the tropical Pacific island of Palmyra. At stations over the open ocean, wind speed spectra have been computed by Byshev and Ivanov (1969), Millard (1971) and Dorman (1974). A summary of the results of these investigators together with the important data parameters, is found in Table II. When comparing these results, differences in the experiments of the various investigators must be considered. Millard (1971), Burt et. al. (1974), Frye et. al. (1972), Hwang (1970) and Van der Hoven (1957) used data that did not cover a complete year. Thus their spectra is biased due to the seasonal variability of the wind speed spectra. In addition, different methods of computing and smoothing were used. However, for comparison of a broad band feature like the synoptic peak these differences are not critical. Furthermore, the number of locations available for comparison is very limited so that any discussion of regional patterns must be regarded as tentative.

A summary of the period and level (f•φ) cf the syncptic peak of the wind speed spectra as determined by varicus investigatcrs. Z is the height cf the anemometer and U is the mean wind speed cf the data analyzed. In cases where these values were nct available, a '-' is shcwn.

Investigators	Location	Z (m)	U m/sec	Data Period	Synoptic Period (days)	Synoptic Level (m/sec)[2]
Van der Hoven(1957)	40N 73W	108	-	Aug. 1955 To Feb. 1956	4	5
Oort and Taylor(1969)	47N 68W	11	-	Jan. 1949 Tc Dec. 1958	3.9	3
Byshev and Ivanov(1969)	53N 36W 44N 41W	-	-	Jan. 1961 tc Dec. 1963	6.4	5
	8S 14W 16S 6W	-	-	July 1957 tc July 1958	12	1
Hwang(1970)	6N 162W	2	-	Mar. 1967 to May 1967	5.9	1.1
Millard(1971)	30N 70W	-	5.7	Apr. 1967 tc June 1967	4	6
Frye et. al.(1972)	45N 125W	20	-	July 1970 Tc Aug. 1970	2 5	3.5 1.5
Burt et. al.(1974)	45N 125W	10	11.8	Aug. 1970	3.0	7.5
Dorman(1974)	30N 140W	25	6.2	Jan. 1951 tc Dec. 1970	8	2.9
This Study	50N 145W	22	10.1	Jan. 1958 tc Dec. 1967	3	8.2

The period of the synoptic peaks range from about 12 days at the Ascension(8S 14W) and St. Helena(16S 6W) Islands to the period of 3 days found at Station 'Papa' (50N 145W) in this study and off the Oregon coast (45N 125W) reported by Burt et. al.(1974). An intermediate value of 8 days is reported by Dorman(1974) at Station N (30N 140W) located near the northern limit of the Trade Wind belt in the Pacific Ocean. These results suggest, as might be expected, a general pattern of increasing frequency of synoptic activity with increasing latitude.

A comparison of the various spectra also reveal large zonal variations in the period. Station 'Papa'(50N 145W) and the Oregon coast(45N 125W) both have a period of about 3 days while at Caribou, Maine(47N 68W), Cort and Taylor report a peak period of 3.9 days. Van der Hoven(1957) finds a peak period of approximately 4 days at Brookhaven, New York(41N 73W). Further to the east, Byshev and Ivanov(1969) found a period of 6.4 days for the synoptic peaks at Station C (53N 36W) and Station D (44N 41W). A similar variation is seen at a latitude of about 30N, with Millard(1971) reporting a period of 4 days at 30N 70W compared to a period of 8 days reported by Dorman(1974) at 30N 140W. (In fact, this comparison understates the difference, since Millard's results are for April and May, when the peak period is probably higher than the yearly value). These zonal variations indicate the importance of the local environment in determining time variations of the surface boundary layer.

The intensity of the synoptic peak exhibits large regional variations. Just as the period of the synoptic peak decreased

with increasing latitude, the intensity shows a corresponding increase. At low latitudes the peak level is low $(f\phi \sim 1.0$ $m^2/sec^2)$ at the Ascension and St. Helena Islands, (Byshev and Ivanov,1969) and it increases at higher latitudes $(f\phi = 8.2$ m^2/sec^2 at Station 'Papa'). Pronounced zonal variations exist as well with the $f\phi$ of Station 'Papa' compared against $f\phi = 3.0$ m^2/sec^2 at Caribou, Maine (Oort and Taylor,1969) and $f\phi = 5$ m^2/sec^2 at Stations C and D (Byshev and Ivanov, 1969). The zonal variation of both synoptic peak period and intensity appear to be related to more localized effects. One such effect could be the presence of topographic features of synoptic scale size in the vicinity of the observation station. For example, at land stations the presence of surface features such as moun-tain ranges, may reduce the intensity and frequency of synoptic scale disturbances, in contrast to the open ocean with its very long fetches. Another factor may be the position of the station in relation to anomalous meteorological regions such as areas associated with frequent cyclogenesis or frequent blocking pat-terns.

The activity found at the diurnal and semi-diurnal frequen-cies differ considerably between ocean stations and land and coastal stations. At 'Papa' there is no significant diurnal peak and the semi-diurnal peak is very small. Millard(1971) found a similar result over the open Atlantic ocean while Dorman's(1974) results show very small diurnal and semi-diurnal peaks, with the diurnal peak being the larger of the two. In contrast, Oort and Taylor's(1969) spectra at Caribou and five other land stations, show a large diurnal wind speed variation

and a very much smaller semi-diurnal peak. At coastal stations, a large diurnal peak and smaller semi-diurnal peak is found.

Over land, Blackadar(1959) has explained the diurnal variability of the wind as a result of the diurnal change in stability. During the daylight hours, as the surface layer is heated it becomes less stable, allowing more convective mixing with the layer above. The two layers become more strongly coupled with a resulting increase in wind speed in the surface layer. At night cooling of the surface layer due to radiative losses, makes it more stable and reduces its coupling with the layer above, decreasing the surface layer wind speed. Frye et. al. (1972) argue that along a coast, the diurnal wind variation is due to the land-sea temperature difference producing a sea breeze during the day and a weaker land breeze at night. Over the open ocean, neither of these mechanisms are very powerful and thus the diurnal wind variation is small.

The semi-diurnal peak, though small, appears to be significant indicating that at least sometimes the wind speed has two maxima and minima each day. One possible explanation is that this periodic motion is associated with the well known semi-diurnal variation of air pressure (Butler, 1962) which is found in the spectral analysis of air pressure.

Figure 4 shows the rotary wind spectrum. The synoptic peak dominates both the anti-clockwise and clockwise spectra with each having the peak occuring at a period of 3 days. The levels of the peaks differ: the clockwise peak has $f\phi=18.4$ (m/sec)^2 compared to $f\phi=13.5$(m/sec)^2 for the anti-clockwise peak. This result can be explained by the general pattern of synoptic wea-

ROTARY WIND

CLOCKWISE

ANTI-CLOCKWISE

Figure 4: The rotary auto-spectrum of the wind computed from five two-yearly blocks covering the period 1958 to 1967. The vertical error bars represent approximate 95% confidence intervals of the mean.

ther system movements in the N E. Pacific. The most common storm track is to the north of Station 'Papa' over the Gulf of Alaska (see U. S Navy, Marine Climatic Atlases). Eastward moving weather systems, whether cyclonic or anti-cyclonic, when passing to the north of the observation station, cause the observed wind to rotate in a clockwise manner. Consider, for example, the passage of an eastward moving cyclonic system to the north of the observation station (the most common situation at Station 'Papa'). As it passes by, this would cause the observed wind to change from southwesterly to westerly to northwesterly in direction. That is, the wind rotates in a clockwise sense. Weather systems moving to the south of Station 'Papa', make greater contributions to the anti-clockwise spectrum. Of course, the situation is complicated by such events as the passage of storm fronts with their abrupt changes in wind direction. Nevertheless, the computed rotary spectrum appears to differentiate between the passage of weather systems to the north and south of the observation station and is consistent with the known pattern of pressure system movements.

A comparison of the wind speed spectrum (figure 2) with the rotary wind spectrum (figure 4) is revealing. In both spectra, the dominant synoptic peak is found to occur at the same period. However, the important annual peak found in the wind speed spectrum is much less pronounced in the rotary spectrum, with no such peak for clockwise rotations and a relatively small peak for anti-clockwise rotations. This difference is due to the long period variation of the wind direction. Wind roses compiled from the data show that the wind tends to be from the

south in winter and generally from the west in summer. The variation of the wind direction over a period of a year is not a uniform rotation but rather an irregular shift. This type of variation in wind direction probably causes the spectral energy of the annual wind speed to be found at shorter periods in the rotary wind spectrum. Indeed, the rotary spectrum shows a less regular rise from a period of one year to the synoptic peak than does the wind speed spectrum.

The seasonal rotary wind spectra are displayed in figure 5. The synoptic peak for both the clockwise and anti-clockwise spectra follows the same pattern of the wind speed spectra: higher levels and a shorter period of the peak in fall and winter in comparison with spring and summer. The relative contributions of the clockwise and anti-clockwise synoptic peaks does not vary appreciably with season.

An examination of single harmonic spectral values indicates no significant diurnal peak but a significant semi-diurnal peak (see Table I). The semi-diurnal peak is found only in the clockwise part of the rotary spectrum, with an energy of 0.045 (m/sec)^2. This result agrees with the findings of Kuhlbrodt and Reger in the Trade Wind zone (discussed by Roll, 1965) who reported a semi-diurnal wind variation from the mean wind which rotated in a clockwise sense during the course of the day. The clockwise semi-diurnal peak is reduced in size in winter and remains relatively constant through the remainder of the year. No significant peak was found in any of the rotary wind spectra at a period of one-third of a day or at the inertial frequency. A small peak was found in the the anti-clockwise spectra at one-

ROTARY WIND

CLOCKWISE   ANTI-CLOCKWISE
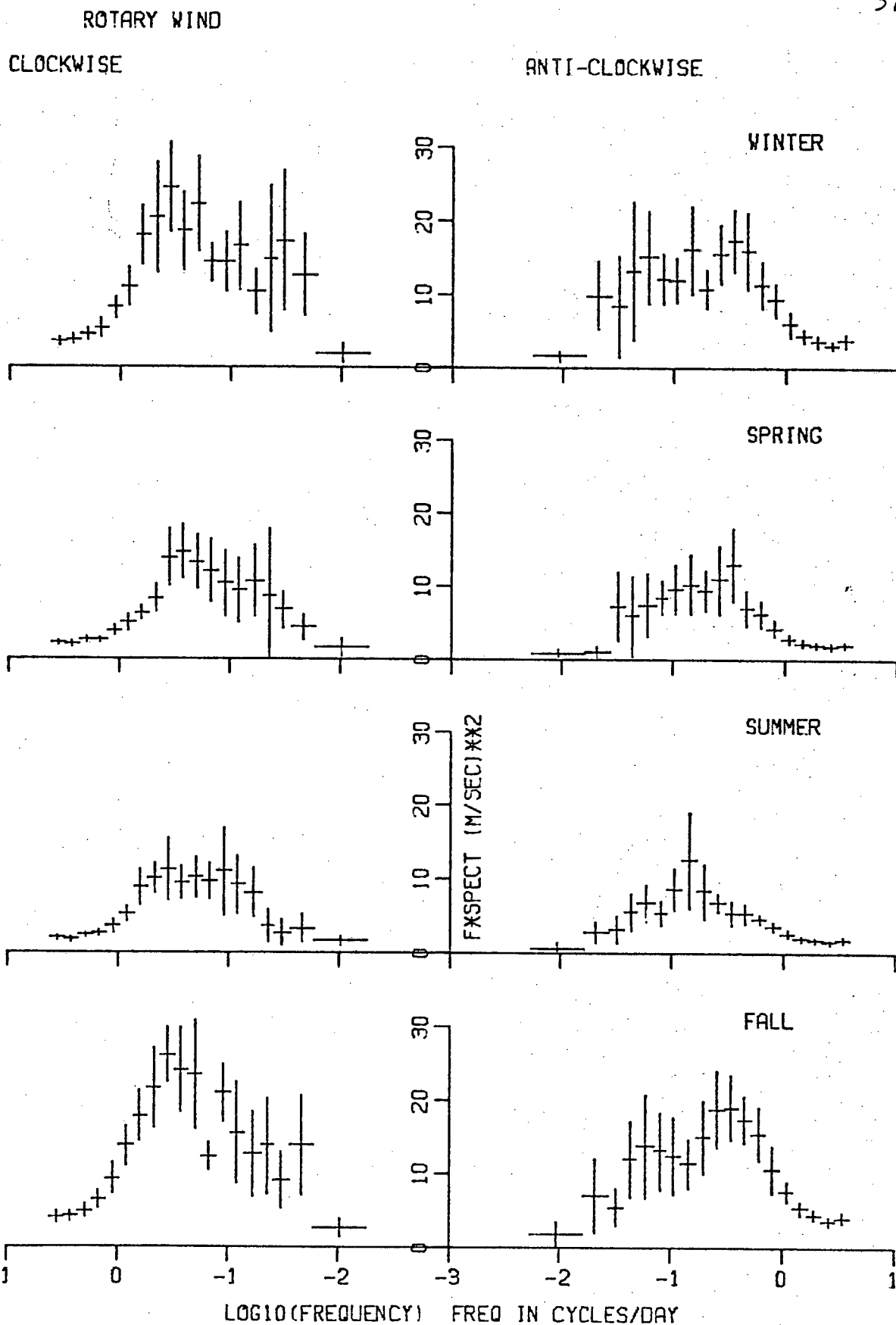
Figure 5: The seasonal rotary auto-spectra of the wind averaged
over the ten years, 1958 to 1967. The vertical error bars
represent approximate 95% confidence intervals of the mean.

quarter of a day.

Rotary wind spectra at other locations are uncommon. Dorman(1974) has computed rotary wind spectra for Station N (30N 140W) in the Pacific, a location even further away from the main storm track. His results show good qualitative agreement with those of this study. The spectral levels are lower due to the smaller amount of synoptic activity in that area. The clockwise rotational spectral peak is larger than the anti-clockwise peak as in this study, while the difference in the levels of the two spectra is even more pronounced.

4.3 Air Pressure

The spectrum of atmospheric pressure (see Figure 6) like the wind speed spectrum, is dominated by a broad, somewhat irregular peak at intermediate periods. However, this peak ranges over longer periods than that of the wind speed, having its half-power points at periods of 70 days and 3 days. The highest spectral level is found at 17 days where $f\phi = 55.8$ (mbar)^2. The spectrum also reveals a large annual periodicity in the air pressure by the presence of a peak at one year and a smaller peak at a period of one-half year. The annual peak has a total variance of 30.8 (mbar)^2 corresponding to an annual range of 16 mbar (about a mean of 1012 mbar). The spectrum at the shortest periods is notable for its very low levels. There is no evidence of any aliasing at these periods.

Important changes take place in the pressure spectrum between one season and another. The seasonal pressure spectra (see Figure 7) show pronounced changes in the spectral levels with large values in fall and winter, intermediate values in spring
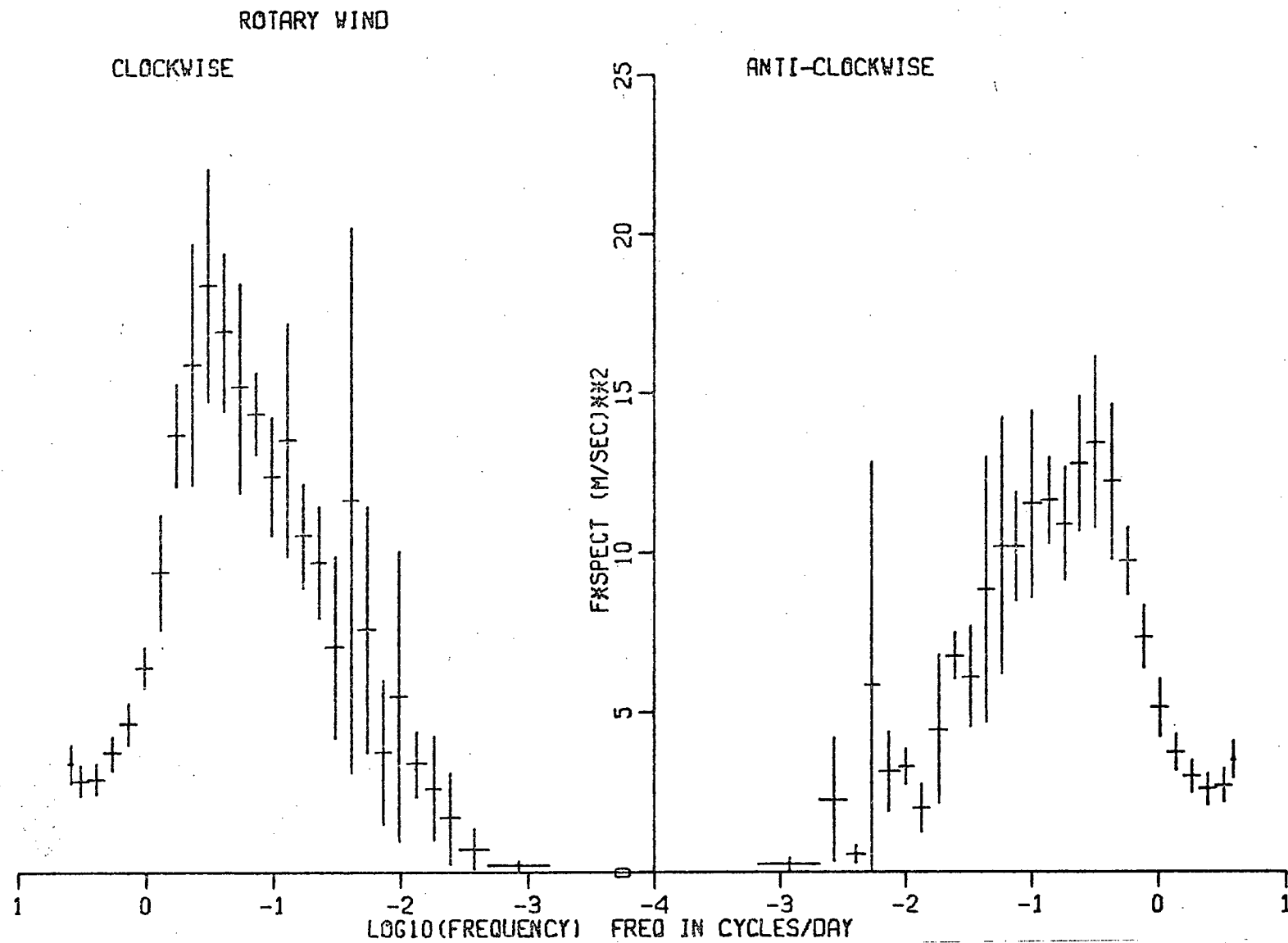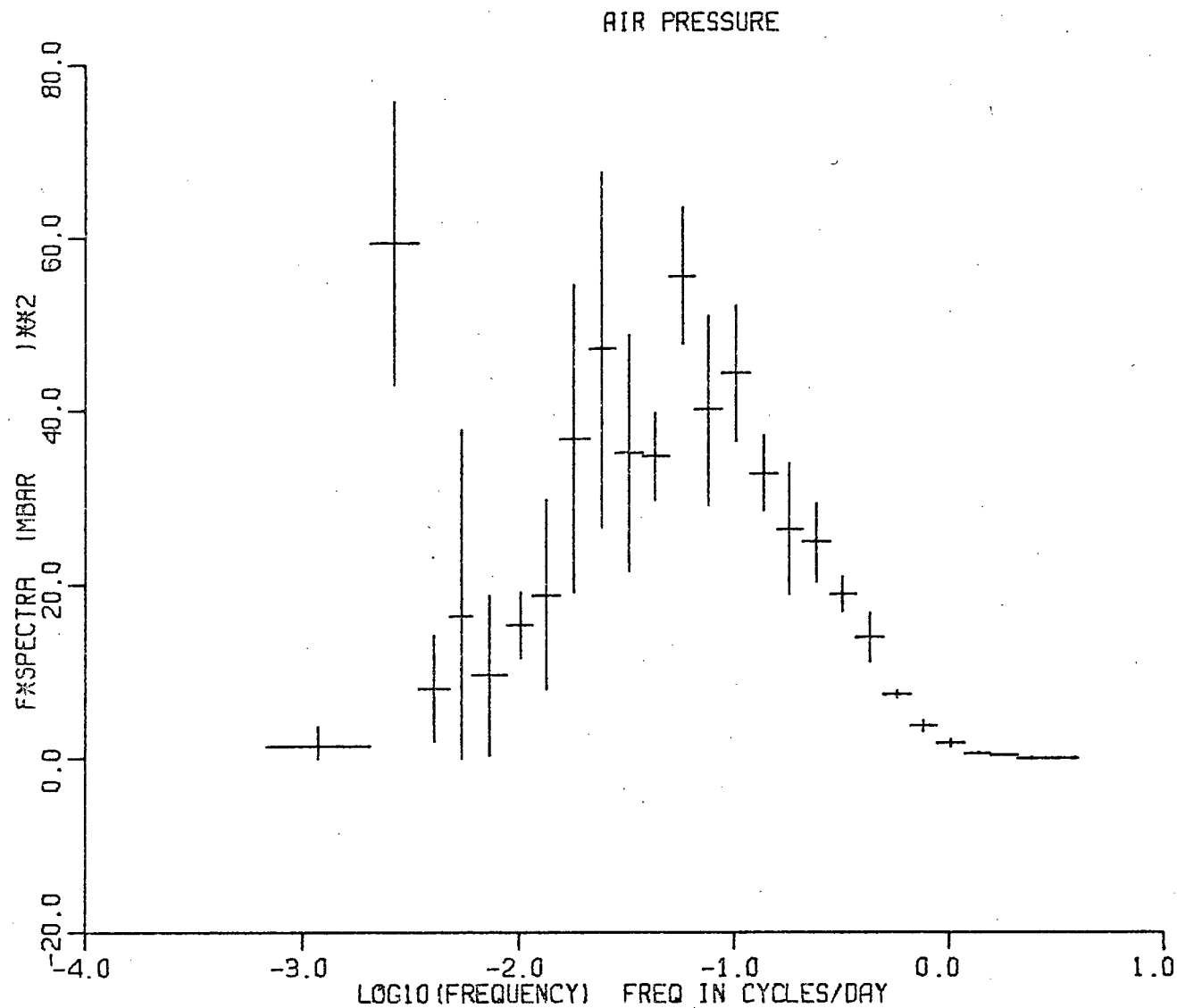
Figure 6: The power spectrum of air pressure computed from five two-yearly data blocks covering the period, 1958 to 1967. The vertical error bars represent approximate 95% confidence intervals of the mean.
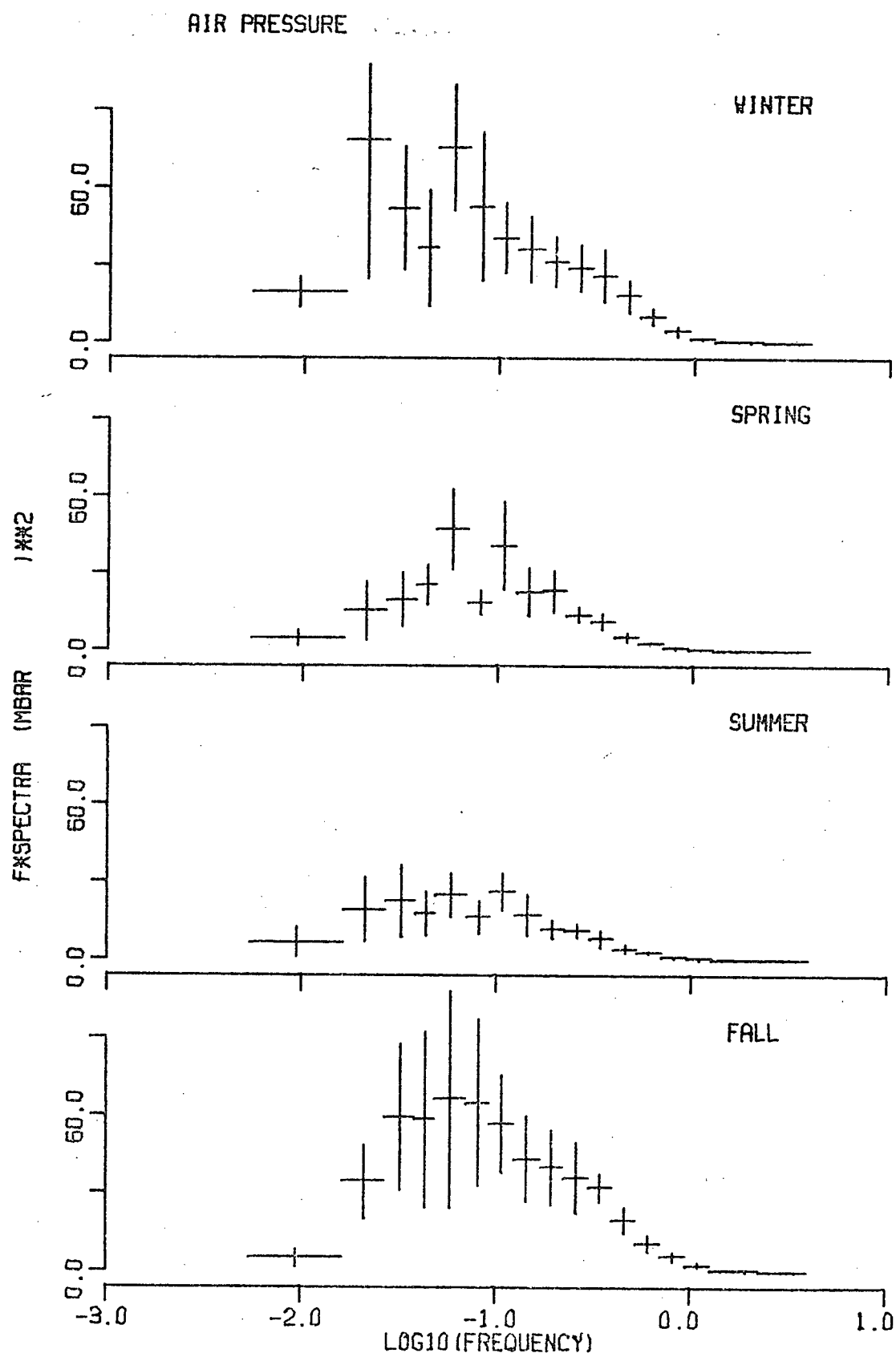
Figure 7: The seasonal power spectra of air pressure; each spectrum is averaged over the ten years, 1958 to 1967. The vertical error bars represent approximate 95% confidence intervals of the mean.

and small values in summer. The seasonal variaticns of the period of the peaks are more complicated. In fall, a single peak is found at 17 days. This peak is also present in winter together with a large contribution from periods around 45 days. In spring the 17 day peak is accompanied by a peak at 9.2 days while the longer period variations are markedly reduced. In summer, while all spectral levels are greatly reduced, the relative contribution from longer periods (say periods greater than 20 days) is larger than in spring.

An examination of the single harmcnic spectral values of the air pressure reveals a sharp semi-diurnal peak with a variance of 0.037 $(mbar)^2$ corresponding to an average range of 0.55 mbar. Smaller variations (see Table III) are found at periods of one day and one-third of a day. These variations are larger in fall and winter at the one-half and one-third of a day periods but the diurnal variations are larger in spring and summer.

The air pressure spectral results are generally consistent with the results of other investigators. Roden(1965) has computed the annual and semi-annual pressure oscillaticns for stations on the Pacific coast of North America. The annual variation found at Station 'Papa' agrees well with the annual variation found at Prince Rupert, B.C. and Alaskan coastal stations but it is considerably larger than that fcund at Victoria, B.C. and Washington and Oregon stations. Air pressure spectra covering the synoptic and seasonal scales have been computed by Dorman(1974) for Ocean Station N (30N 140W) and by Eyshev and Ivanov(1969) for Ocean Stations C and D located at 53N 36W and

TABLE III

The energy of single harmonic spectral peaks of air pressure, air temperature, absolute humidity and sea surface temperature found at periods of one day, one-half day and one-third day.

Quantity (units)	Period	Annual	Winter	Spring	Summer	Fall
Air P $(mbar)^2$	1.0 S.D.	0.0118 ±.0086	–	0.034 ±.022	0.019 ±.017	–
	0.5 S.D.	0.037 ±.0035	0.044 ±.018	0.035 ±.008	0.030 ±.007	0.043 ±.017
	0.333 S.D.	0.0040 ±.0008	0.0064 ±.0068	0.0014 ±.0013	0.0017 ±.0012	0.0070 ±.0052
Air T $(C^o)^2$	1.0 S.D.	0.0446 ±.0240	0.0281 ±.0290	0.0862 ±.0378	0.0692 ±.0245	0.0169 ±.0244
	0.5 S.D.	0.0047 ±.0012	0.0043 ±.0017	0.0040 ±.0020	0.0068 ±.0035	0.0055 ±.0029
Air q $(gm/m^3)^2$	1.0 S.D.	0.0014 ±.0011	0.0006 ±.0008	0.0027 ±.0029	0.0016 ±.0023	0.0003 ±.0013
	0.5 S.D.	0.0001 ±.0001	–	–	–	–
Sea T $(C^o)^2$	1.0 S.D.	0.0020 ±.0011	0.0003 ±.0002	0.0045 ±.0024	0.0027 ±.0016	0.0007 ±.0006
	0.5 S.D.	0.0002 ±.0002	–	–	–	–

44N 41W, respectively. Both of these air pressure spectra reveal a broad peak similar to that found at Station 'Papa' (17 days) with the period of the peak being 16 days at Station N and about 12 days at Stations C and D. While the periods of the peaks were in reasonably good agreement, the levels differed considerably. At 'Papa' the peak level was $f\phi=56$ (mbar)^2 compared to 9 (mbar)^2 at Station N and about 8 (mbar)^2 at Stations C and D. This reflects at least in part, the difference in the level of synoptic activity between these locations. The semidiurnal and diurnal variation of air pressure has been reported at many locations (Butler,1962) including Station N (Dorman,1974), San Diego (Gossard,1960) Bermuda (Wunsch,1972) and Palmyra Island (Hwang,1970). As expected the size of the variation found at 'Papa' is smaller than that found at the more southerly locations cited above.

4.4 Sea Surface Temperature

The spectrum of sea temperature is shown in Figure 8. As previously mentioned (see Chapter 2), the sea temperature was erroneously measured over the first five years on one of the two weatherships. The effect of this error on the spectrum was examined by comparing the spectrum computed from all ten years with the spectrum computed from only the last five years of data. At the diurnal period, the ten year spectral value is more than twice the corresponding value computed from the last five years. However, at other periods, while the smoothed spectral estimates differ by as much as 40% for individual estimates, the differences are within the 95% confidence interval computed from the separate spectral estimates of each data block. Thus, the
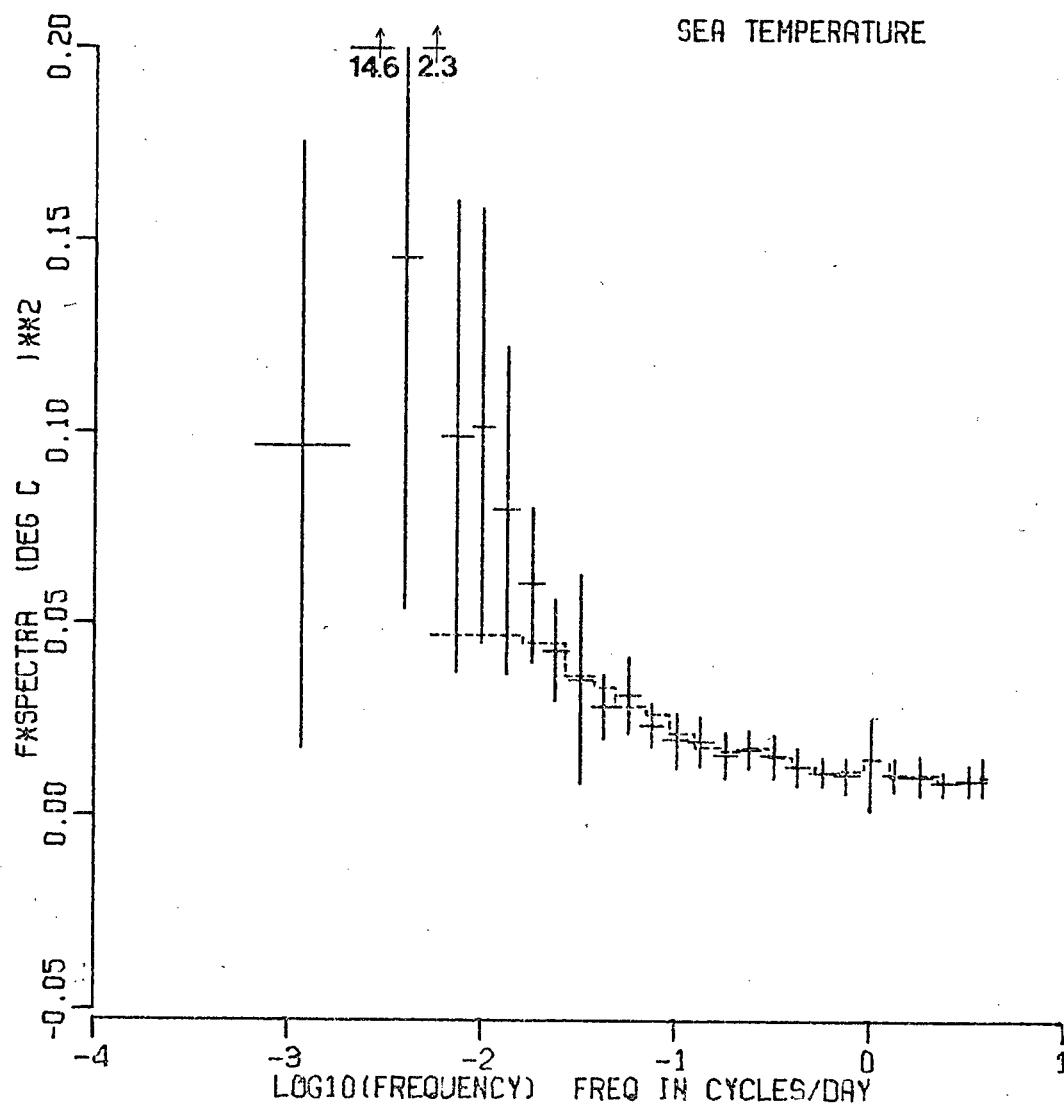
Figure 8: The power spectrum of sea temperature computed from five two-yearly blocks covering the period, 1958 to 1967 and for comparison, the power spectrum computed by averaging the seasonal estimates (as a dashed line). A correction is made to the spectrum at the period of one day to compensate for erroneous sea temperature measurements of the first five years. The vertical error bars represent approximate 95% confidence intervals of the mean.

two yearly and seasonal temperature spectra are computed from
all ten years of data but corrected at the diurnal period to
agree with the diurnal spectral value computed from the last
five years of data. The single harmonic spectral values dis-
cussed below are computed from the last five years of data as
well.

The two-yearly sea temperature spectrum is dominated by the
annual cycle with peaks at the annual and semi-annual periods.
Over 95% of the total energy of the spectrum is contributed at
these periods. The annual period has an energy of 7.50 $(C^o)^2$
corresponding to an average range of 7.9 C^o while the semi-
annual period has an energy of 0.56 $(C^o)^2$ corresponding to a
range of 2.2 C^o. (The mean sea temperature is 8.46 ^oC). With
the exception of the diurnal peak, the remainder of the spectrum
is featureless, declining steadily with decreasing periods.

The data from which each seasonal spectrum was computed,
was digitally filtered to remove the large annual variation (as
explained in Chapter 3). However, at the frequencies resolved
and displayed on the seasonal spectra (Figure 9), this filtering
should have little effect. To test this, the seasonal spectral
values were averaged and the results are plotted as a dashed
line in Figure 8. As expected, the agreement is good except at
the lowest seasonal frequency band. This discrepency is due to
the fact that the lowest band includes contributions from
periods of 182 days to 105 days, which were zeroed by the fil-
tering.

The seasonal spectra of sea temperature (see Figure 9), in
contrast to the wind and air pressure spectra, have their lar-

Figure 9: The seasonal power spectra of sea temperature; each
spectrum is averaged over the ten years, 1958 to 1967. A
correction is made to the spectra at the period of one day to
compensate for erroneous sea temperature measurements of the
first five years. The vertical error bars represent approximate
95% confidence intervals of the mean.

gest spectral values in summer and the smallest spectral values in winter. The largest changes in the seasonal spectra occur at periods ranging from 10 to 100 days. In spring the largest values are found at periods of 12 to 30 days, while the other seasons show the largest spectral values at longer periods. In all cases, the 95% confidence intervals are large indicating a large year to year variability and the fact that the longest period spectral estimates have the least amount of smoothing.

The single harmonic spectral values of the last five years were examined. They show a sharp peak at a period of one day and a weaker peak at one-half day. No significant peaks were found at one-third or one-quarter of a day. The diurnal peak has an energy of 0.0020 $(C^0)^2$ corresponding to an average daily range of 0.13 C^0 (see Table III). The semi-diurnal peak has an energy of 0.00015 $(C^0)^2$ corresponding to a range of 0.04 C^0. The diurnal variability of sea temperature also shows a marked seasonal variability. The energy is largest in spring and decreases by more than an order of magnitude to its lowest value in winter. It is not surprising that the greatest diurnal variation occurs in spring since this season, which for the purposes of the analysis includes all of June, has the greatest amount of solar insolation. In addition, downwards heat transport is reduced at this time of year due to the presence of a shallow seasonal thermocline (see Tabata,1961). The combination of more heat input on a daily cycle, together with less transport of heat away from the surface results in this large diurnal variation. In winter, the situation is reversed, and the result is a very small diurnal variation.

Other sea temperature spectra can be compared with the above results. Dorman(1974) has computed seasonal spectra at Ocean Station N (30N 140W). The summer spectrum agrees well with that found at Station 'Papa' while the winter spectrum shows more activity at periods of 2 to 10 days. Sea temperature oscillations with periods of 25 to 45 days have been reported by Koizumi at Ocean Station 'Extra' (39N 153E), located off the coast of Japan (Roll, 1965). These oscillations were related to meandering ocean currents. Gill(1974) has computed a surface temperature spectrum for Ocean Weather Station E (35N 48W) which shows a peak at a period of approximately one-fifth of a year (70 days) believed to be related to mid-ocean eddies. The lack of any equivalent spectral features at 'Papa' is perhaps due to the great distance separating Station 'Papa' from any intense ocean currents.

Both Koizumi and Dorman have studied the diurnal variation of sea temperature. Koizumi finds an average annual range of 0.28 C° while Dorman determined a range of 0.13 C° very close to the range found at 'Papa'. Koizumi and Dorman both find a change in the diurnal variation with season. In both cases, the diurnal variation is largest in summer and smallest in winter. However, at 'Papa' the relative change is larger, reflecting its more northerly position with more pronounced seasons. Denman(1972) has developed a model of the upper layer of the ocean which was tested for the months of May and June at Station 'Papa'. His model, using a constant wind speed of 8 m/sec, predicts a diurnal sea temperature range of 0.18 C°. This result is very close to the spring value found in this analysis of 0.19

C⁰.

4.5 Air Temperature

The air temperature spectrum (see Figure 10), like the sea temperature spectrum, is dominated by the annual and semi-annual variations. The annual peak has an energy of 8.29 $(C^0)^2$ while the semi-annual peak has an energy of 0.79 $(C^0)^2$, which together account for 84% of the total energy. The corresponding average air temperature ranges are 8.3 C^0 for the annual period and 2.6 C^0 for the semi-annual period (as compared to the mean air temperature of 8.2 ^0C).

At periods between the semi-annual and diurnal, the air and sea temperature spectra differ considerably. The sea temperature spectrum decreases uniformly from the semi-annual peak while the air temperature spectrum reveals a very broad, uneven peak between periods of 2 days and 60 days with spectral levels that are an order of magnitude larger than the corresponding sea temperature spectrum. This broad region of increased activity seems to be associated with the passage of different air masses. At the shortest periods, the spectrum increases. This result indicates that there are air temperature variations of periods less than one-quarter day which are aliased back to longer periods.

The seasonal spectra (see Figure 11) reveal a striking difference between the high spectral levels of fall and winter in contrast to the low spectral levels of spring and summer. In addition, it appears that a 'gap' may exist in the fall and winter spectra at periods of about 12 days separating the spectra into a synoptic peak centered at about 6 days and a longer

Figure 10: The power spectrum of air temperature computed from five two-yearly data blocks covering the period, 1958 to 1967. The vertical error bars represent approximate 95% confidence intervals of the mean.

AIR TEMPERATURE
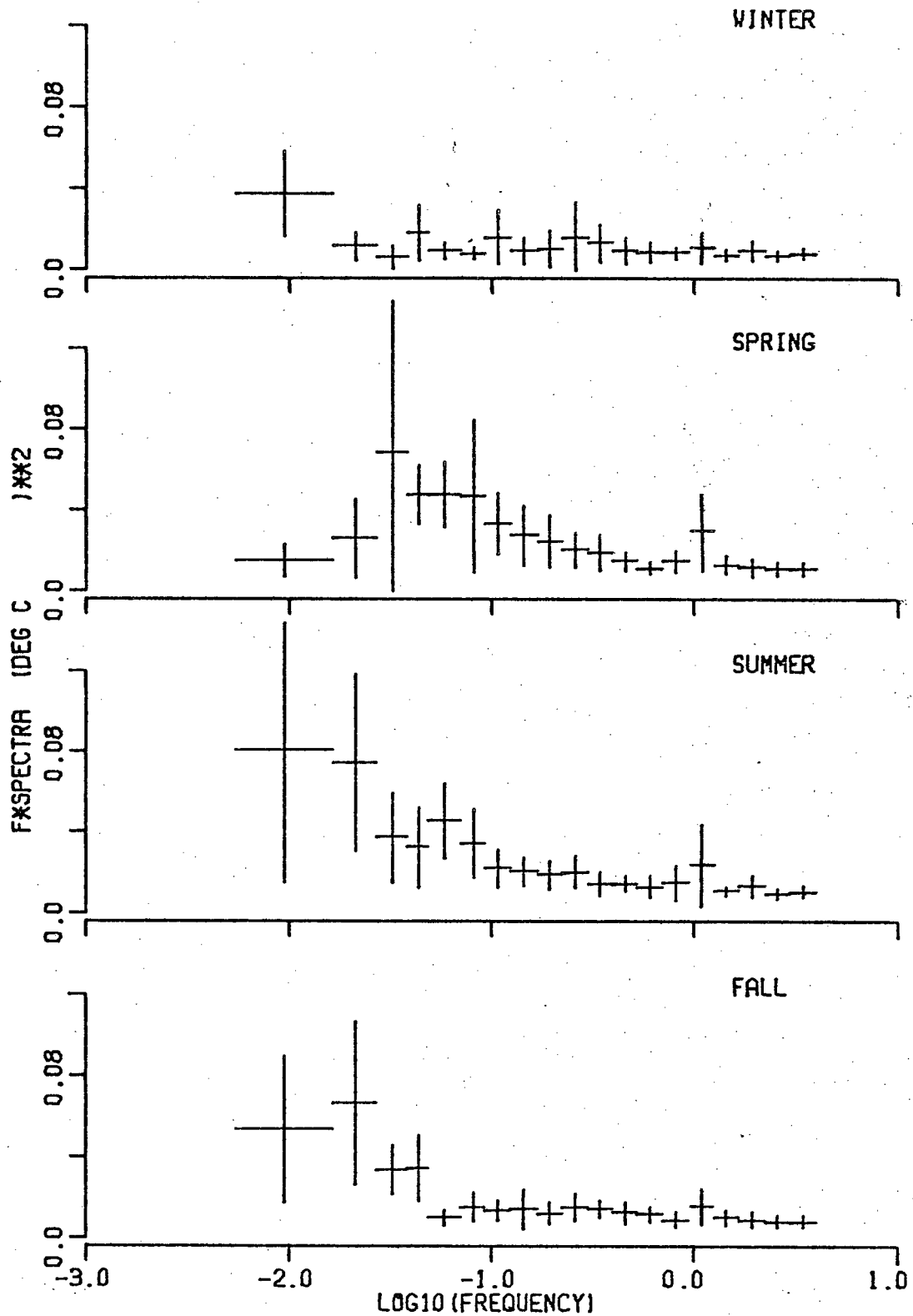

Figure 11: The seasonal power spectra of air temperature; each spectrum is averaged over the ten years, 1958 to 1967. The vertical error bars represent approximate 95% confidence intervals of the mean.

period peak centered at about 23 days.

Both the two-year and seasonal spectra show a pronounced diurnal peak. An examination of the single harmonic spectral values (see Table III) reveal a significant but much smaller semi-diurnal peak as well. The diurnal peak energy is 0.045 $(C^o)^2$ corresponding to an average daily temperature range of 0.64 C^o. The semi-diurnal peak energy is only 0.0047 $(C^o)^2$ corresponding to an average range of 0.20 C^o. As might be expected, the largest diurnal variations are found in spring and summer when the solar insolation is the greatest.

The annual and diurnal variations of air temperature over the sea are well known and have been studied by a number of investigators. Roll(1965) provides a useful summary of these results. The diurnal and annual air temperature ranges found at Station 'Papa' are in good agreement with the findings of others at similar latitudes.

Studies of periodicities of the air temperature at periods between one day and one year are much less common. Powalchuk and Panofsky(1968) have computed the spectra at a number of stations in North America in winter. They find a peak occuring at each station with periods of the peak ranging from 4 days to 20 days. The peaks with longest periods are for stations on the western side of North America in maritime climates. Byshev and Ivanov(1969) have computed the air temperature spectrum over the ocean. At stations of approximately the same latitude as Station 'Papa', their spectral results show a broad peak centered at about 11 days. Dorman(1974) for Station N (30N 140W) further to the south, found a peak in winter at periods of 6 to

11 days. The behavior of the air temperature spectra at Station 'Papa' is generally consistent with these results over synoptic periods, but additional energy is found at longer periods (15-60 days).

4.6 Absolute Humidity

The absolute humidity spectrum (see Figure 12) reveals the largest variations at the annual and semi-annual periods. The annual variation amounts to an energy of 2.28 $(gm/m^3)^2$ corresponding to an average annual range of 4.4 gm/m^3. The semi-annual variation has an energy of 0.36 $(gm/m^3)^2$ corresponding to a range of 1.7 gm/m^3 (the mean absolute humidity is 7.35 gm/m^3). The absolute humidity spectrum features a broad well defined synoptic peak at 5.5 days with half power points at 1.5 days and 48 days. The increase in spectral values at the shortest periods is an indication of shorter period variations being aliased back to longer periods.

Figure 13 reveals important seasonal variations in the absolute humidity spectrum. The spectral levels are largest in fall and lowest in spring. In each of the seasons a synoptic peak is found, with the peak value at periods ranging from 3.8 days (fall) to 6.8 days (summer). The longer period activity appears to be more variable. In winter, and to a lesser extent, in spring and fall, a peak is found at periods of 17 to 23 days. In summer, the longer period activity is greatly reduced.

An examination of the single harmonics (see Table III) shows a sharp peak at a period of one day and a weak peak at a period of half a day. The diurnal peak has an energy of 0.0014 $(gm/m^3)^2$ corresponding to an average daily range of 0.11 gm/m^3
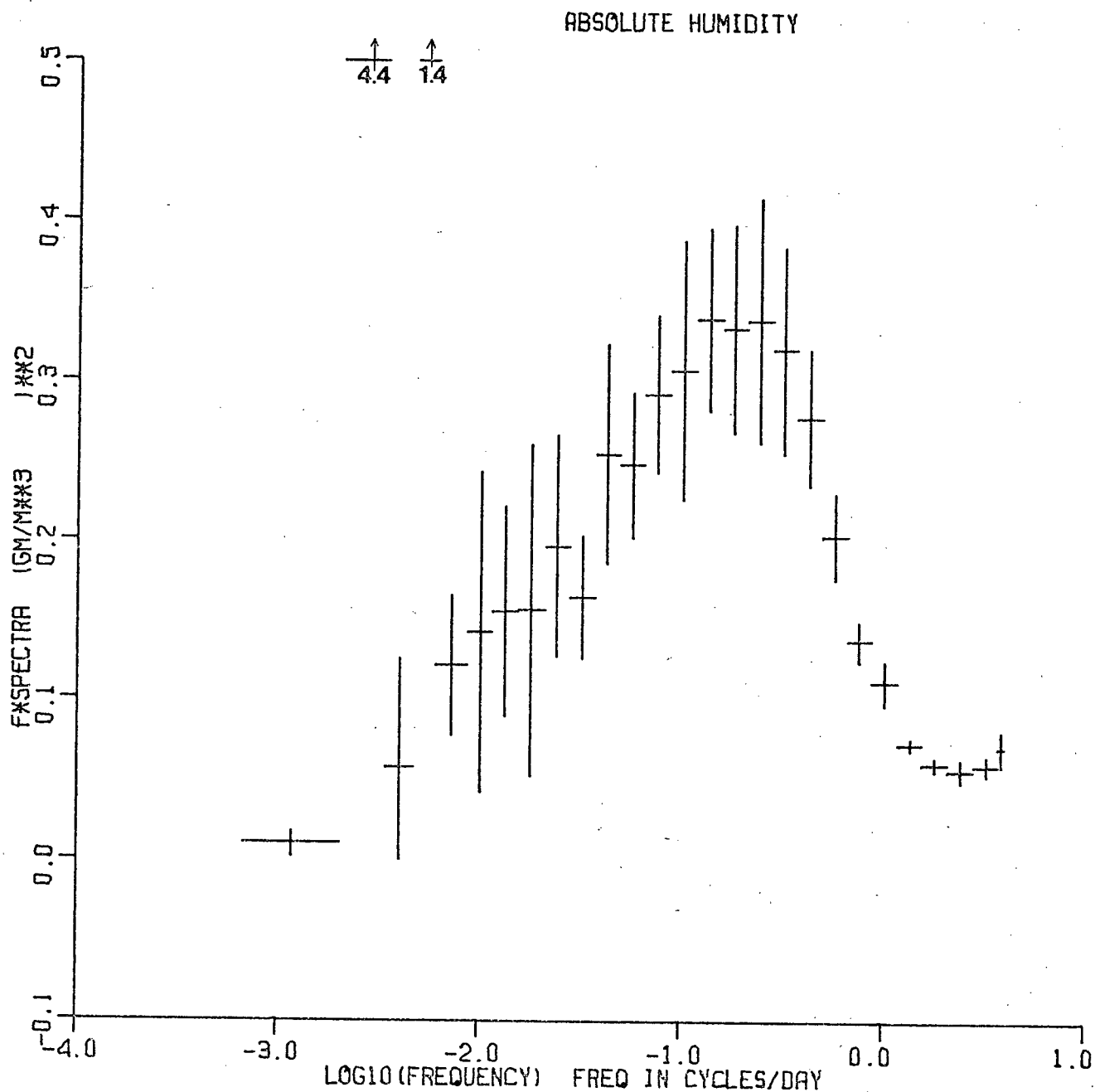
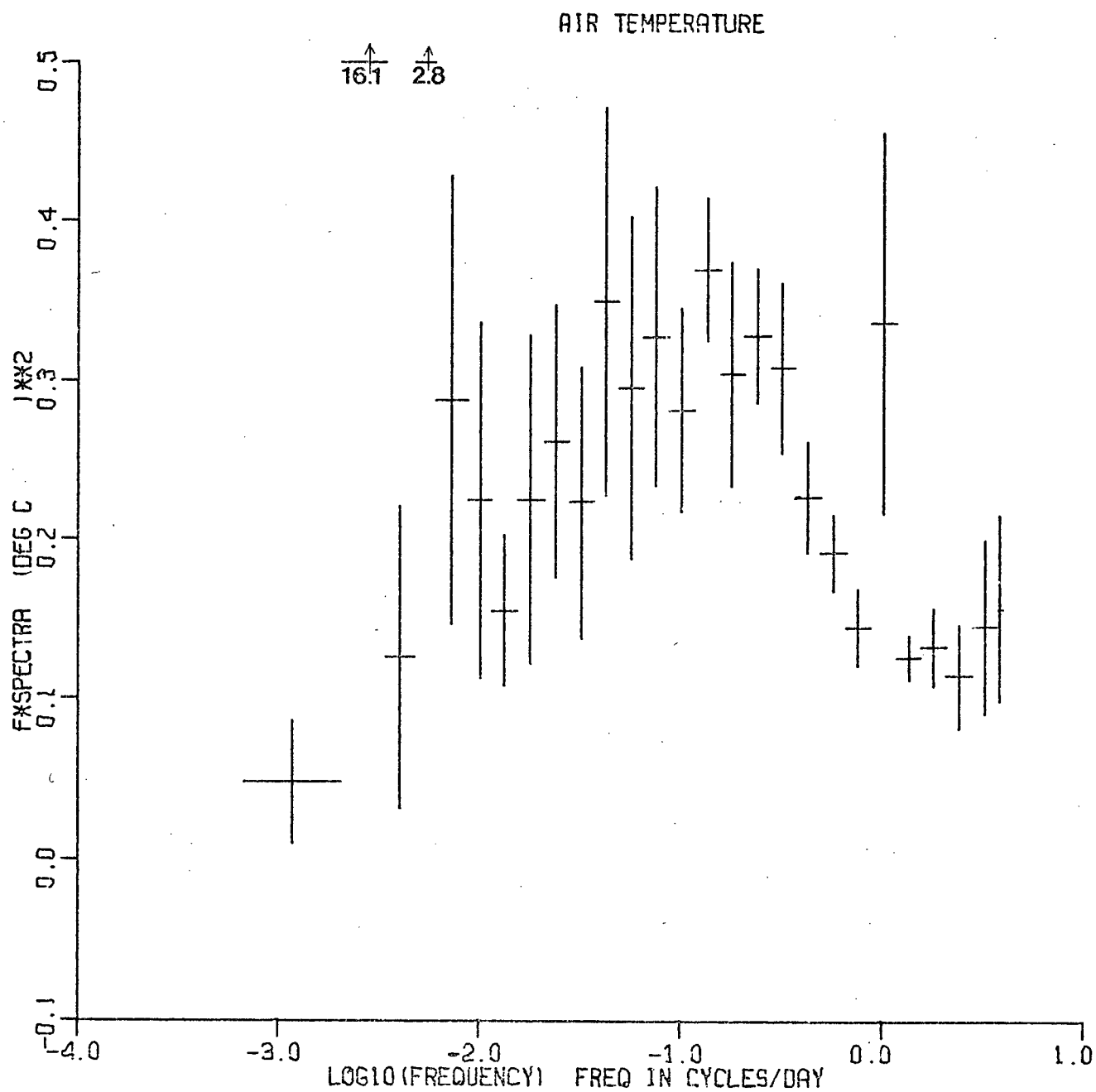Figure 12: The power spectrum of absolute humidity computed from five two-yearly data blocks covering the period, 1958 to 1967. The vertical error bars represent approximate 95% confidence

ABSOLUTE HUMIDITY

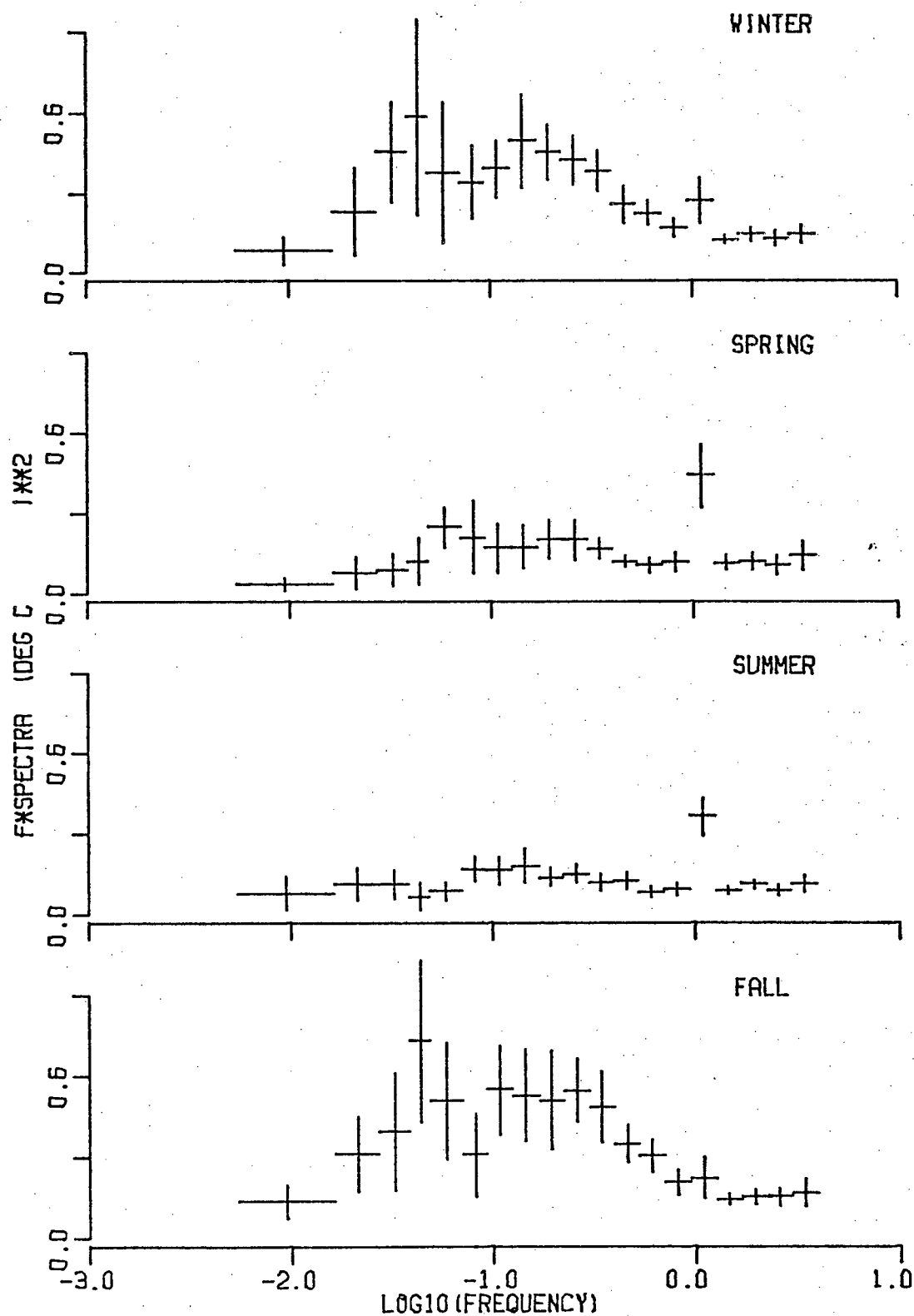Figure 13: The seasonal power spectra of absolute humidity; each spectrum is averaged over the ten years, 1958 to 1967. The vertical error bars represent 95% confidence intervals of the mean.

while the semi-diurnal peak has an energy of 0.0001 $(gm/m^3)^2$ corresponding to a range of 0.03 gm/m^3. As might be expected, the diurnal variation is largest in spring and summer when the increased solar radiation evaporates more water at the sea surface. The single harmonic spectral values show no peak at the semi-diurnal period because of the reduced frequency resolution. The semi-diurnal peak, which was only marginally defined with the resolution of a two-year time series, is lost in the background with time series of 91 days length.

It is interesting to compare the spectra of the air temperature and absolute humidity. While both spectra are dominated by the annual peak, they show considerable differences at shorter periods. The absolute humidity spectrum shows a well defined peak at 5.5 days while the air temperature spectrum shows no single peak but somewhat increased levels between 2 days and 60 days. The relative contribution from these periods to the total variance is much larger for humidity than temperature. Such differences in the spectra, suggest that considerable differences exist in the moisture and temperature fields and their interactions with the ocean, on synoptic and seasonal scales.

Spectra of humidity are very rare indeed. Dorman (1974) has presented a spectrum of dew point temperature for Ocean Station N (140W 30N). Because dew point temperature is a deterministic and approximately linear function of absolute humidity (over the rather narrow range of temperature and humidities encountered), the relative energy found at various frequencies can be meaningfully compared. Dorman's results reveal the same features found

at 'Papa'. He finds a large annual variation and a much smaller diurnal variation. In addition, he finds a synoptic peak at about 5.8 days for each of the seasons.

4.7 Turbulent Fluxes

The spectra of quantities which are representative of the turbulent fluxes of momentum, sensible heat flux and latent heat flux are computed. Figure 14 is a plot of the rotary spectrum of the vector time series (UU_x, UU_y), proportional through the bulk aerodynamic parameterization (equation 1) to the wind stress (also called the momentum flux). The rotary wind stress spectrum is similar to the rotary wind spectrum with both clockwise and anti-clockwise rotations having a synoptic peak at 3 days. The clockwise rotations dominate the wind stress rotary spectrum to a greater extent than the wind rotary spectrum.

The seasonal wind stress spectra (see Figure 15) show very marked differences. The spectral levels in fall are four to five times greater than in summer as a result of the increased storm activity. These levels decrease from fall through winter and spring to the lowest levels in summer. The spectra also reveal that a greater proportion of the fall and winter spectral energy is found at shorter periods than is the case for spring and summer. The relative contributions from the clockwise and anti-clockwise spectra to the total rotary spectrum over all periods remains remarkably constant for all seasons. However, changes are found between the clockwise and anti-clockwise contributions at individual frequency bands. The most noticeable of these changes is found in summer when the clockwise spectrum has a broad peak over periods from 1.5 to 9 days while the anti-

ROTARY WIND STRESS

CLOCKWISE   ANTI-CLOCKWISE
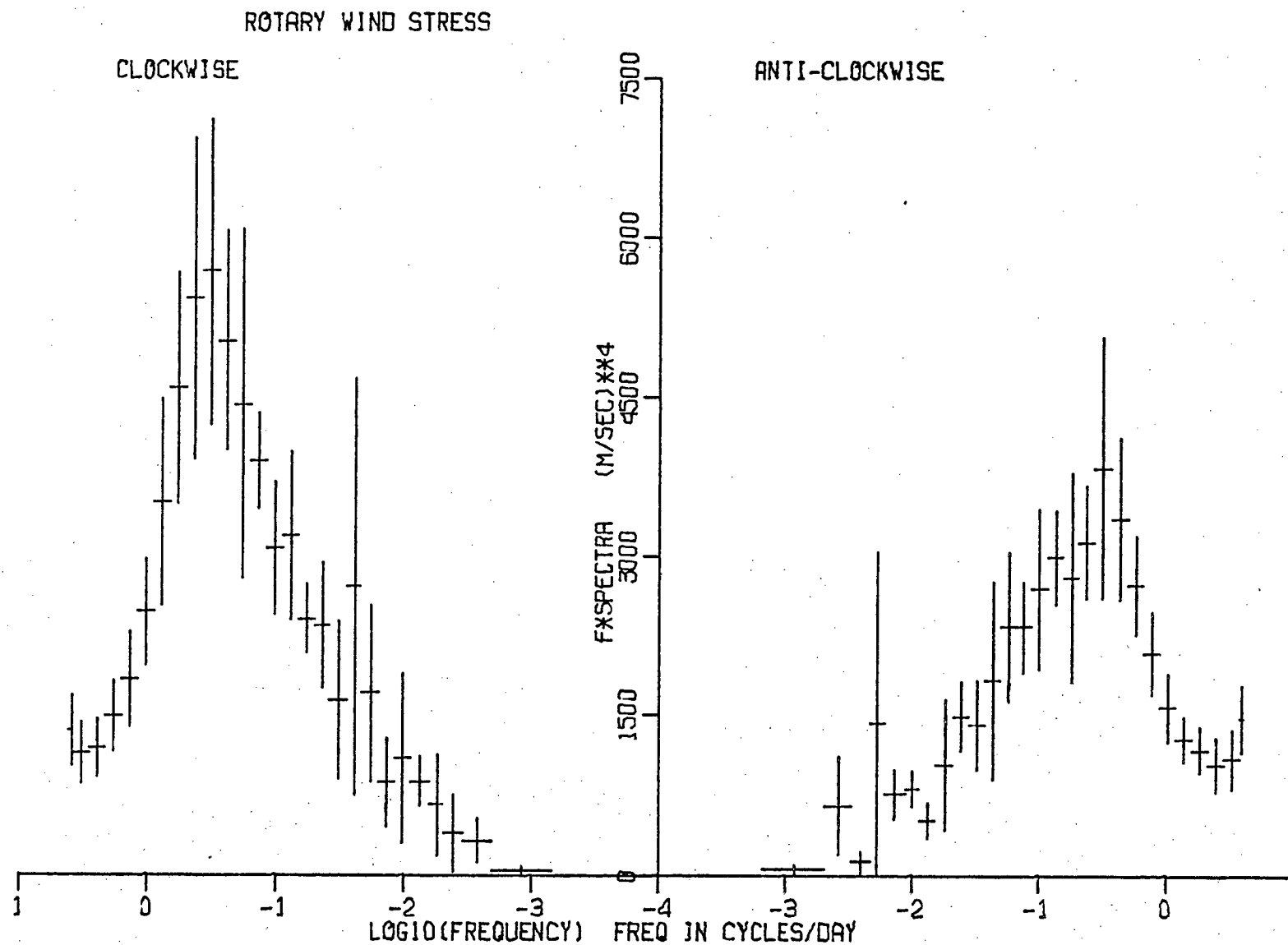
Figure 14: The rotary auto-spectrum of $|\vec{U}|\vec{U}$, a quantity which is proportional to the wind stress, computed frcm five two-yearly blocks covering the period 1958 to 1967. The vertical error bars represent 95 % confidence intervals of the mean.

ROTARY WIND STRESS

CLOCKWISE   ANTI-CLOCKWISE

LOG10(FREQUENCY)   FREQ IN CYCLES/DAY
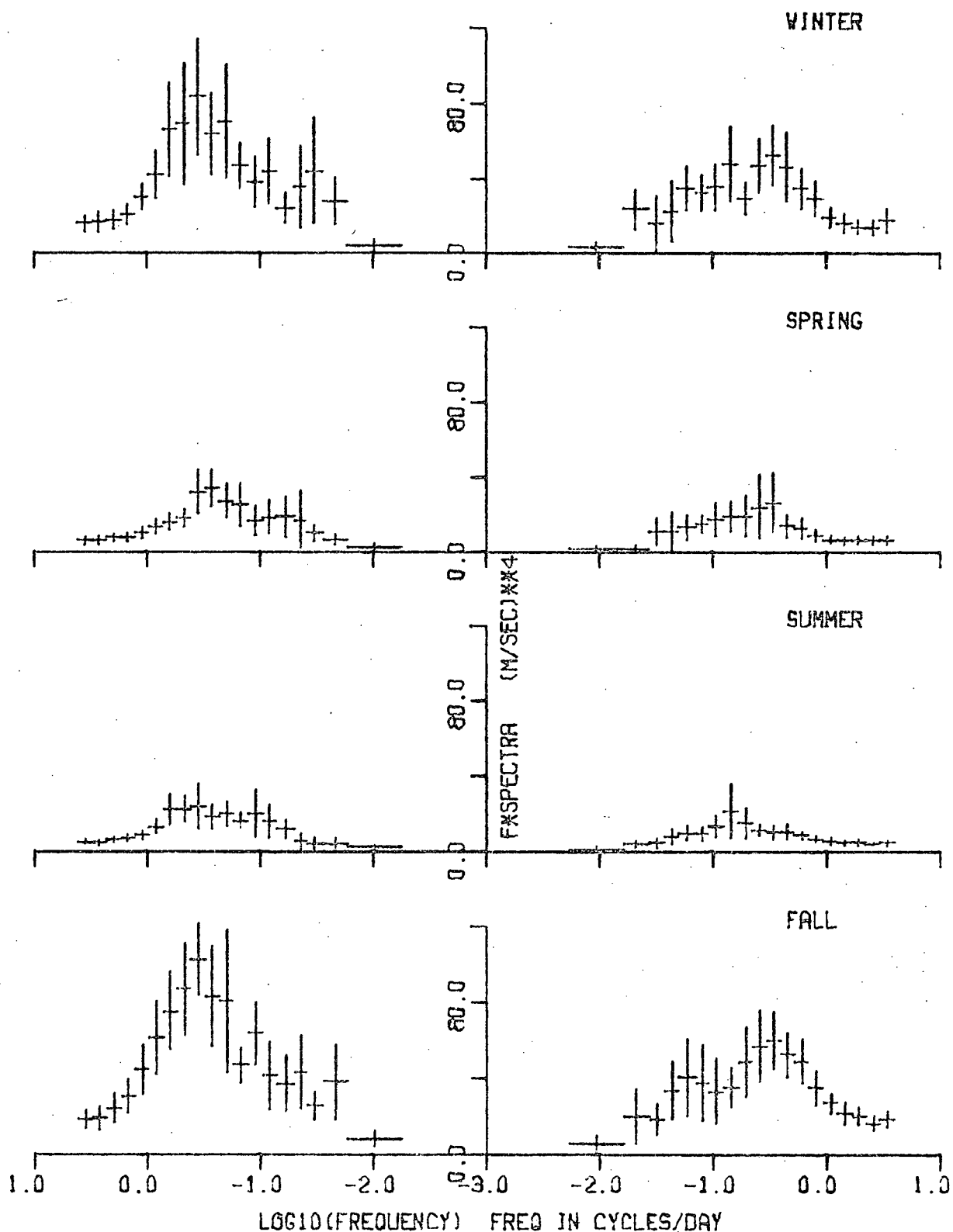
Figure 15:   The seasonal rotary auto-spectra of |Ū|Ū, a quantity
which is proportional to the wind   stress,   computed   from   five
two-yearly blocks covering   the   period,   1958   tc   1967.   The
vertical   error   bars   represent   approximate   95%   confidence
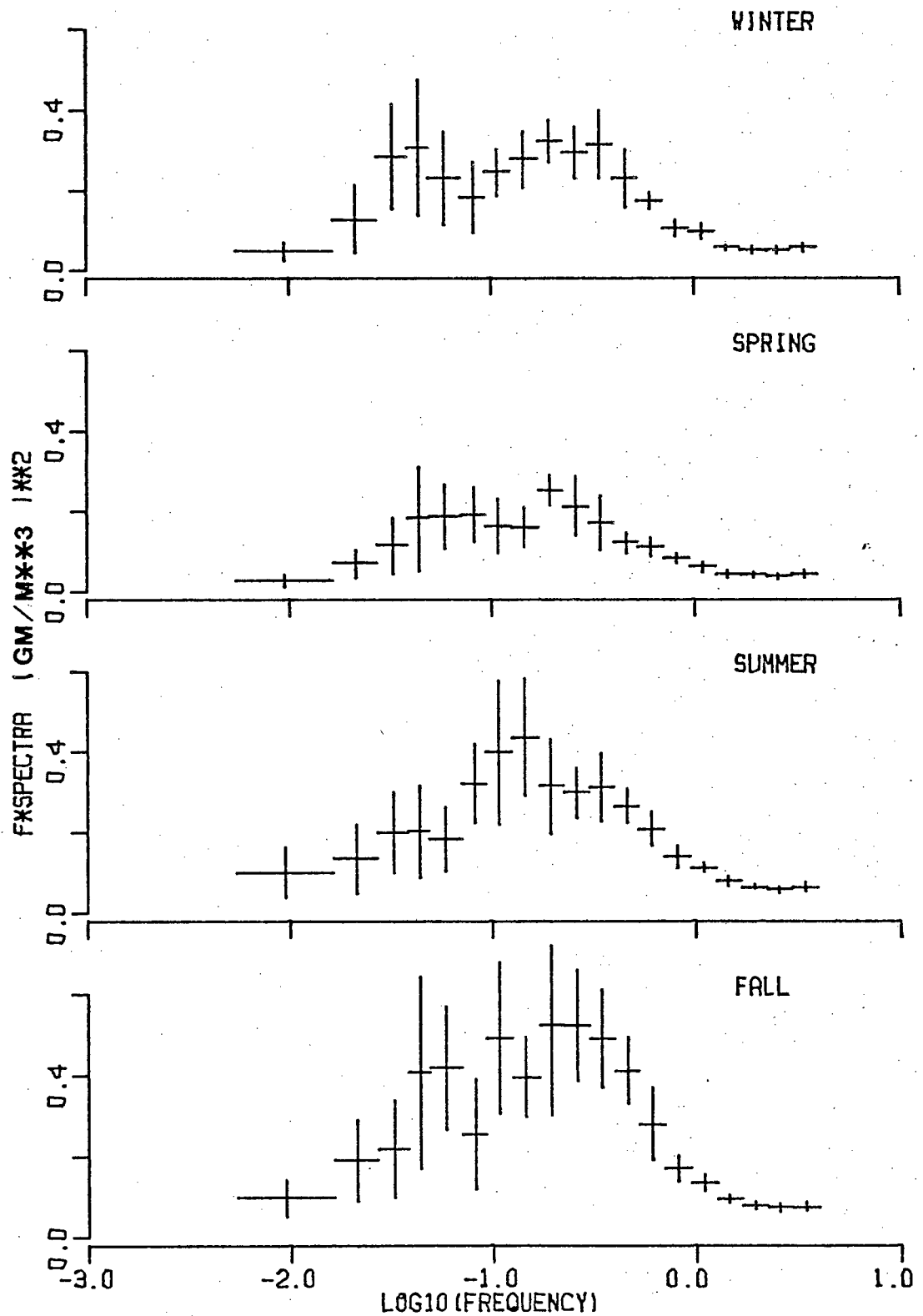intervals of the mean.

clockwise spectrum has a rather sharp peak at 6.8 days. This deviation from the dominant fall and winter spectra could be the result of a change in the pattern of the passage cf synoptic disturbances over the N. E. Pacific between summer and winter. Further study is required to test this hypothesis.

An examination of the single harmonic spectral values (see Table IV) reveals a very sharp semi-diurnal peak in the clockwise spectrum. This peak has an energy of 10.8 (m/sec)^4 which amounts to an average range of 9.5 (m/sec)^2. No peaks are found at periods of one day, one-third of a day, one-quarter of a day, or the inertial period. The anti-clockwise spectral values show no peaks other than a very small one at one-half day.

Two-yearly spectra of quantities that are representative of turbulent heat transports are displayed in Figure 16. Figure 16 contains three plots: a plot of the spectrum of $U\Delta T$ which by equation (2) is proportional to the sensible heat flux, a plot of the spectrum of $U\Delta q$ which by equation (3) is proportional to the latent heat flux and a plot of the spectrum of $1.2U\Delta T + 2.44U\Delta q$ which is proportional to the total turbulent heat transport (taking $\rho = 1.2 \times 10^{-3}$ gm/cm^3, L=2440 joules/gm, C_p=1.00 joules/gm-^{0}C and $C_T=C_q$ in equations (2) and (3)). Each plot in Figure 16 is scaled in such a way that equal displacements from the horizontal axis represent equal contributions to the variance of the total heat flux. Each spectrum has the same general features: relatively small but significant annual and semi-annual peaks and a broad synoptic peak that contains most of the energy. The synoptic peak has its highest levels at periods of 7 and 4 days for each of the quantities.

TABLE IV

The energy of single harmonic spectral peaks of quantities which are representative of the wind stress (U•Ū), the sensible heat flux, the latent heat flux and the total turbulent heat flux found at periods of one day, one-half day and one-quarter day.

Quantity (units)	Period	Energy				
		Annual	Winter	Spring	Summer	Fall
Clock-wise UŪ (m/sec)^4	1.0	–	–	–	–	–
	0.5	10.83	4.07	8.58	7.42	14.64
	S.D.	±8.27	13.18	10.19	10.80	30.26
Anti-clock-wise UŪ (m/sec)^4	1.0	–	–	–	–	–
	0.5	0.558	–	–	–	–
	S.D.	±0.911				
Sensible Heat (cal/cm^2/day)^2	1.0	34.4	30.0	45.5	35.7	29.2
	S.D.	±18.5	±27.7	±19.7	±20.1	±36.0
	0.5	5.15	6.11	1.88	5.90	8.76
	S.D.	±1.09	±3.11	±2.54	±3.97	±8.79
Latent Heat (cal/cm^2/day)^2	1.0	–	–	–	–	–
	0.5	1.78	2.84	–	4.34	4.05
	S.D.	±2.10	±7.279	–	±5.16	±24.6
	0.25	0.201	–	–	–	2.18
	S.D.	±0.197	–	–	–	±7.22
Total Heat (cal/cm^2/day)^2	1.0	42.4	50.9	62.1	23.4	–
	S.D.	±14.2	±54.1	±48.4	±39.1	–
	0.5	5.63	8.10	1.36	11.4	9.45
	S.D.	±4.27	±15.5	±4.01	±12.8	±25.5
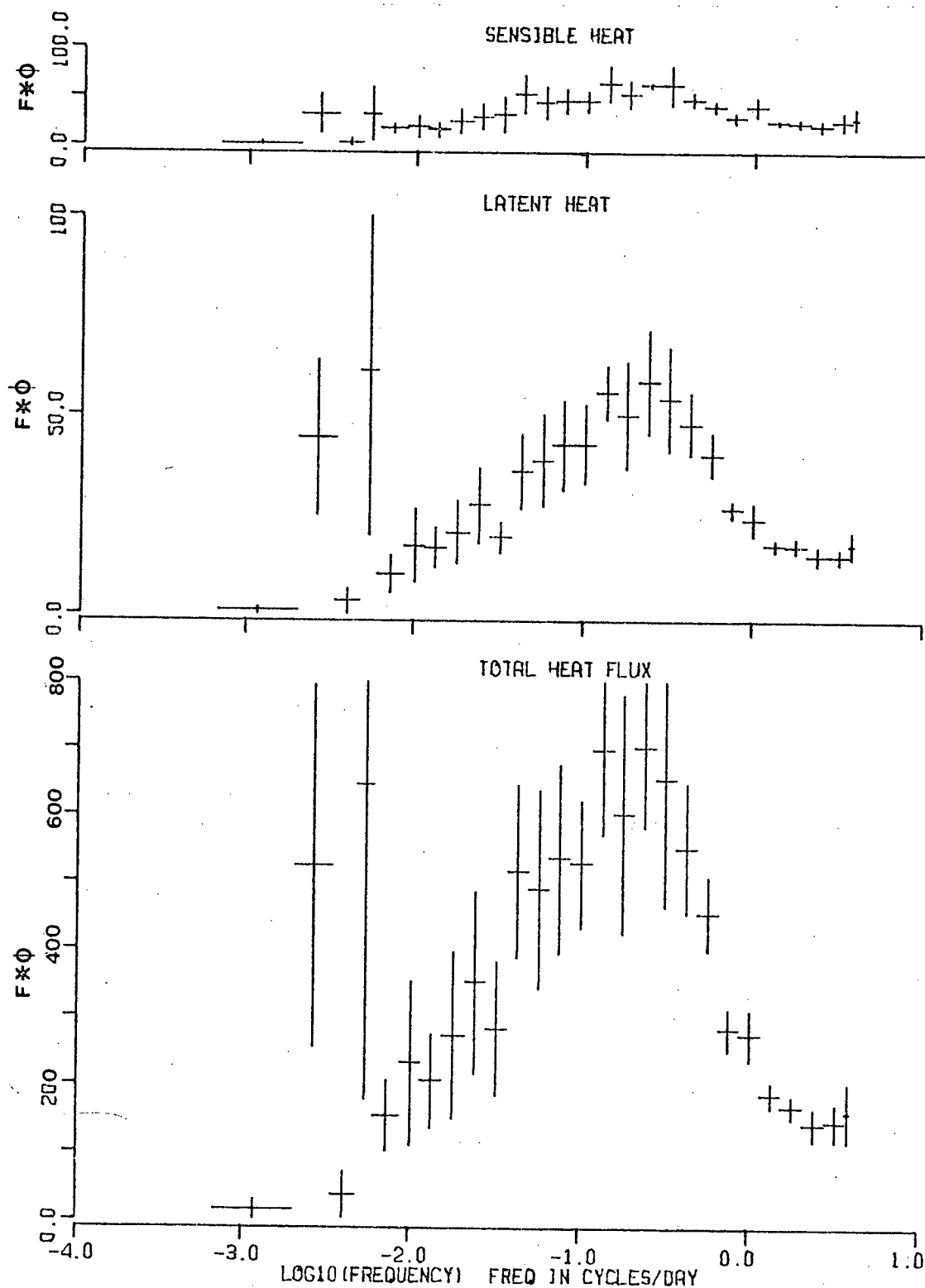
Figure 16: The power spectra of $U\Delta T$ (in $(°C-m/sec)^2$, proportional to the sensible heat flux), $U\Delta q$ (in $(gm/m^2-sec)^2$, proportional to the latent heat flux) and $1.2U\Delta T + 2.44U\Delta q$ (proportional to the total turbulent heat flux), computed from five two-yearly blocks covering the period, 1958 to 1967. The vertical error bars represent approximate 95% confidence intervals of the mean.

It is clear from Figure 16 that the auto-spectral values of the total heat flux represent considerabley more heat transfer variations than the the sum of the sensible and latent heat flux auto-spectral values at all periods greater than one day. This is a result of the high correlation between $U \cdot \Delta T$ and $U \cdot \Delta q$ variations. Over periods from two days to two years, the correlation between $U \cdot \Delta T$ and $U \cdot \Delta q$ is 0.7 or greater.

On the plots in Figure 16, the semi-annual peaks are larger than the annual peaks because in the log f plots the bandwidth is narrower at the semi-annual period. However, the contribution to the variance from the semi-annual period is less than that from the annual period.

The annual variation of the latent heat flux, as computed from the spectral values of $U \Delta q$ using $C_q = 1.5 \times 10^{-3}$, has an average range of 103 cal/cm²-day while the semi-annual energy peak corresponds to a range of 86.4 cal/cm²-day indicating large annual and semi-annual variations about the average of 88.9 cal/cm²-day. These values are considerably larger that the corresponding values for the sensible heat flux (annual range of 46 cal/cm²-day and a semi-annual range of 32 cal/cm²-day). The average sensible heat transfer was 11.7 cal/cm²-day. The total turbulent heat transfer has an annual range of 147 cal/cm²-day and a semi-annual range of 105 cal/cm²-day about a mean of 100 cal/cm²-day. That the semi-annual variations are a large fraction of the annual variations is a reflection of the presence of a secondary maximum in these heat fluxes in March in addition to the maximum heat transport which occurs in the fall.

An inspection of the single harmonic values (see Table IV)

shows a very sharp diurnal peak in the $U\Delta T$ spectrum. This peak has an energy of 2.27 $(C^\circ\text{-m/sec})^2$ corresponding to an average daily range of the sensible heat flux of 16.9 $\text{cal/cm}^2\text{-day}$. A smaller semi-diurnal peak is found as well. The seasonal variation of the diurnal peak is rather small with the largest diurnal variation occuring in spring (a sensible heat range of 19.5 $\text{cal/cm}^2\text{-day}$) and the smallest diurnal variation in fall (a range of 15.6 $\text{cal/cm}^2\text{-day}$). The $U\Delta q$ spectrum shows no diurnal peak and only a very small semi-diurnal peak. Thus, there exists no daily cycle in latent heat transport similar to that of sensible heat transport. The spectrum of the total heat flux shows a prominent diurnal peak and a smaller semi-diurnal peak. The average diurnal range is 18.9 $\text{cal/cm}^2\text{-day}$, very nearly equal to that of the sensible heat flux, which suggests the variation is largely due to the daily sensible heat cycle.

Large changes in the spectra of turbulent heat fluxes (see Figures 17, 18, and 19) are found with the seasons. The sensible heat flux spectra show the largest differences in spectral levels with the summer spectral values being an order of magnitude less than those of fall and winter. The relative contributions from various frequencies show less pronounced changes. In all spectra, a peak is found at periods of 3 to 4 days. A longer period peak of marginal significance at about 23 days is prominent in fall and is present in all the seasonal spectra except that of summer.

The seasonal spectra of the latent heat flux also show marked changes with the seasons but not to the same extent as the sensible heat flux. Unlike the case of sensible heat flux,
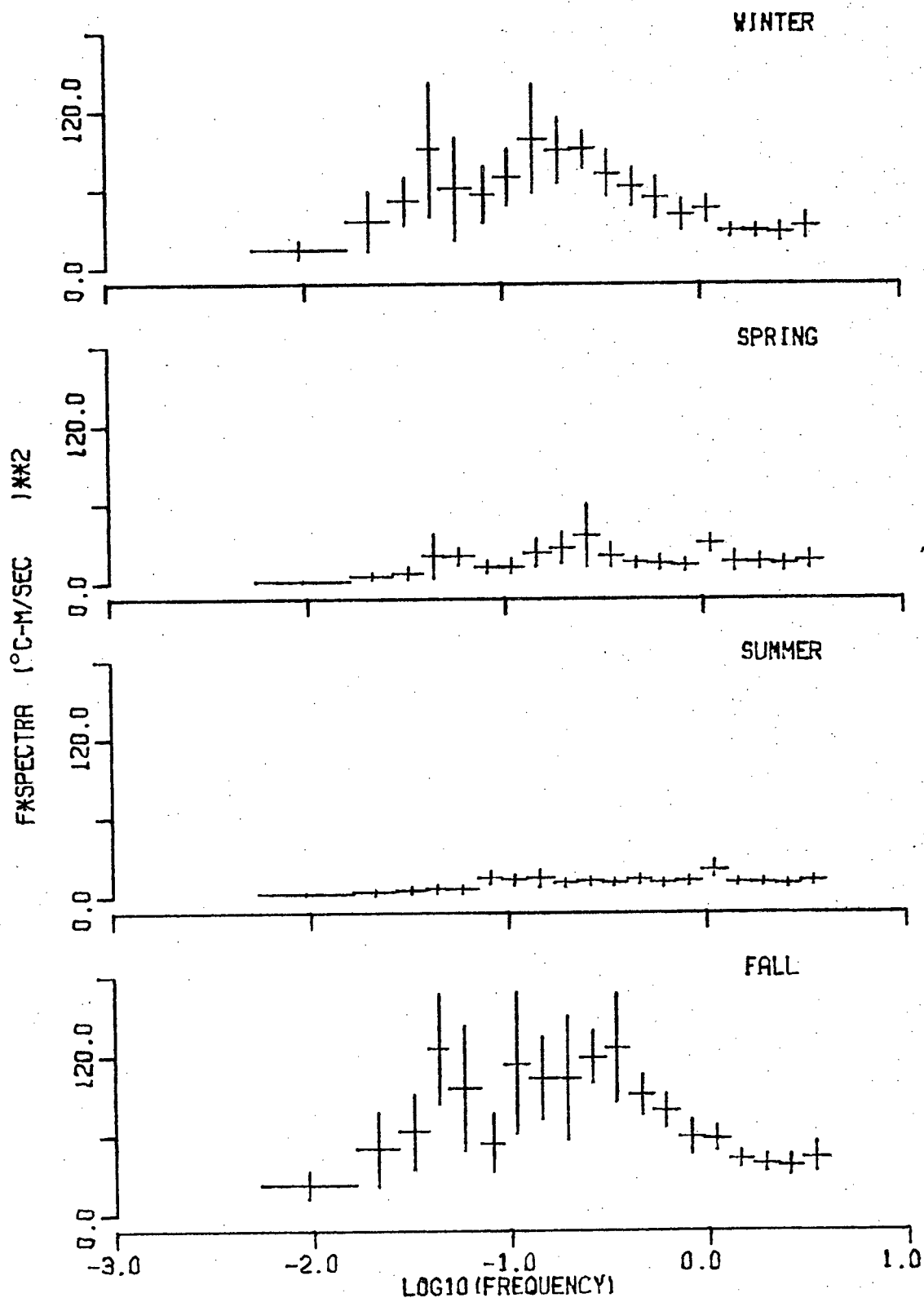
Figure 17: The seasonal power spectra of UΔT (proportional to the sensible heat flux). Each spectrum is averaged over the ten years, 1958 to 1967. The vertical error bars represent approximate 95% confidence intervals of the mean.
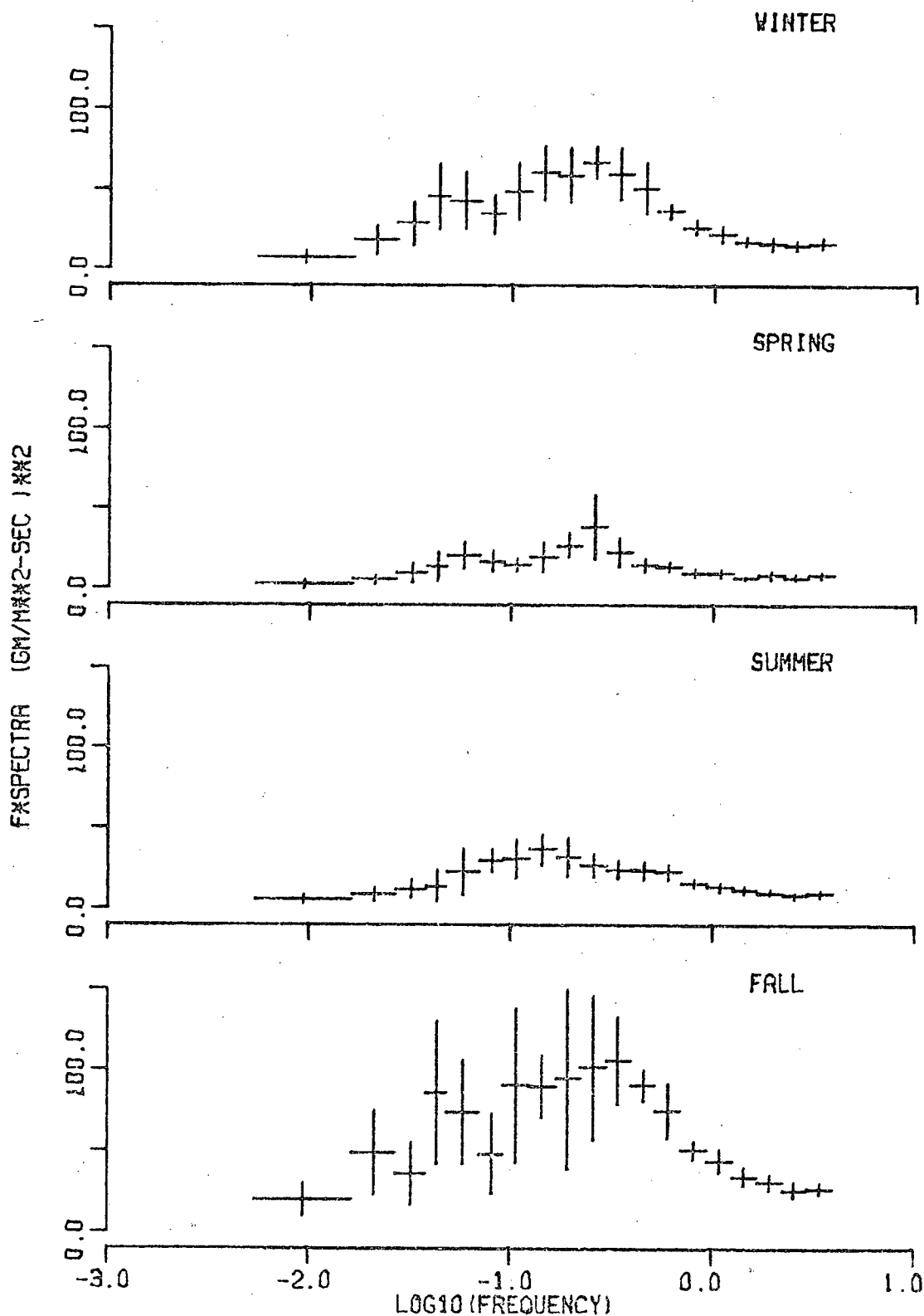
Figure 18: The seasonal power spectra of U∆q (proportional to the latent heat flux). Each spectrum is averaged over the ten years, 1958 to 1967. The vertical error bars represent approximate 95% confidence intervals of the mean.
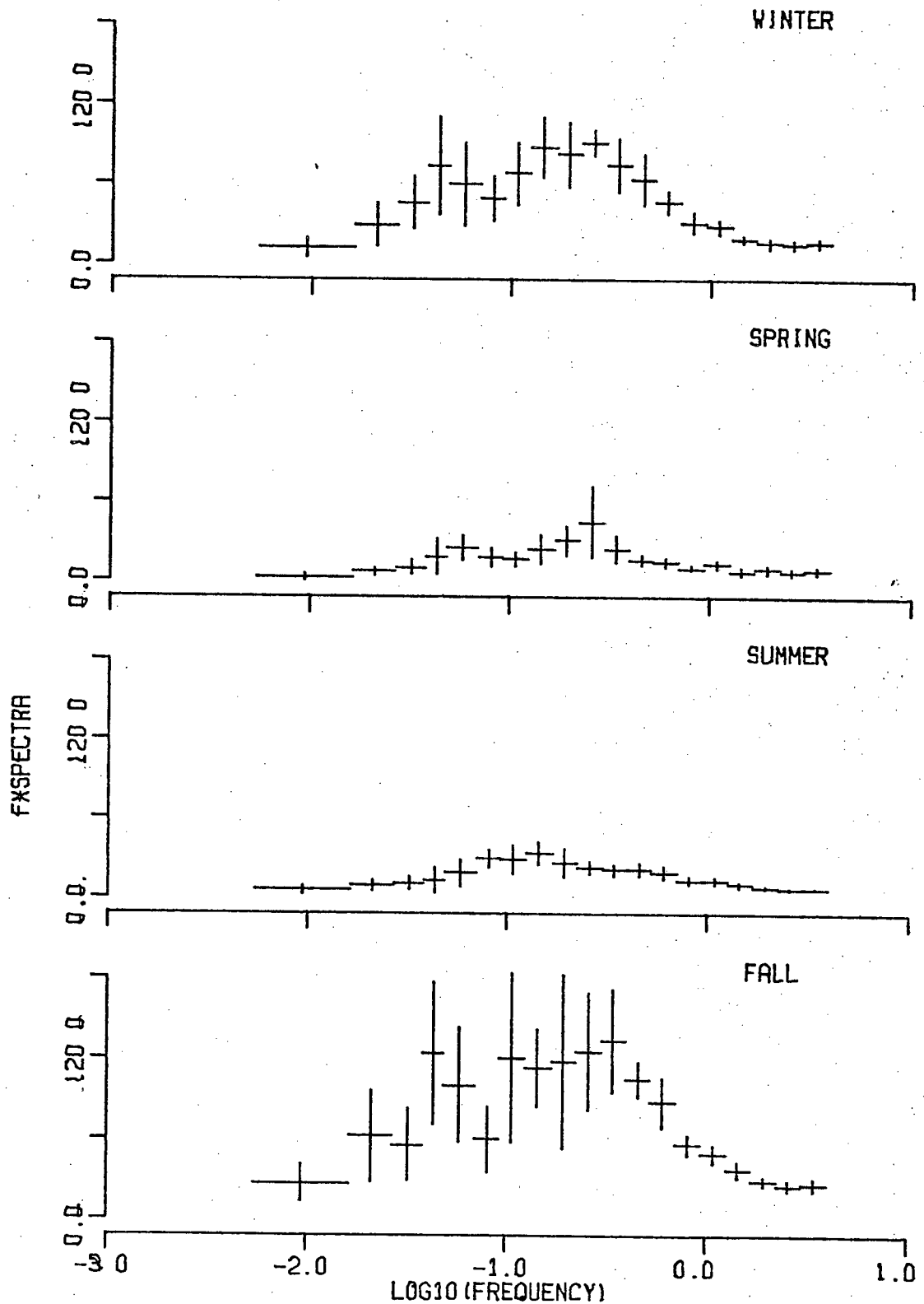
Figure 19: The seasonal spectra of $1.2U\Delta T + 2.44U\Delta q$ (proportional to the total turbulent heat flux). Each spectrum is averaged over the ten years, 1958 to 1967. The vertical error bars represent approximate 95% confidence intervals of the mean.

the summer spectrum of latent heat is much the same as the spring spectrum. Both these seasons have spectral levels about one-third of those of fall and winter. The period of the synoptic peak shifts with the seasons, being shortest in fall (2.9 days), at an intermediate value in winter and spring (3.8 days) and longest in summer (6.8 days). A longer period peak is found in fall and winter at about 23 days. The seasonal spectra of the total turbulent heat flux is very similar in character to that of latent heat flux since over the periods resolved, the total heat flux is dominated by the contributions of the latent heat flux.

Chapter 5

CROSS-SPECTRAL RESULTS

5.1 Introduction

Cross-spectral analysis provides information on the relatedness of pairs of quantities over the periods resolved. Because the number of basic measured quantities plus the number of quantities which may be derived from these (wind stress, sensible heat flux, latent heat flux, total turbulent heat flux) is relatively large, there are many possible pairs of quantities that could be subjected to cross-spectral analysis. Due to time and space limitations, it is not possible to present an analysis of each of these pairs. In this study, cross-spectral analysis is used to examine the relationship of each of the basic surface scalar quantities (air pressure, air temperature, absolute humidity and sea temperature) with those factors which are capable of modifying the surface scalar quantities. Such factors (which are available from the data) are the wind and the parameterized turbulent heat fluxes. In addition, the relationships between some of the pairs of scalar quantities are also examined.

The cross-spectral results are displayed by means of four graphs for each pair of quantities studied. These are plots of phase, coherence, the transfer spectrum of the first quantity and the transfer spectrum of the second quantity (see Chapter 3 for the definitions of these cross-spectral values). On the coherence plot, the dashed line represents those coherence values below which there is a 95% probability that a randomly coherent signal will fall. The computed coherence estimates

which lie above this line are described as 'good' and 'very good' while those below the dashed line are described as 'fair' and 'poor' (as described in Chapter 3). It should be noted that for the shorter periods, the number of degrees of freedom are so large that it is possible to find statistical significance in coherence estimates that are small (say less than 0.3). Such small coherence estimates, though statistically significant are of little value in attempting to predict the behavior of one quantity from that of another quantity. The transfer spectral values, (fraction of spectral energy of one quantity that is coherent with the other quantity) shown as dashed lines, are plotted beneath the auto-spectral values for the same quantity.

5.2 Air Pressure

A study of the cross-spectra between wind and air pressure provides some insight into the dynamics of the surface atmospheric layer over the ocean. The rotary cross-spectra between vector wind and air pressure as well as the cross-spectrum between wind speed and air pressure are computed (see Figure 20).

A discussion of the coherence relationship between wind and air pressure can be conveniently divided into three parts according to the scale ranges resolved: the climatic/seasonal scales, the longer synoptic scales and the shorter synoptic scales. The mesoscale is unimportant since pressure fluctuations at these periods are very small. Over climatic/seasonal scales, the coherence spectra show generally poor levels of coherence. One exception to this statement is found at the annual cycle in the wind speed-pressure coherence spectrum where the coherence of 0.91 is very good. The two quantities, as one would expect are

Figure 20: Graphs of phase, coherence and the transfer spectra between the wind and air pressure. The cross-spectral quantities are displayed for both the vector wind (as rotary spectra) and the wind speed.

very nearly 180 degrees out of phase. Due to the effect of wind direction changes, the annual cycle found in the wind rotary auto-spectra is greatly reduced and as a result, there is a smaller annual peak in the rotary coherence spectra.

The most significant levels of wind-pressure coherence are found at the shorter synoptic scales (periods ranging from one to ten days). Over this range of periods, a prominent peak of statistically very good coherence appears in the clockwise co-herence spectrum (peak level of 0.70) and anti-clockwise co-herence spectrum (peak level of 0.57) as well as the wind speed-pressure coherence spectrum (peak level of 0.47). The higher coherences found for the clockwise and anti-clockwise rotating wind in comparison with those of the wind speed, emphasize the importance of cyclonic and anti-cyclonic pressure systems in determining the wind field over the shorter synoptic scales. A passing cyclone or anti-cyclone should be characterized by a rotation of the wind vector in association with the pressure change. The wind speed would also be expected to change with the pressure, but with a more complicated response.

A simple model can be used to illustrate this point. Con-sider the passage of an eastward-moving low pressure cyclonic system with its center slightly to the north of the observation station. The air pressure will go through one-half a cycle during the passage of the system (from intermediate to low to intermediate values). Neglecting the effect of frontal discon-tinuities and other complications of pressure system airflows, the wind vector will rotate from pointing very nearly due north to pointing very nearly due south in a clockwise sense. Thus,

the half-cycle change in air pressure is clearly coherent with the 180 degree clockwise rotation of the wind. However, the wind speed of a typical middle latitude depression (see McIntosh and Thom, p. 150) will first increase and then decrease as the low pressure center approaches and then increase and decrease again after the center passes by. Clearly, the response of the wind speed should be less coherent with air pressure than the response of the rotating clockwise wind component for these atmospheric pressure systems.

A marked difference is found in the coherence results at longer synoptic periods (greater than 10 days) in comparison with the coherence results at the shorter synoptic periods. At these longer periods, the rotary coherence levels are considerably lower. These results suggest that, at the longer synoptic periods, the variation of the wind can no longer be thought of as a relatively simple response to travelling atmospheric circulation systems. Instead, the relation between the wind and air pressure appears to be considerably more complicated at such scales. Interestingly, the coherence between the wind speed and air pressure remains much the same at the longer periods as that found at shorter synoptic periods. Also, the phase difference between wind speed and air pressure remains fairly constant (being nearly out of phase) throughout the synoptic scale.

5.3 Air Temperature

The cross-spectral results (see Figure 21) show a significant amount of coupling between the air temperature and the wind over a wide range of scales. The most significant levels of coherence are found at synoptic scales. The clockwise rotary coherence ranges from 0.4 to 0.7 over periods cf 1.5 to 35 days while the anti-clockwise rotary coherence levels are somewhat lower, ranging from 0.25 to 0.6 cver the same interval of periods. These results suggest that the air temperature has a greater response to clockwise rotations of the wind than anti-clockwise rotations.

This differential response of air temperature, cn synoptic scales, is understandable in terms of the passage of synoptic circulation systems over the North Pacific Ocean. Synoptic pressure disturbances travelling eastward to the north of Station 'Papa' (resulting in a clockwise wind rctaticn at 'Papa') are more likely to be associated with cold airmasses than pressure systems passing to the scuth (anti-clcckwise wind rotations) due to the difference in latitude. It would seem that these cold airmasses produce more coherent changes in the air temperature than the relatively warmer pressure systems passing to the south.

When the wind direction is excluded from the analysis ty computing the wind speed-air temperature cross-spectrum, the coherence levels are found to be much lower but still generally significant. At synoptic scales, the coherence spectrum shows a peak from 1.3 to 3.5 days but with coherence levels of only 0.20. This region of statistically very good coherence is se-
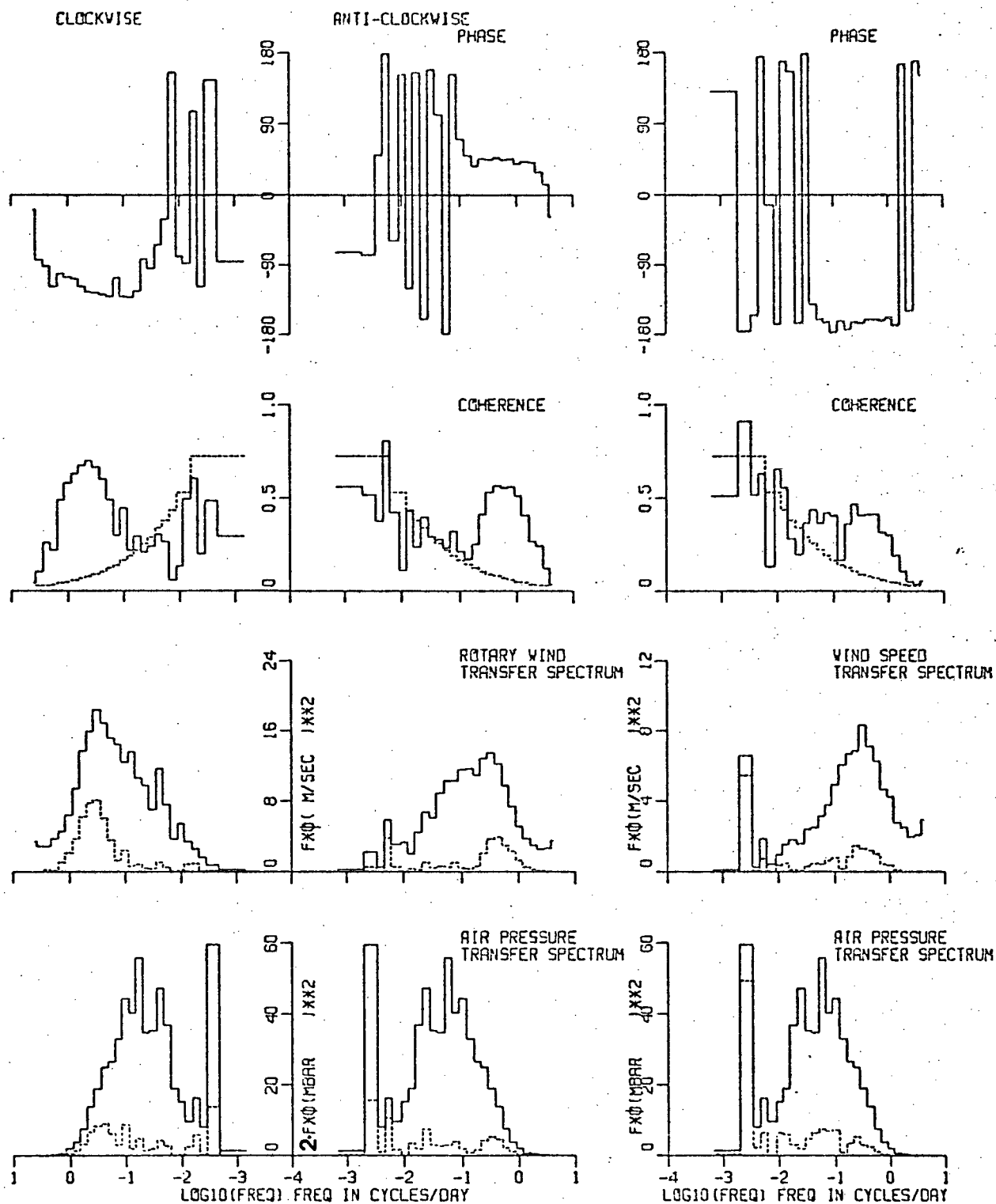
Figure 21: Graphs of phase, coherence and the transfer spectra between the wind and air temperature. The cross-spectral quantities are displayed for both the vector wind (as rotary spectra) and the wind speed. The annual and semi-annual peaks of the air temperature auto-spectra are off-scale.

parated from the fair to good coherence found at longer periods by a region of poor coherence found at 6.5 to 11 days. The phase at the synoptic peak ranges from -30 degrees to 30 degrees, indicating that the air temperature is nearly in phase with the wind speed.

At periods longer than the synoptic scale, the coupling between air temperature and the wind remains at significant levels. The clockwise coherence is very good out to periods of about 200 days and remains fair and good at the periods of one year and two years, respectively. The anti-clockwise coherence exhibits a somewhat different behavior: it remains good out to periods of 64 days but for longer periods (with the exception of a peak of very good coherence at 100 days) it declines to poor coherence levels. The wind speed-temperature coherence is generally good at the longer periods with two sharp peaks at the annual and semi-annual cycles. The annual coherence is, of course, extremely good with a value of 0.99. Air temperature leads wind speed by 125 degrees over the annual cycle.

We have seen that changes in the air temperature are significantly coherent with wind rotations. Such changes in the air temperature are due to advection of different airmasses past the observation point. The effect of more localized modifications is examined by computing the cross-spectrum between the air temperature and $U \Delta T$ (a quantity which through the bulk aerodynamic parameterization, equation (2), is representative of the upward turbulent transport of sensible heat). The cross-spectral results, displayed in Figure 22, show a very significant and high level of coherence between these quantities at all scales less

Figure 22: Graphs of phase, coherence and the transfer spectra between the air temperature and UΔT (a quantity representative of the sensible heat flux). The annual and semi-annual peaks of the air temperature auto-spectra are off-scale.

than or equal to one-half year. At periods longer than one-half year, the coherence levels are poor, with the exception of very good coherence at the annual cycle.

Over the synoptic and mesoscale periods, the phase between the two signals is very uniform, remaining within 10 degrees of being exactly out of phase. Over these scales, then, an increase in temperature is accompanied by a decrease in $U\Delta T$ and a decrease in temperature is accompanied by an increase in $U \cdot \Delta T$. The high coherence found here suggests that the fluctuations in the air temperature may be used to predict the corresponding fluctuations in $U \cdot \Delta T$. While the coherence levels for air temperature with $U \Delta T$ are large (0.7 to 0.9) the coherence levels of air temperature with the sensible heat flux may be lower because of the scatter found in experimental comparisons of direct measurements of sensible heat and the calculated value of sensible heat through equation (2) (see for example, Pond et. al. (1971)).

5.4 Absolute Humidity

The absolute humidity is an airmass characteristic, which like air temperature, is modified by means of turbulent exchanges with surrounding parcels of air. It is further related to air temperature since the air temperature determines the upper limit (saturation value) of absolute humidity. As one would expect, then, the air temperature-absolute humidity cross-spectrum, displayed in Figure 23 indicates a strong correlation over most scales, as seen from the high coherence levels and small phase values. For periods less than 3 days, the coupling declines sharply although the coherence between the signals does remain statistically significant.

Figure 23: Graphs of phase, coherence and the transfer spectra between the air temperature and the absolute humidity. The annual and semi-annual peaks of both the air temperature and absolute humidity auto-spectra are off-scale.

The absolute humidity-wind cross-spectrum (see Figure 24) is remarkably similar to the air temperature-wind cross-spectrum previously discussed. Both cross-spectra show that the most significant coherence levels occur at synoptic periods and that the clockwise wind rotations are more coherent with air temperature and absolute humidity than anti-clockwise wind rotations or the wind's speed. The major difference between the two cross-spectra are to be found at shorter periods. Over periods ranging from 4 days to 0.5 days, the absolute humidity is more coherent with the rotary wind and wind speed than air temperature. The largest change is found for the case of the clockwise rotating wind. Such differences between temperature and humidity in relation to the wind as well as the reduced temperature-humidity coherence suggest that over the smaller synoptic period, processes other than the wind are important. Apparently one manifestation of such processes is to reduce the wind-air temperature coherence. One possible process which would have a different effect on temperature than humidity would be heat transfers by long wave radiation.

The cross-spectrum between absolute humidity and $U\Delta q$ (a quantity which is representative of the turbulent water vapour transfer by means of equation (3)) was computed. The cross-spectral results, displayed in Figure 25, show very similar features to the air temperature-$U\Delta T$ spectral results previously discussed. The absolute humidity variations dominate $U\bullet\Delta q$ changes but not to the same extent as temperature variations dominate the $U\bullet\Delta T$ changes. Over a considerable part of the resolved periods (periods less than 100 days) the coherence is
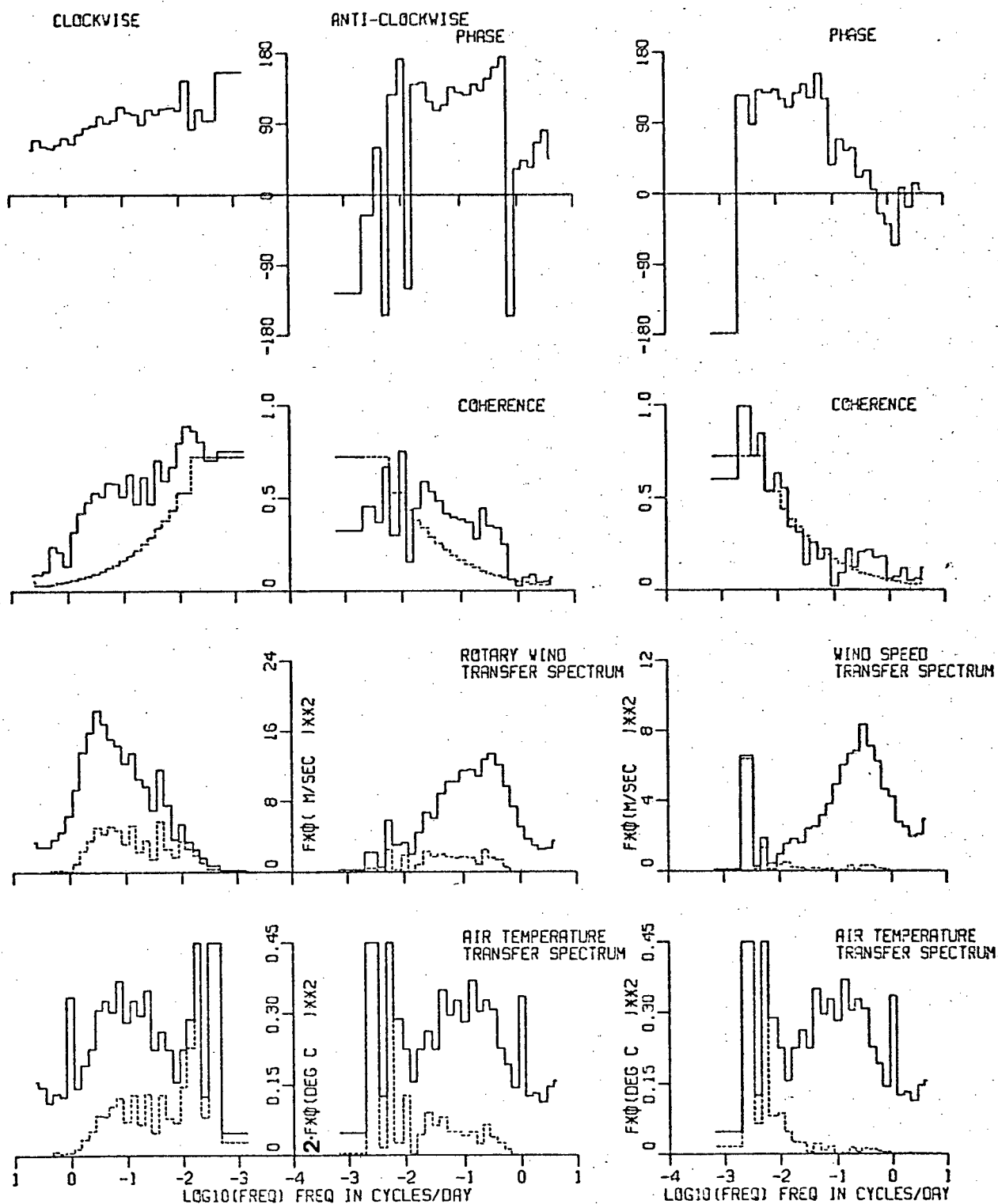
Figure 24: Graphs of phase, coherence and the transfer spectra between the wind and absolute humidity. The cross-spectral quantities are displayed for both the vector wind (as rotary spectra) and the wind speed. The annual and semi-annual peaks of the absolute humidity auto-spectrum are off-scale.
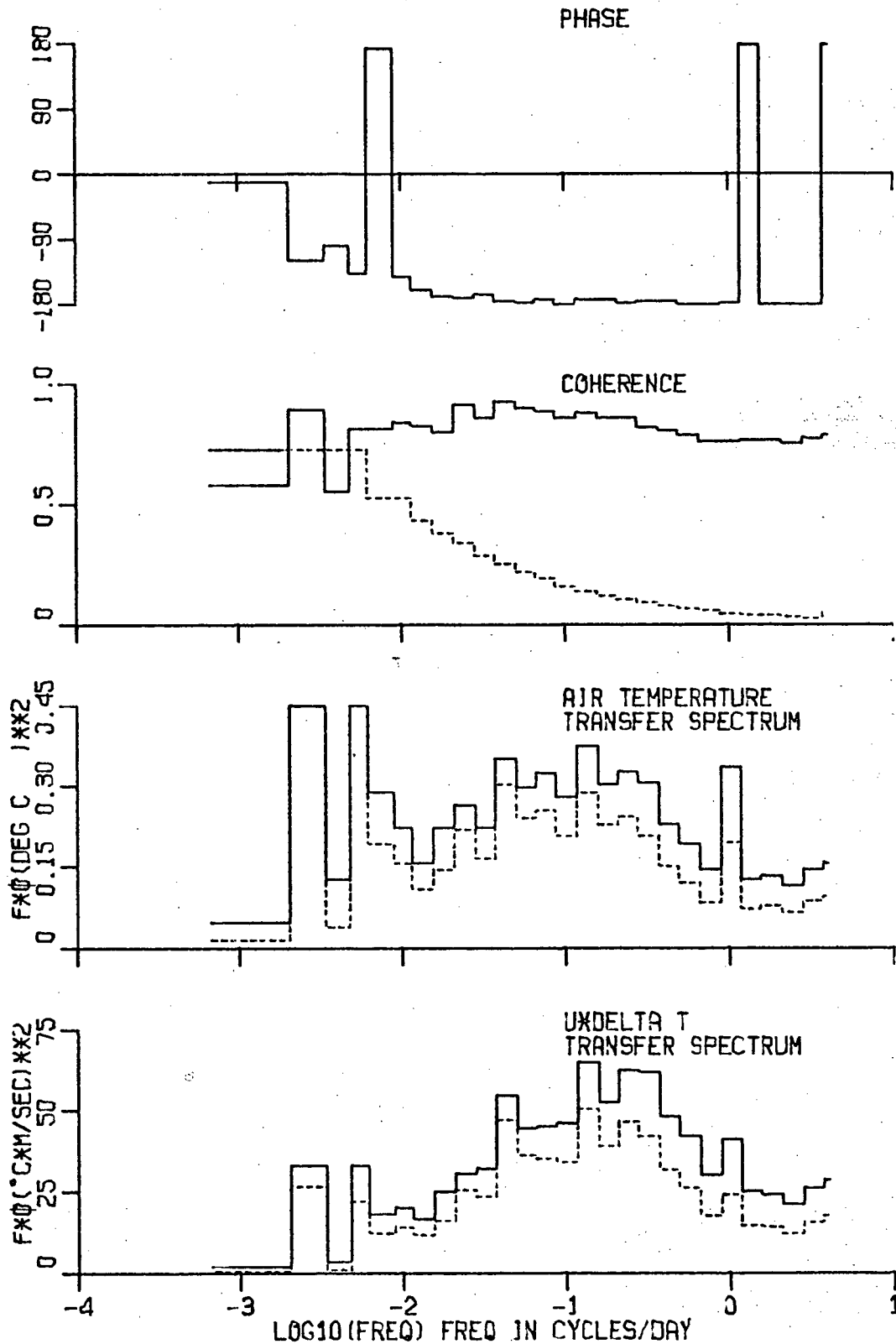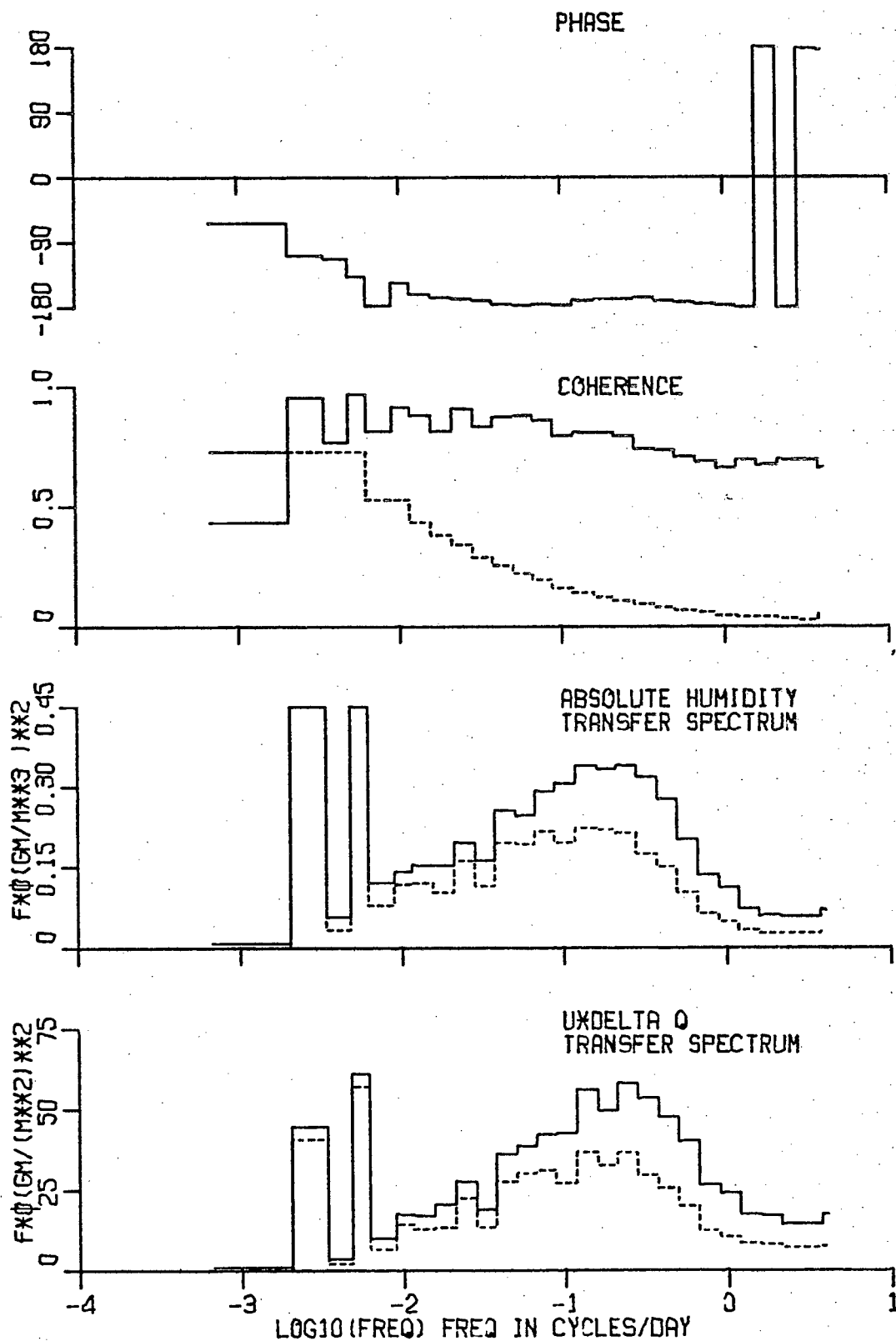
Figure 25: Graphs of phase, coherence and the transfer spectra between the absolute humidity and UΔq (a quantity representative of the latent heat flux). The annual and semi-annual peaks of the absolute humidity auto-spectrum are off-scale.

statistically very good, ranging from 0.90 to 0.65 and the phase remains within 20 degrees of the signals being exactly out of phase. While it must be remembered that the correlation between water vapour (or latent heat) transfer and $U\Delta q$ is not perfect, the results suggest a strong inverse relationship between absolute humidity and water vapour transfer.

5.5 Sea Temperature

The cross-spectral results of sea temperature with various surface meteorological quantities can be used to study the coupling between the ocean and the atmosphere. As previously mentioned in Chapter 2, the sea temperature recorded over the first five years contain some apparently erroneous values. The major effect of these errors on the spectrum is to distort the diurnal spectral estimate (as discussed in Chapter 4). For the cross-spectral results that follow, all ten years of the data were used in computing them. As a check on their reliabilty, the same cross-spectra were computed using only the last five years of the data. The same general features were found in both sets of cross-spectra.

The cross-spectrum between the sea temperature and the air temperature is shown in Figure 26. It shows statistically very good levels of coherence at all periods but the levels are rather small to make a good predictor except at periods longer than 100 days. The highest coherence is found at the annual and semi-annual cycles and the coherence levels generally decline with decreasing periods. Over the synoptic scales, the coherence ranges from 0.3 to 0.5 and seems to vary about a fairly constant level. The phase difference between the air and sea
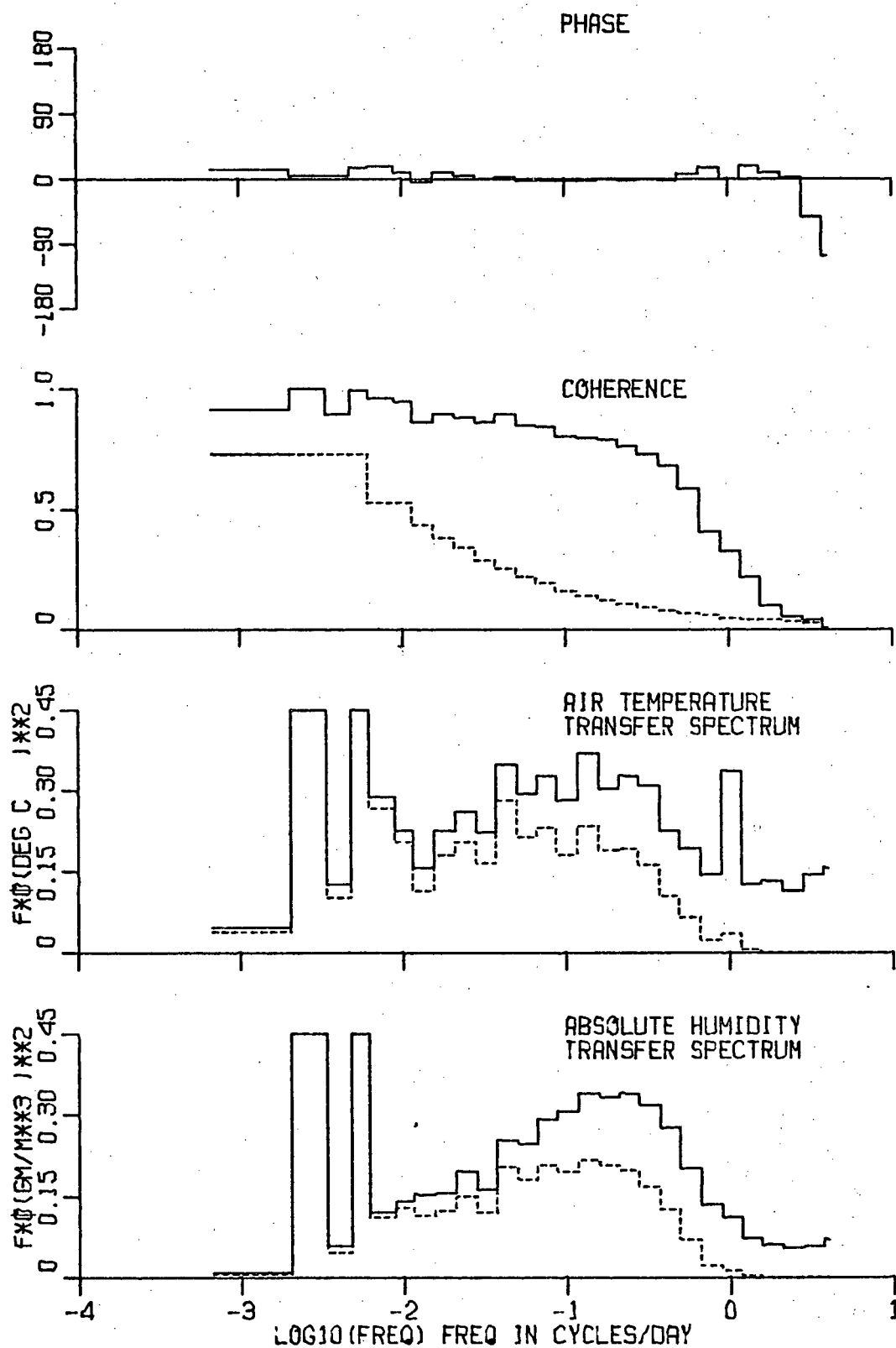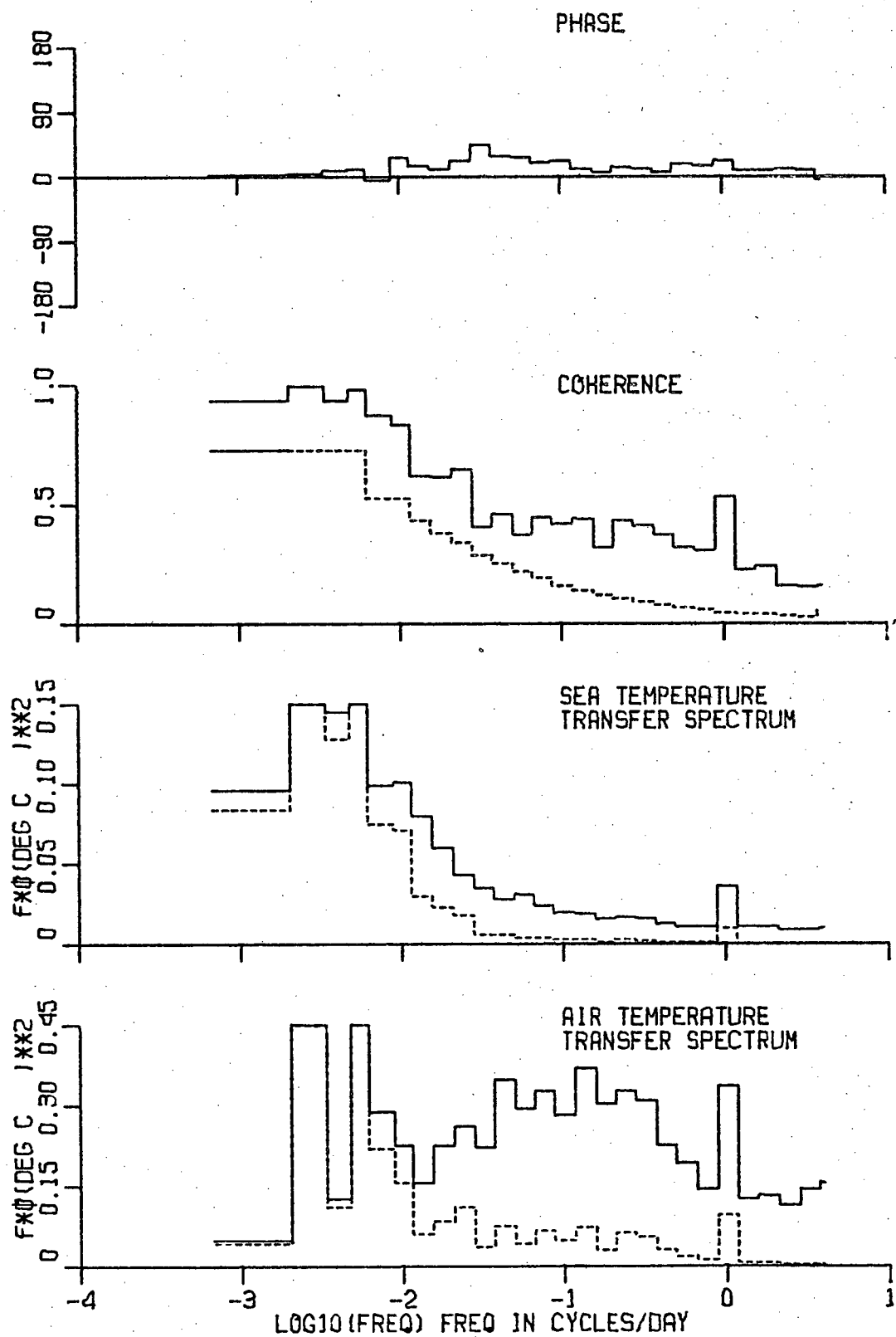
Figure 26: Graphs of phase, coherence and the transfer spectra between the air temperature and the sea temperature. The annual and semi-annual peaks of both the sea and air temperature auto-spectra are offscale.

temperature is small, being less than 40 degrees over most periods. The air temperature generally leads the sea temperature.

The wind-sea temperature cross-spectra are displayed in Figure 27. The rotary cross-spectrum shows statistically good to very good coherence levels over all periods. However the coherence levels are too low to be useful as a predictor. The clockwise coherence levels are somewhat higher than the anti-clockwise coherence levels, particularily at synoptic periods. Apparently this difference is a reflection of the difference between synoptic disturbances passing to the north (resulting in clockwise wind rotations) and those passing to the south (resulting in anti-clockwise wind rotations). Previously, we have seen that disturbances passing to the north are more strongly coupled to the air temperature, apparently because they originate at higher latitudes and therefore have more pronounced airmass temperature differences from the air they replace. One would then expect that the sea temperature will be modified to a greater extent by such synoptic disturbances as well, resulting in higher coherence levels.

The cross-spectrum between the wind speed and the sea temperature shows statistically very good levels of coherence over periods ranging from one year to one day. These levels are generally larger than those for the rotary wind at the longer synoptic and seasonal/climatic scales. The coherence decreases steadily with decreasing period. The phase plot indicates that except for the very longest and the very shortest periods resolved, the sea temperature leads the wind speed by 90 to 135
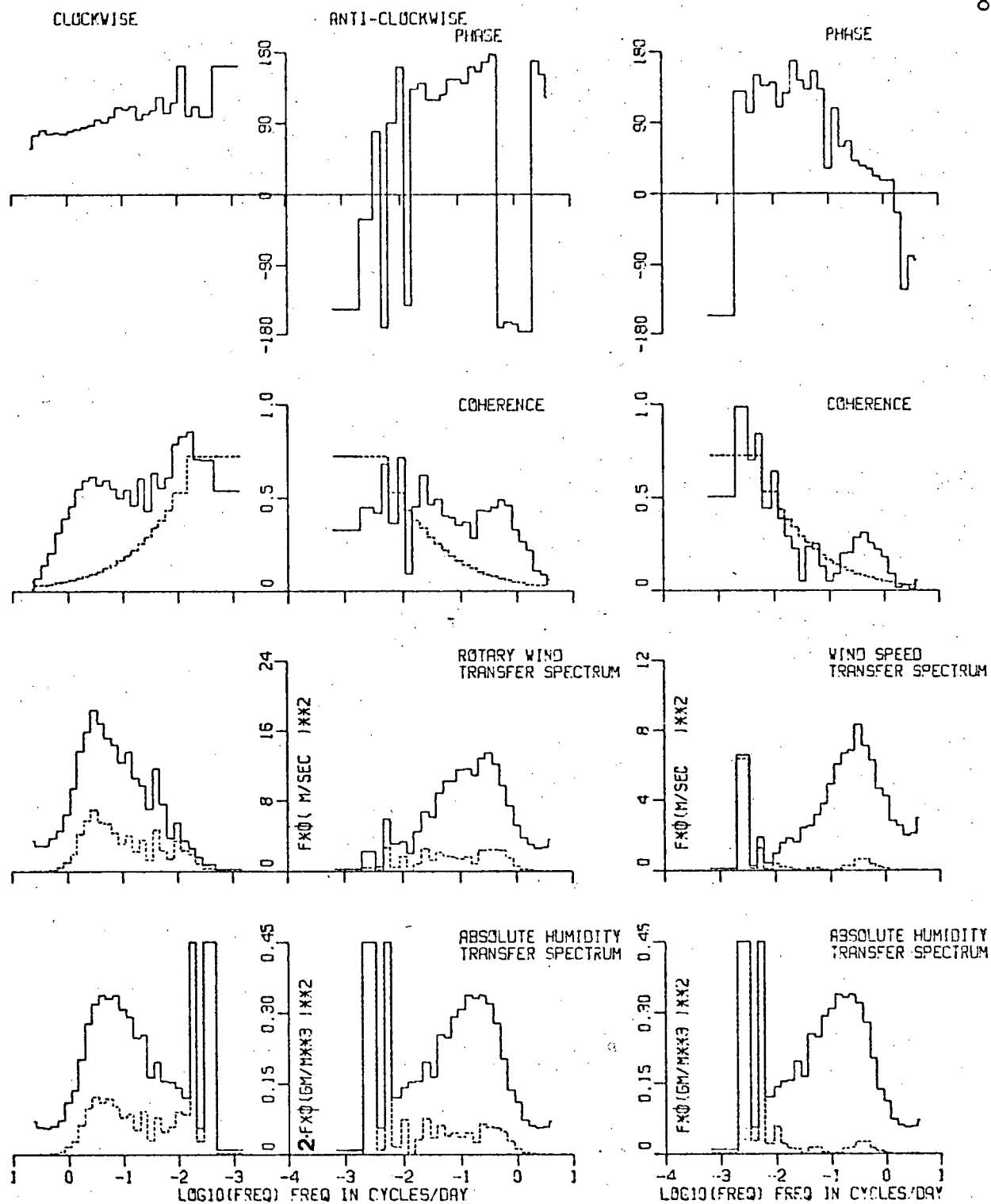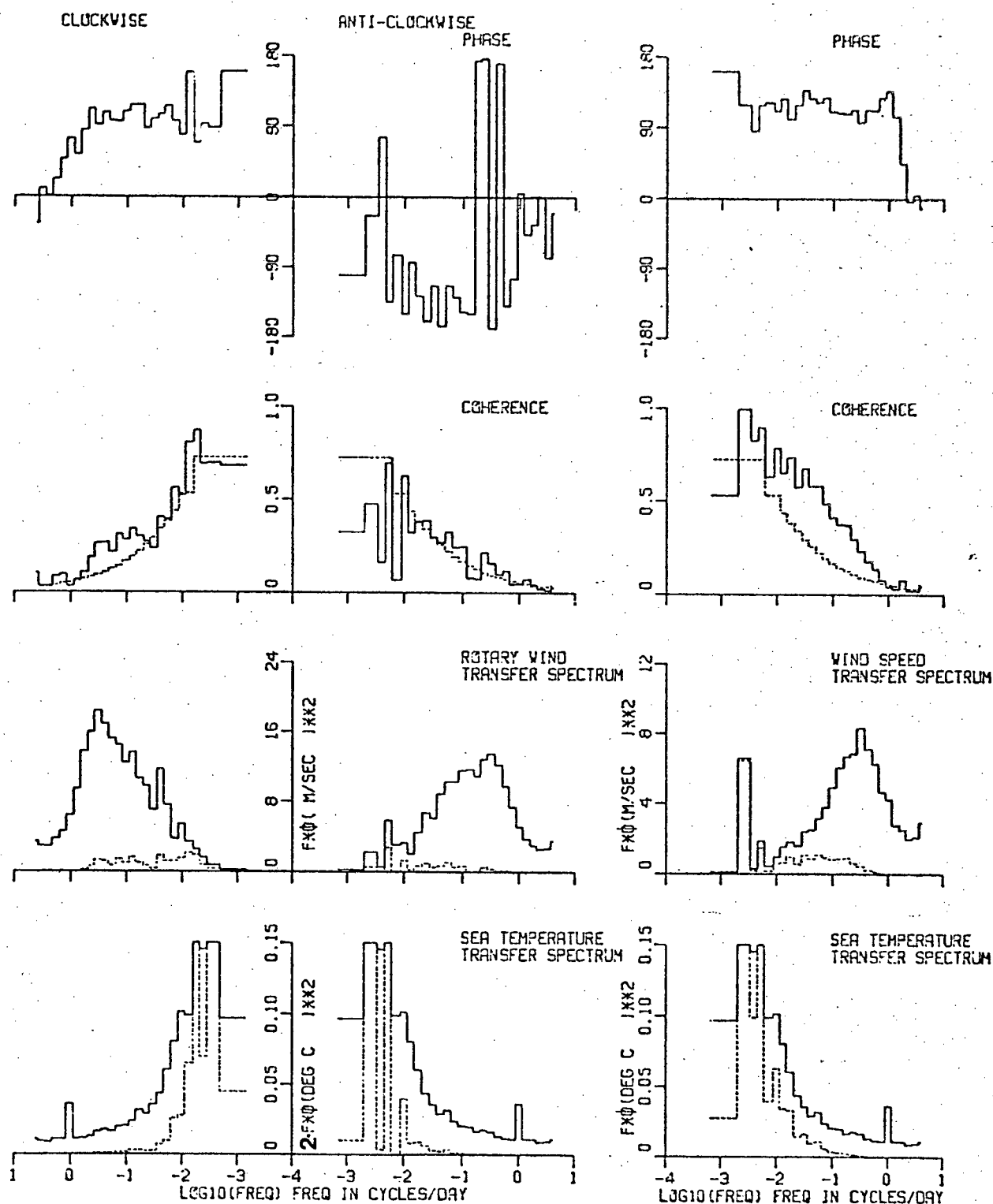
Figure 27: Graphs of phase, coherence and the transfer spectra between the wind and sea temperature. The cross-spectral quantities are displayed for both the vector wind (as rotary spectra) and the wind speed. The annual and semi-annual peaks of the sea temperature auto-spectrum are off-scale.

degrees.

It is instructive to compare the cross-spectral results for the wind and the sea temperature with those of the wind and the air temperature. The wind speed is more coherent with the sea temperature than the air temperature while the rotary wind components are more coherent with the air temperature than the sea temperature for periods greater than 3 days. This result indicates a greater degree of coupling of the wind speed with sea temperature than air temperature on such scales. Ocean-atmospheric coupling processes which could account for the high degree of coupling with the wind speed include turbulent heat exchanges and wind driving of the ocean's upper layer, both of which are related to the wind speed. Similarily, the lower coherence of sea temperature with the rotary wind shows that the sea temperature is less directly related to the passage of synoptic scale pressure disturbances.

The relatedness of the sea temperature with air pressure is examined by computing their cross-spectral values (see Figure 28). The major features of the coherence spectrum are very good coherence levels at the annual period (0.92) and at shorter synoptic periods (ranging from 2 to 7 days). Over the longer synoptic periods and the seasonal/climatic periods, the coherence shows marked variations about the 95% significance level. At periods between 65 days and the annual period, the coherence is only fair to poor. A bulge in the spectrum to levels of statistically good and very good coherence is found between 10 and 30 day periods. The phase spectrum indicates that air pressure leads the sea temperature over most periods.
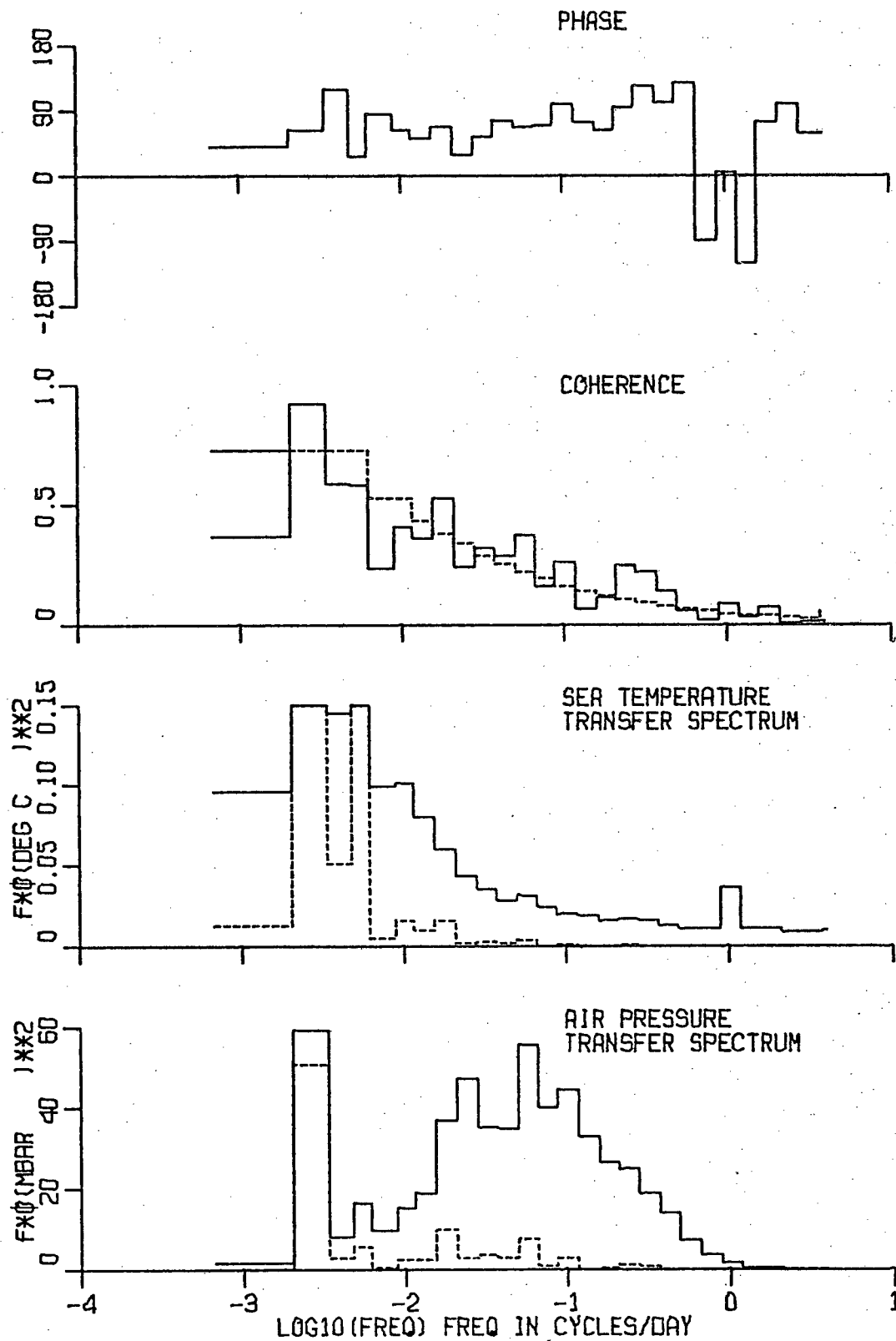
Figure 28: Graphs of phase, coherence, and the transfer spectra between the sea temperature and air pressure. The annual and semi-annual peaks of the sea temperature auto-spectrum are off-scale.
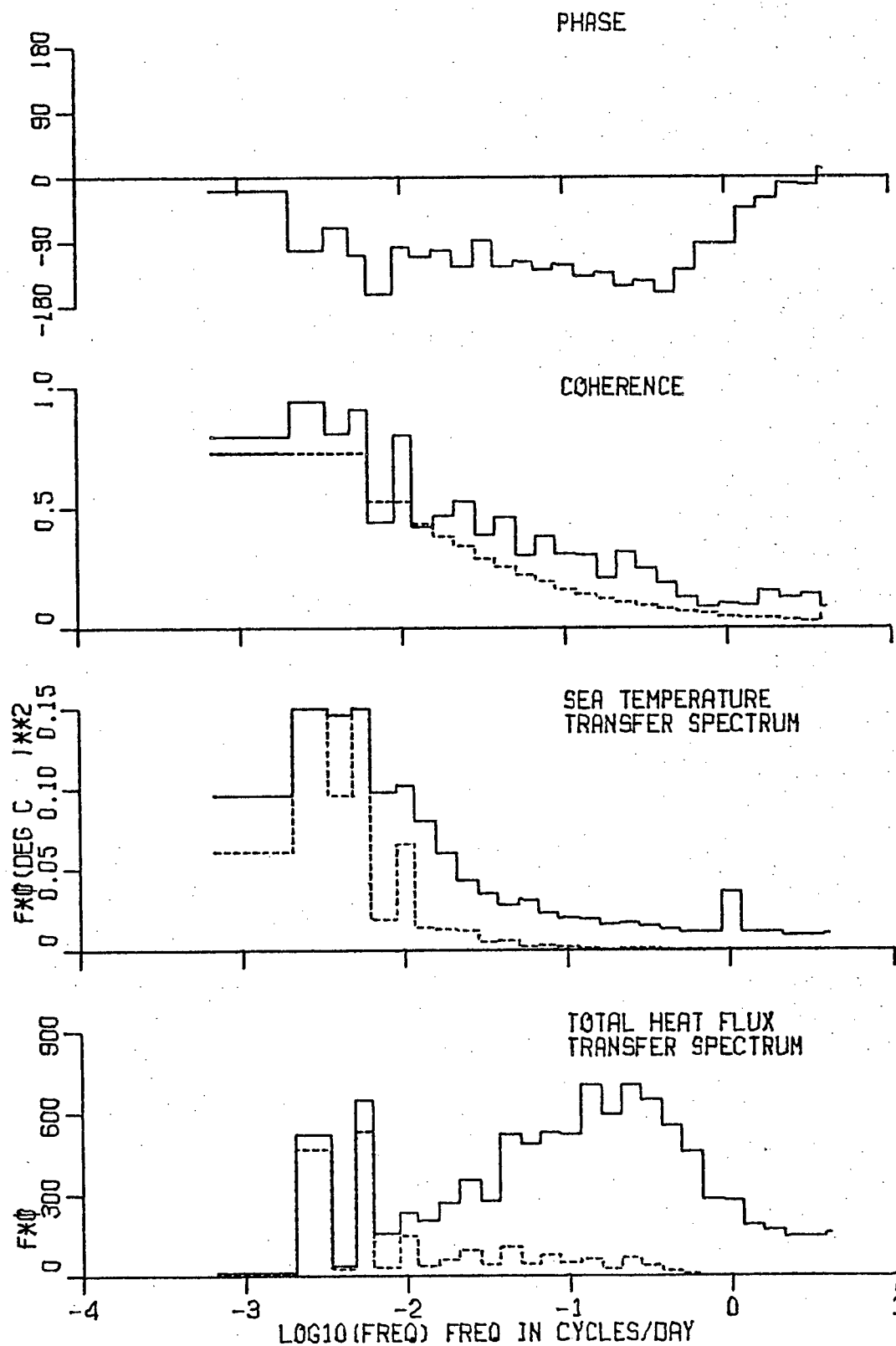
Figure 29: Graphs of phase, coherence and the transfer spectra between the sea temperature and 1.2*UΔT + 2.44*UΔq (a quantity representative of the total turbulent heat flux). The annual and semi-annual peaks of the sea temperature auto-spectrum are off-scale.

The cross-spectrum between sea temperature and the total turbulent heat flux (see Figure 29) reveals generally very good coherence levels over most periods. However, the coherence is only large enough to be of practical use for predictive purposes at the longest periods. The phase difference between the two quantities ranges from 90 to 180 degrees, with the sea temperature leading. Over periods from one year to one day, a comparison of Figure 29 with Figures 22 and 25 shows that the sea temperature-heat flux coherence levels are considerably lower at periods less than 100 days, than the air temperature-$U\Delta T$ or the absolute humidity-$U\Delta q$ levels.

5.6 Co-spectra Between Quantities Used To Compute Bulk Fluxes

The bulk parameterization formula for momentum flux (or wind stress) is a relationship which allows east-west and north-south components of the wind stress to be computed from the product of the wind speed and the east-west and north-south wind components ($U \cdot U_x, U \cdot U_y$). Similarily, the sensible and latent heat fluxes are determined from the products, $U\Delta T$ and $U\Delta q$, respectively (equations (2) and (3)). To assess at which scales important contributions are made to these products (and hence to the fluxes), the co-spectra between each quantity were computed for each of the products.

The co-spectrum ϕ_{xy} resolves the contributions to the co-variance XY due to in-phase oscillations from various periods. In the co-spectral plots following, $f\phi_{xy}$ is plotted to produce the correct weighting for a logarithmic frequency scale.

The co-spectra between the wind speed and each wind component are displayed in Figure 30. The contributions to the
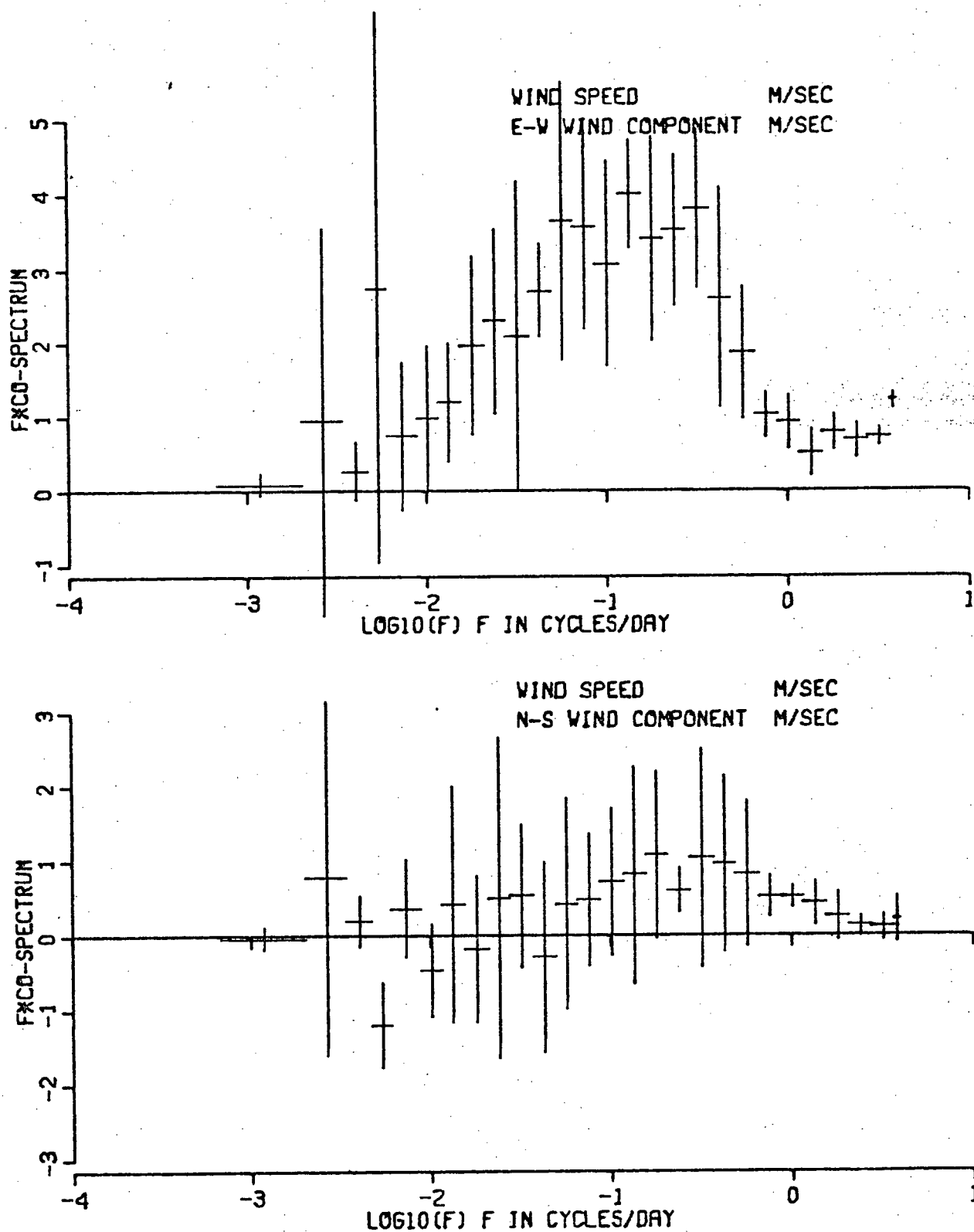
Figure 30: The co-spectrum between the wind speed and the east-west wind component and between the wind speed and the north-south wind component computed from five two-yearly blocks. The vertical error bars represent approximate 95% confidence intervals of the mean co-spectral estimate.

covariance (as computed from the area under the graph of co-spectral values) from all periods resolved by the co-spectral analysis is 14.9 (m/sec)^2 for the $U \cdot U_x$ co-spectra and 3.1 (m/sec)^2 for the $U \cdot U_y$ co-spectra. To put these values into perspective, it should be noted that the contribution to covariance from the product of the long-term averages ($\bar{U} \cdot \bar{U}_x$ and $\bar{U} \cdot \bar{U}_y$) are 41.5 (m/sec)^2 and 14.4 (m/sec)^2, respectively.

The $U \cdot U_x$ co-spectral values are always positive and show peak levels at periods of about seven days with a marked decline at the shorter periods. The contributions to the covariance from periods of 2 days to 6 hours amounts to only 12% of the total spectral covariance and less than 3% of the total covariance ($\overline{U \cdot U}_x = \int \phi_{UU_x} + \bar{U} \cdot \bar{U}_x$). Similarily, the $U \cdot U_y$ co-spectral levels are generally positive with the highest levels found at periods of about 4 days. As with the east-west case, the north-south covariance has relatively small contributions from periods less than 2 days. These results suggest that when computing the long-term wind stress, using the bulk aerodynamic parameterization, one must have measurements at intervals separated by no more than 2 or 3 days to obtain reliable wind stress estimates.

The co-spectra of the wind speed with the sea-air temperature difference ($U \cdot \Delta T$) and of the wind speed with the sea-air humidity difference ($U \cdot \Delta q$) are displayed in Figure 31. Both co-spectra follow the same pattern: relatively large positive contributions from the annual and semi-annual cycles, while at shorter periods between 7 days and 2 days, relatively large negative co-spectral levels are found. These negative cospectral values are not unexpected since strong winds cause increased
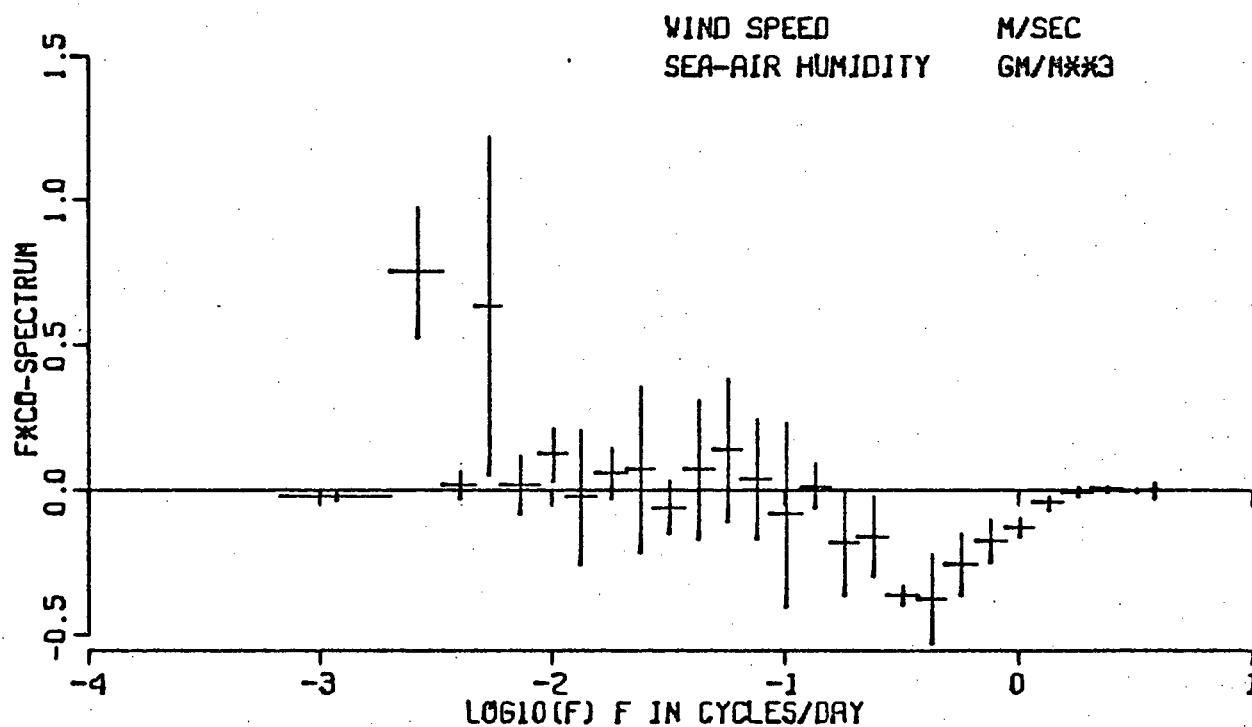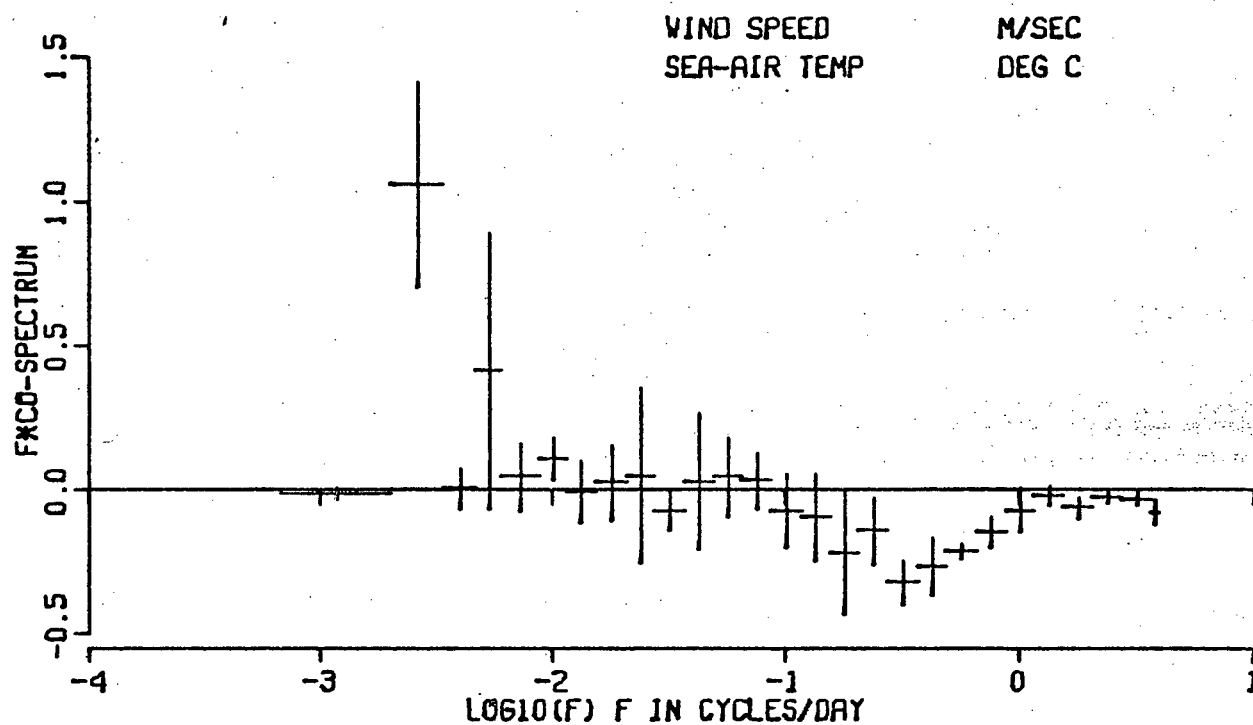
Figure 31:   The co-spectrum between the wind speed and the
sea-air temperature difference and between the wind speed and
the sea-air humidity difference from five two-yearly blocks.
The vertical error bars represent approximate 95% confidence
intervals of the mean co-spectral estimate.

mixing of the surface layers of both the atmosphere and the ocean which decreases air-sea temperature and humidity differences.

In relation to the total co-variance of the wind speed and sea-air humidity difference ($U \cdot \Delta q$), the annual and semi-annual variation accounts for only 4.7% of the total and the shorter period variation account for only 3.8%. In addition, because of their opposite signs, these two variations partially cancel one another out. Clearly, the long term latent heat transfer can be determined adequately from long-term averages of the wind speed and the sea-air humidity difference.

In terms of the total covariance of the wind speed and the sea-air temperature difference, contributions from the annual cycle and the shorter periods (2 to 7 days) are more important. The annual and semi-annual cycle peaks accounts for 24% of the total covariance ($U \cdot \Delta T$) while the shorter periods account for approximately 12%. Thus, in computing the long term sensible heat flux by means of the bulk aerodynamic parameterization, it is important to include the effects of these periods by choosing a sufficiently small sampling interval.

Chapter 6

THE EFFECT OF DATA SMOOTHING ON WIND STRESS COMPUTATIONS

6.1 Introduction

In this chapter a study is made of the effect of using the smoothed data that are readily available over the oceans on the computation of wind stress (or momentum flux) by means of the bulk parameterization formula (equation (1)). The two sources of wind field data which are available over the entire ocean for long periods are wind roses (as compiled in climatic atlases) or mean pressure maps from surface weather charts (from which the wind can be computed geostrophically and then corrected for the frictional effect of the surface). Both of these data sources are organized in such a way that the wind data are inherently averaged or smoothed. The effect that this smoothing has on the computed wind stress is examined by smoothing the basic 3-hourly wind data at Station 'Papa' in a similar fashion and then applying the equation (1) to this smoothed data. The resulting value of wind stress is then compared with the estimate of wind stress made by applying the bulk parameterization formula directly to the 3-hourly data.

Two previous studies of this kind have been made by Malkus(1962) and Frye(1972). Malkus computed the wind stress by various means at two locations: one in the tropical Atlantic and the other at Weather Station 'C' (53N 36W) in the North Atlantic. However, the data used at both locations covered a period of less than a month. Wind roses are generally compiled from many years of data for each month of the year. The stress

magnitude calculated from the wind roses agreed with the direct calculation to within 25%. The stress magnitude computed from the vector averaged wind (which is similar to what can be computed from surface pressure maps) showed good agreement with the direct calculation at the tropical location. However at the more northerly location, it was low by a factor greater than 2 as a result of the much greater variability of the wind direction in the latitudes of the westerlies.

Frye(1972) studied the effect that the averaging distance (or period) used in obtaining the mean wind speed has on the computed wind stress at an Oregon coastal location. Because his basic data did not include complete wind direction measurements, he chose a data run where the wind was consistently blowing from the north. His results showed that the wind stress steadily decreased with the size of the averaging period. At a period of about a week, this change was approximately 20%.

Because the drag coefficient, C_D may be a weak function of the wind speed, two different drag coefficients were used. These include a constant drag coefficient (Pond et. al.,1974):

$$C_D = 1.5 \times 10^{-3} \tag{30}$$

and a linear drag coefficient (Deacon and Webb,1962):

$$C_D = (1.0 + 0.07 \cdot U) \times 10^{-3} \tag{31}$$

where U is the mean wind speed in m/sec. More recent measurements indicate that the weighting factor of 0.07 used in the linear drag coefficient is too large. However, it useful for this study in that it provides an upper bound of the possible effects of the non-constant drag coefficient.

The drag coefficient may depend on the atmospheric stabili-

ty as well (Roll,1965). This effect may be important in coastal regions, but it is not likely to be important over the open ocean, where the air-sea temperature difference (ΔT) is relatively small. At Station 'Papa', the absolute value of ΔT exceeds 2 C° in fewer than 10% of the observations. Furthermore, large values of ΔT often coincide with low wind speed values (Figure 31), so that the effect of non-neutral stability is limited to periods when the contributions to the wind stress are small.

Since the examination of the effect of smoothing in this study is limited to one location, the conclusions must be considered tentative. It would be desirable to apply the same analysis at other locations to see how the effects vary geographically. The effect of smoothing over spatial scales also needs to be examined.

6.2 Direct Wind Stress Computation

In order to determine the effects of smoothing on the wind stress computation, the wind stress is first computed directly from the 3-hourly observations (i.e. no data smoothing). The directly calculated values will be compared in later sections with the wind stress computed from smoothed data. In addition, the directly calculated values are useful to illustrate the variability of the wind stress over monthly and yearly periods.

The direct calculation of the wind stress was made by computing both wind stress components for each three-hourly measurement and averaging these over the data record used:

$$\tau_x = \frac{\sum_{i=1}^{N} \rho C_D (U_i{}^2 + V_i{}^2)^{1/2} U_i}{N} \quad ; \tau_y = \frac{\sum_{i=1}^{N} \rho C_D (U_i{}^2 + V_i{}^2)^{1/2} V_i}{N} \tag{32}$$

where N is the number of data points, τ_x, τ_y are the east-west

and north-south stress components, respectively and U_i, V_i are the east-west and north-south wind components. The density ρ is 1.25×10^{-3} gm/cm³ (based on Table F-9, Handbook of Chemistry and Physics, 51st edition using an air temperature of 8.2 °C, absolute humidity of 7.4 gm/m³ and air pressure of 1010 mbar). The wind stress was computed using both the constant (equation (30)) and linear (equation (31)) drag coefficients.

The stress was calculated from 2916 observations for each year (out of a total of 2920 observations in an ordinary year and 2928 observations in a leap year). The observations were centered on the year. The monthly wind stresses were computed from the same number of observations with each 'month' consisting of 243 observations. In months or years which include missing or erroneous data (see Appendix I), the incorrect data is not used and the stress computation was based on the reduced number of good observations.

The wind stress for each of the ten years, 1958 to 1967 inclusive, is displayed in Figure 32. The results are displayed as the magnitude of the wind stress (in dynes/cm²) and the direction of the wind stress (as an angle in degrees clockwise from north). The magnitude of the stress has sizeable variations between different years. These variations are relatively large in comparison with the long term wind stress mean but are small in comparison with the fluctuations of the wind stress at smaller scales. The direction of the wind stress has smaller year to year variations, ranging in size from 60 to 90 degrees eastward of north in direction.

The directly calculated stresses computed using the linear
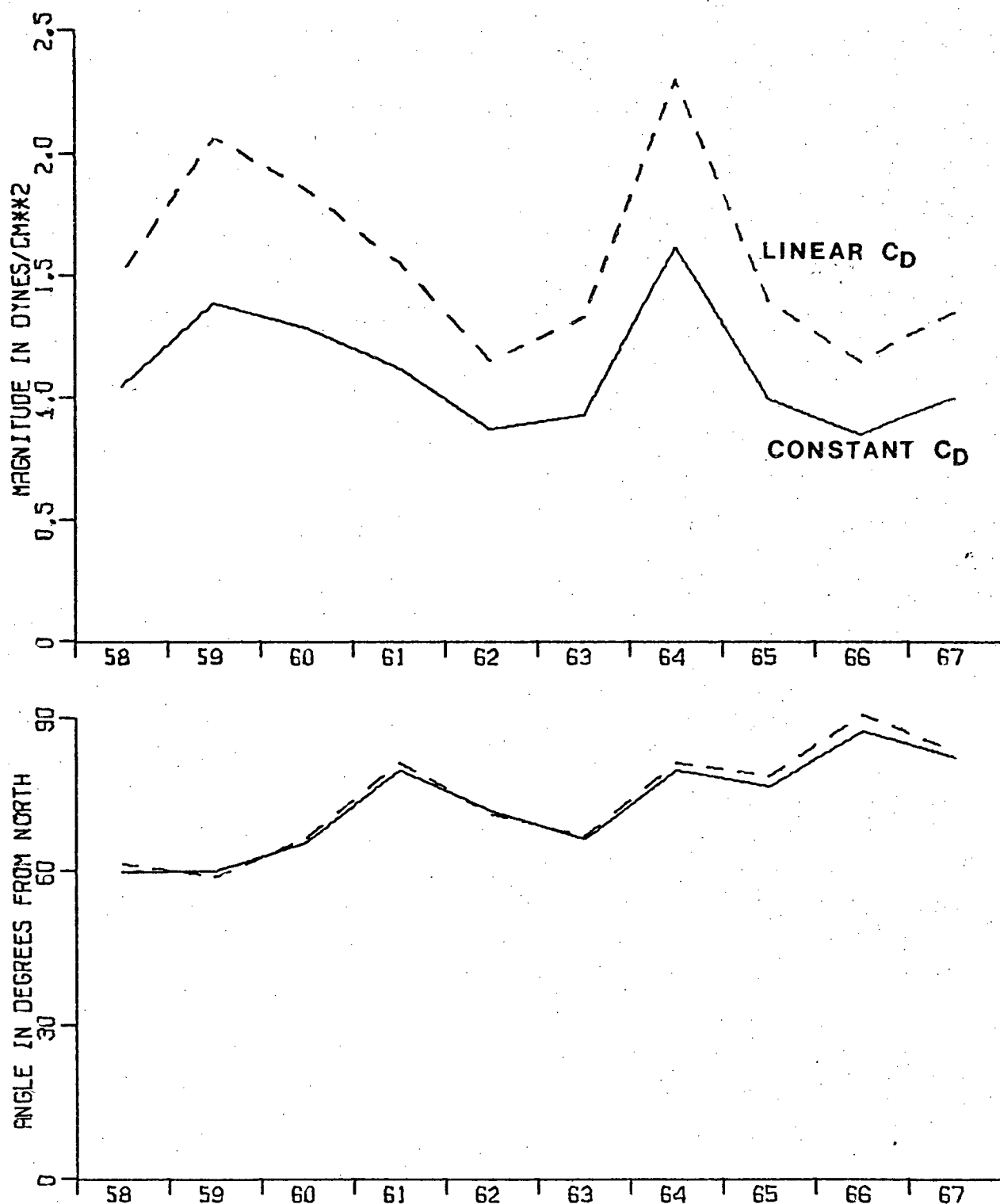
Figure 32: The directly calculated wind stress for each year from 1958 to 1967. The wind stress computed using the constant drag coefficient is plotted as a solid line while the dashed line represents the wind stress computed using the linear drag coefficient.

drag coefficient are somewhat larger in magnitude but have nearly the same direction. The the ratio of the magnitude increase over the constant drag coefficient case ranges from 1.32 (1962) to 1.50 (1959).

A large seasonal variation is found in the wind stress calculated for each month and averaged over each of the ten years (see Figure 33). The magnitude of the wind stress is largest in the fall and smallest in the summer. The larger error bars shown on the graph indicate the large year to year differences in the wind stress magnitude for each month. As an example of this variation, consider the month of Febuary which in 1958 and 1962 was the month of the lowest wind stress for each year and which in 1967 was the month of the greatest wind stress.

The monthly wind stress direction displayed in Figure 31 is computed as the mean of the ten direction values available for each month. The graph indicates that for all months, the stress direction is generally northward (0°) to south eastward (135°).

The monthly wind stresses computed using the linear drag coefficient show larger magnitudes. The relative size of the increase is related to the mean wind speed of each month. In fall and winter, when the mean wind is larger, the increase in the magnitude is approximately 50% while in summer when the mean wind is smaller, the increase is 25 to 30%. The difference in wind stress direction as a result of using the linear drag coefficient is small, being less than 5 degrees for each month.
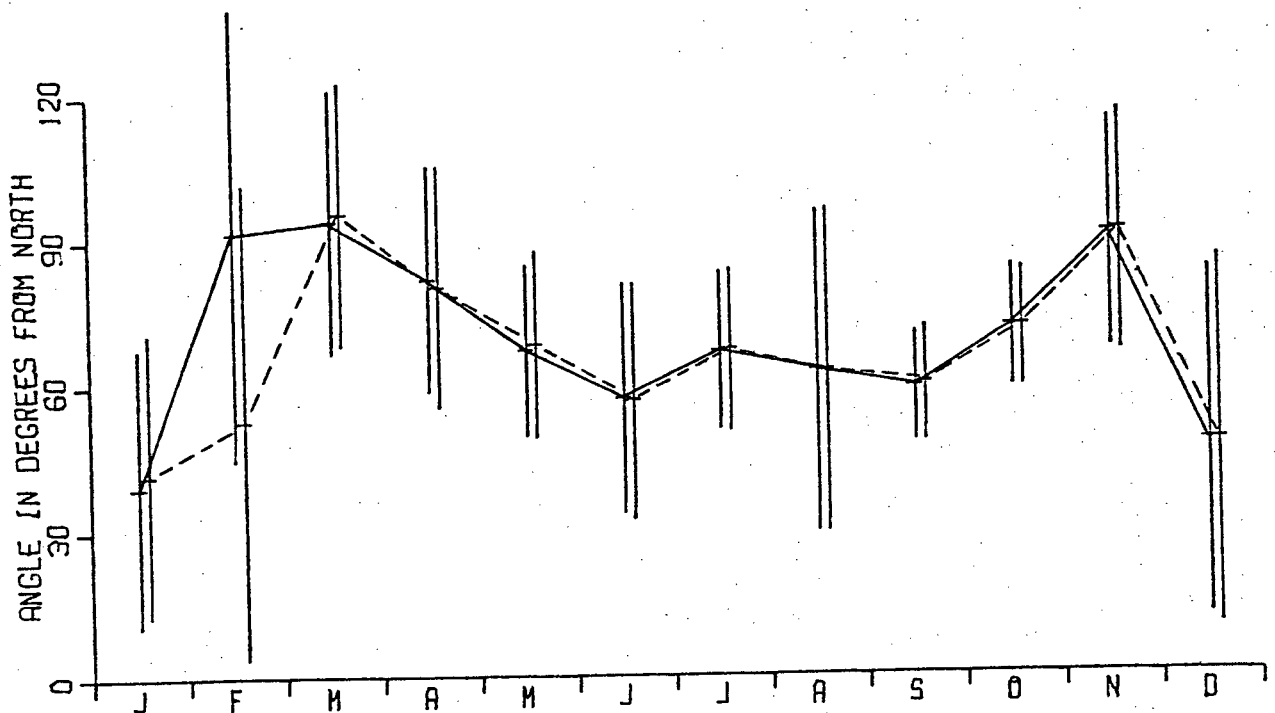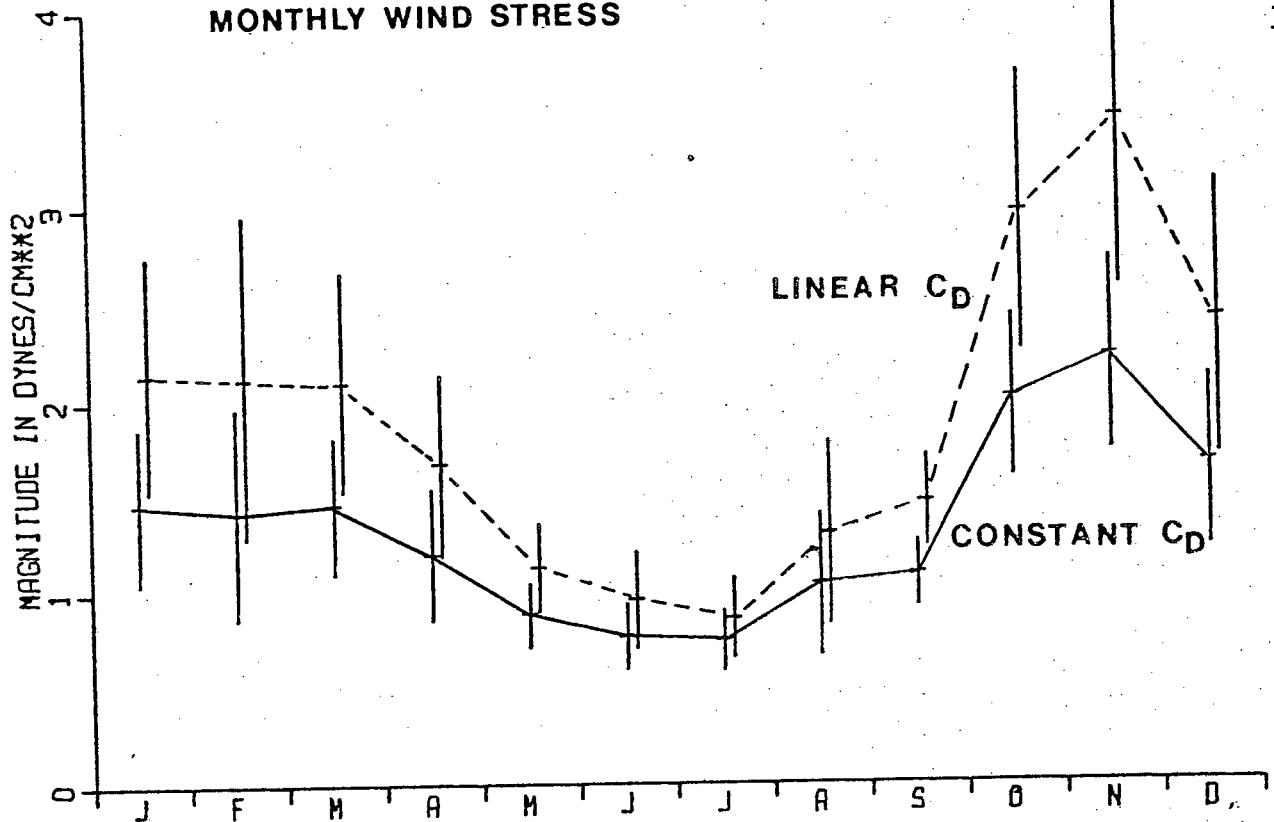
Figure 33: The directly calculated wind stress for each month. The vertical error bars represent the 95% confidence intervals of the mean computed from the separate estimates for each of the ten years, 1958 to 1967. The solid line represents the wind stress computed using the constant drag coefficient while the dashed line represents the wind stress computed using the linear drag coefficient.

6.3 Wind Stress From Climatic Atlases

The impetus for studies of the wind stress field over the ocean was provided by Sverdrup(1947) who related the strength of ocean currents to the curl of the wind stress. Shortly after the appearance of this pioneering work, the Scripps Institute of Oceanography computed the wind stress field over the North Pacific (1948) and the North Atlantic (1950). Hidaka(1958) later extended the computations to cover the Indian and Southern Hemisphere Oceans.

The basic data used in these computations were wind roses tabulated from many years of observations. For the North Pacific, Indian and Southern Hemisphere Oceans, these wind roses provided only the frequency of winds blowing in a given direction. The wind data for the Atlantic Ocean gave the wind speed distribution in each direction, as well, but in rather coarse groups.

With the publication of the Marine Climatic Atlas of the World, volumes I-VIII (1955 to 1969), a better data set for wind stress computations became available. Using this atlas, Hellerman(1967) recomputed the wind stress field over the world's oceans, although the drag coefficient as a function of wind speed that he used was probably not the best choice in the light of more recent measurements.

In order to assess the effect of this data format on the wind stress computation, the data were sorted and tabulated in the format of the Marine Climatic Atlas wind roses for each month from all ten years of data. The intervals of the wind speed distribution of each direction and of the overall wind

speed distribution are given in Table V. As in the Marine Climatic Atlas, the wind speed distribution values were rounded off to the nearest single percentage of the total number of data points used in constructing the wind rose. The symbol '+' used in the Marine Climatic Atlas to represent percentages which are non-zero but less than one-half of one percent was taken to be 1/4 of one percent for the purposes of calculation.

Twelve directions were used rather than the eight of the Atlas because the original data were provided in 36 directions. Sorting the data into eight directions would result in some bias as some of the eight directions would have contributions from five of the original 36 measured directions while others would have contributions from only four of the measured directions. (For a discussion of this effect see Lea and Helvey(1971)).

The wind stress was computed for each of the twelve directions following the method of Hellerman(1965). The computation was made using two different drag coefficients (equations (31) and (32)). Wind stresses were then added vectorially to obtain the east-west and north-south components. From the components, the magnitude and direction were computed and are used in displaying the results.

The wind stresses, as computed from the data organized in the wind rose format, are given in Table VI. The corresponding directly calculated values are also given for comparison. The results show that the two magnitudes differ by amounts ranging from less than 1% to as much as 14% for the case of the constant drag coefficient. The average of the monthly absolute percent differences is 5.6%. The difference between the magnitudes cal-

TABLE V

The data format used in wind roses presented in the Marine Climatic Atlases. First, the speed distribution that is used to group the wind data in each separated direction is presented. Then, the speed distribution for all wind readings regardless of direction is presented.

For Each Direction:

Interval	Beaufort Numbers	Minimum Speed (knots)
1	2-3	3.5
2	4-5	10.5
3	5-6	21.5
4	8-12	33.5

Overall Speed Distribution:

Interval	Beaufort Numbers	Minimum Speed (knots)
1	0-1	0.0
2	2	3.5
3	3	6.5
4	4	10.5
5	5	16.5
6	6	21.5
7	7	27.5
8	8	33.5
9	9	40.5

TABLE VI

Comparison of the wind stress magnitude and direction as computed from the data organized into the format of the Marine Climatic Atlas ('MCA') with the value computed directly from the 3-hourly data ('Direct'). The results are given for the both the constant and linear forms of the drag coefficient. The stress magnitude has units of dynes/cm²-day and the direction is in degrees clockwise from North.

Constant Drag Coefficient

	Magnitude			Direction		
Month	Direct	MCA	%Diff	Direct	MCA	Diff.
Jan.	1.052	1.043	-0.9	43.44	43.09	-0.35
Feb.	1.226	1.149	-6.3	62.43	59.61	-2.82
Mar.	1.192	1.283	7.6	99.30	97.23	-2.07
Apr.	1.046	1.078	3.1	91.78	88.66	-3.12
May	0.811	0.922	13.7	69.89	65.18	-4.71
June	0.634	0.666	5.0	63.49	66.15	2.66
July	0.679	0.740	9.0	64.98	61.90	-3.08
Aug.	0.943	0.912	-3.3	73.63	73.39	-0.24
Sept	1.066	1.007	-5.5	60.47	53.59	-6.88
Oct.	1.945	1.916	-1.5	75.31	77.96	2.65
Nov.	1.902	1.856	-2.4	83.35	83.71	0.36
Dec.	1.114	1.210	8.6	62.70	65.25	2.55
Year	1.098	1.111	1.1	72.45	71.74	0.71

Linear Drag Coefficient

	Magnitude			Direction		
Month	Direct	MCA	%Diff	Direct	MCA	Diff.
Jan.	1.530	1.552	1.4	47.09	46.74	-0.35
Feb.	1.877	1.708	-9.0	63.40	60.76	-2.64
Mar.	1.701	1.891	11.2	95.37	98.58	3.21
Apr.	1.418	1.501	5.9	90.73	88.80	-1.93
May	1.017	1.200	18.0	71.52	65.46	-6.06
June	0.779	0.828	6.3	65.06	67.86	2.80
July	0.781	0.872	11.7	64.30	60.70	-3.60
Aug.	1.183	1.147	-3.0	73.01	72.66	-0.35
Sept	1.421	1.332	-6.3	61.75	53.38	-8.37
Oct.	2.862	2.842	-0.7	74.85	77.55	2.70
Nov.	2.919	2.831	-3.0	82.01	82.96	0.95
Dec.	1.584	1.759	11.0	65.51	66.97	1.46
Year	1.550	1.571	1.4	72.73	72.50	0.23

culated over all the seasons is only 1.1%. The difference in direction is less than 6 degrees for each month. The corresponding differences for the case of the linear drag coefficient are slightly larger.

These results demonstrate that the effect of organizing the data into the wind rose format of the Marine Climatic Atlas has a rather small effect on the computed wind stress.

6.4 Wind Stress From Surface Weather Charts

Other sources of wind data over the oceans are the surface air pressure charts issued by various meteorological agencies. Such charts display the mean pressure field over various periods, often five days, one month or a season. By assuming that the pressure gradient is balanced by the Coriolis force, the geostrophic wind is calculated. At the earth's surface, the geostrophic wind must be corrected for the frictional effect of the surface. While the relation between the geostrophic wind and the observed surface wind is not well established, it is thought that over the open ocean, this correction is relatively small, amounting to a magnitude reduction of 0.7 and a rotation of less than 10 degrees (Flohn,1969).

The geostrophic wind computed from the pressure gradient is a vector quantity. Averaging the pressure field results in a vector averaging of the resultant geostrophic wind (i.e. each wind component is averaged). To estimate the effect of using a vector averaged wind in the computation of the wind stress, the observed 3-hourly surface wind observations were vector averaged over various periods. The resultant wind was then used in the bulk transfer formula to determine the wind stress. The wind

stress computed from the vector averaged wind was then compared with the directly calculated wind stress.

The comparison scheme described above will only be sensitive to the effect that the vector averaging of wind values has on the computed wind stress. Any variations of the resultant wind from other effects over the averaging periods investigated, will not be detected by this analysis. Other effects which may result in variations include a possible non-uniform surface correction to the geostrophic wind and the breakdown of the assumed geostrophic balance in certain situations (e.g. during the passage of a storm front).

The vector averaging was done separately on each of the 5 blocks of 5832 wind components (each block includes very close to two years of the data).

Each data block was divided into 5832 groups of one data sample, 2916 groups of two data samples, 1458 groups of four data samples, 729 groups of eight data samples, and so on up to one group of 5832 samples. The average of both wind components was computed from the individual components in each group. From these averaged wind components, $(\bar{U}_i, \bar{V}_i)$, $i=1,2,...L$ where L is the number of groups, the wind stress was determined by applying the bulk aerodynamic parameterization:

$$\tau(T) = \rho C_D \cdot \sum_{i=1}^{L} \{ [(\bar{U}_i)^2 + (\bar{V}_i)^2]^{1/2} \cdot (\bar{U}_i, \bar{V}_i) \}/L \qquad (34)$$

where T is the averaging period (T=729/L in days). The density, ρ was assumed to be constant and the calculations were made for both the constant and linear form of the drag coefficients.

Because it was convenient in such a computation scheme to

have complete data blocks, the small amount of missing and erroneous wind data was replaced by wind data taken from the previous two yearly data block sampled at the same time of the year. For example, the two readings of missing wind data on Dec. 23, 1961 were replaced by wind data measurements made on Dec. 23, 1959.

The results are displayed in Figure 34, which plots the ratio of the computed stress magnitude from the vector averaged data to the computed stress magnitude from the 3-hourly data, $|\tau(T)|/|\tau(1/8)|$. Also plotted in Figure 34 is the difference between the wind stress directions, $\theta_\tau(T)-\theta_\tau(1/8)$, computed from the vector averaged values and directly from the 3-hourly values, respectively. The vertical error bars represent approximate 95% confidence intervals of the mean computed from the five two-yearly data blocks.

The magnitude of the wind stress decreases markedly with the vector averaging period. At a period of one month, the computed magnitude is reduced by more than one-half for the case of the constant drag coefficient. At the same averaging period, for the case of the linear drag coefficient the magnitude is reduced to less than one-third of the directly calculated value. The greater reduction for the case of the linear drag coefficient can be partly attributed to the use of the vector mean wind speed in determining the drag coefficient. For longer averaging periods, the value of the drag coefficient is reduced which results in a further reduction to the computed wind stress. The relatively small size of the 95% confidence intervals indicates that the wind stress reduction with averaging
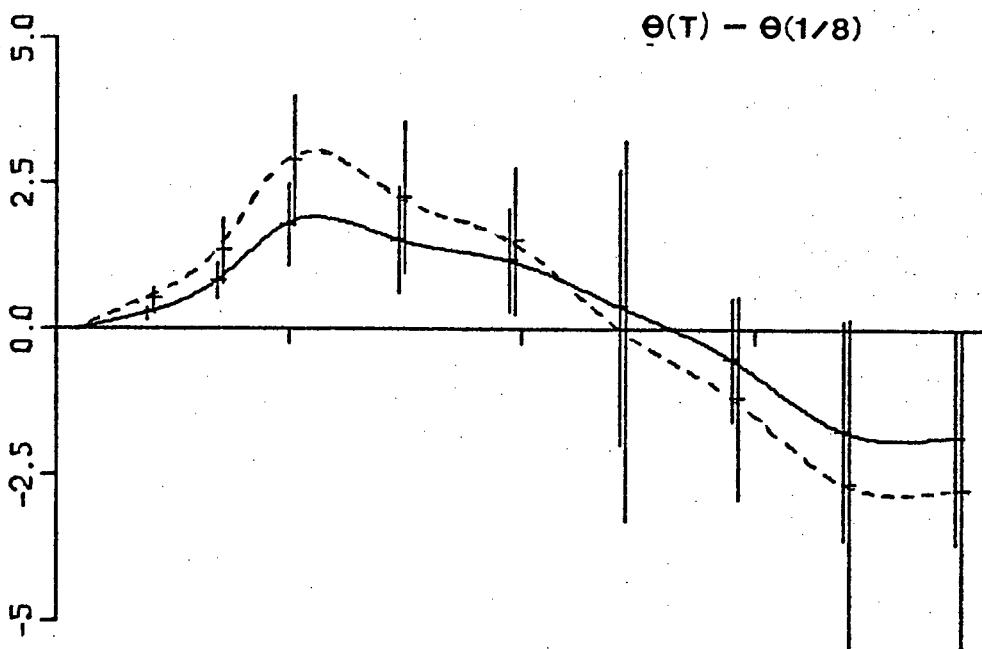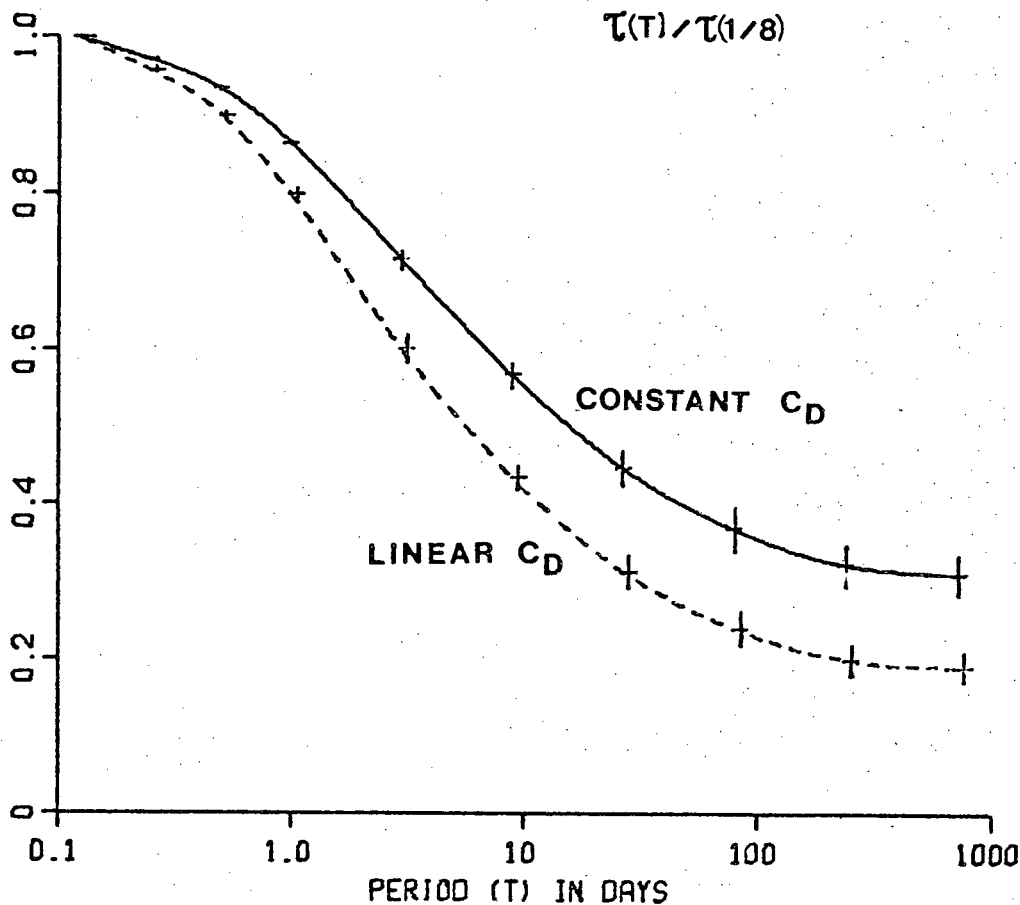
Figure 34: The ratio of the wind stress magnitude computed from wind data that are vector averaged over a period, T to the directly calculated wind stress. The lower plot represents the difference between the direction of the directly calculated wind stress and the direction of the wind stress computed from the vector averaged data. The vertical error bars represent approximate 95% confidence intervals of the mean.

period is much the same for each two-yearly data block.

The effect of vector averaging on the direction of the wind stress is much smaller. Figure 34 shows that the agreement between the direction computed from the vector averaged values is generally within 3 degrees of the direction computed directly over all averaging periods studied.

These results demonstrate that the effect of vector averaging the wind data (which is similar to the use of mean pressure maps for computing the geostrophic wind) is to reduce considerably the magnitude of the computed wind stress over averaging periods of a few days or longer. However, the effect on the stress direction is quite small and averaged data of this type seems to provide a good estimate of the direction the wind stress. These conclusions must be considered tentative as they are based on measurements at one location only. To test the results, the same kind of test should be made on wind data from other locations.

Chapter 7

THE EFFECT OF DATA SMOOTHING ON HEAT FLUXES

7.1 Introduction

When turbulent fluxes of sensible heat and latent heat are needed over large oceanic regions, the only data which are available are inherently smoothed. The effect of this data smoothing on the computation of the turbulent heat fluxes through bulk aerodynamic parameterizations is examined in this chapter.

The bulk transfer formulas for the sensible heat flux and latent heat flux can be written as

$$H_S = \rho C_p\, C_T\, U\Delta T \tag{2}$$

$$H_L = L C_q\, U\, \Delta q \tag{3}$$

respectively where U is the mean wind in m/sec, ΔT is the sea-air temperature differences in $^\circ$C, and Δq is the sea-air humidity difference in gm/m³. The non-dimensional coefficients C_T and C_q are taken to be 1.5×10^{-3}, the heat of vapourization per unit mass, $L=2.46\times10^{10}$ ergs/gm, the specific heat at constant pressure, $C_p=1.00\times10^7$ ergs/gm- C and the density of air, $\rho=1.25\times10^{-3}$ gm/cm³ (based on the average temperature of 8.2 $^\circ$C and average absolute humidity of 7.4 gm/m³).

The basic data set needed for the calculation of the heat fluxes are values of U, ΔT and Δq. Two sources of data available over large oceanic regions are marine climatic atlases and surface weather charts. The wind data format of these sources was described in Chapter 6.

From the climatic atlas, the wind roses used to display the wind data, allow an accurate determination of the mean wind

speed. Climatic atlases also provide the distribution of air temperature, sea temperature and wet-bulb temperature from which ΔT and Δq may be determined.

Alternatively, surface weather charts may be used to obtain the wind information. However, the value determined from this data source corresponds to vector averaged mean wind rather than the mean wind speed (see Chapter 6) used in equations (2) and (3). In addition, surface weather charts may not contain temperature or humidity data so these would have to be obtained from other sources.

7.2 Direct Calculation

In order to compare the effects of data smoothing on the computation of heat fluxes, the fluxes were computed directly from the 3-hourly data. These directly calculated heat fluxes serve as standards for comparison purposes. They are also useful for displaying the year to year and monthly variations.

The data were organized into ten yearly blocks, with each block consisting of 2916 3-hourly readings (out of a possible 2928 readings for a leap year and 2920 readings for a non-leap year). Each block was divided into 12 'months', each being made up of 243 data readings. In those months which had 2 or more incorrect readings, the heat fluxes were computed from the reduced number of only valid readings. When only a single reading was missing (often the slowly varying sea temperature), linear interpolation was used to replace the reading.

The yearly averages of each heat flux are displayed in Figure 35. The latent heat flux has a mean value of 89.2 cal/cm²-day while the sensible heat flux averages 11.6 cal/cm²-
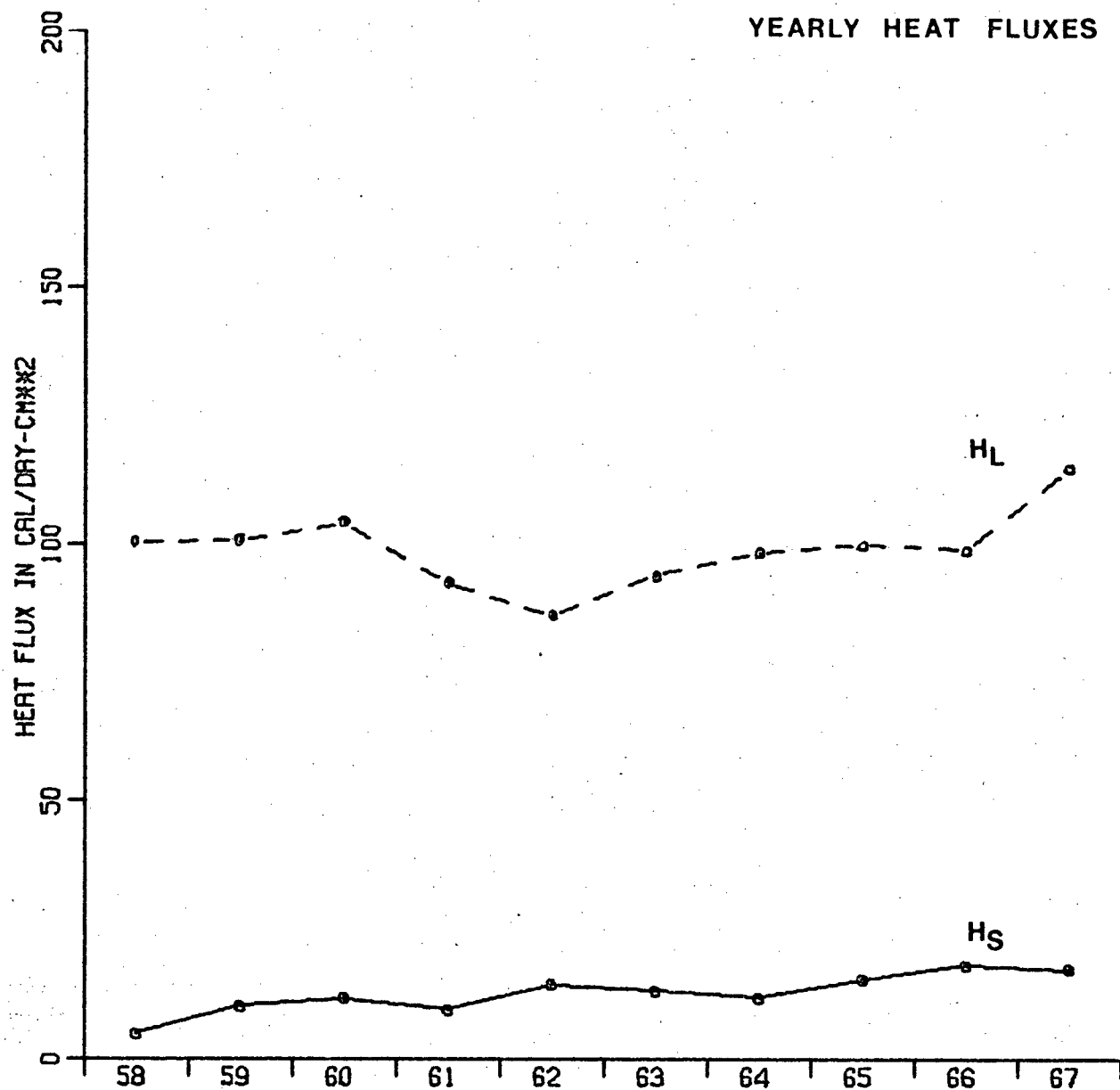
Figure 35: The yearly averages of the directly calculated sensible and latent heat fluxes.

day. (These values of mean heat fluxes differ slightly from the values computed from the spectral analysis as given in Appendix II because the missing and incorrect data were handled differently). Clearly the sensible heat flux is considerably smaller than the latent heat flux as indicated by the Bowen's ratio (H_S/H_L) which ranges from 0.05 (1958) to 0.18 (1966) about the overall mean value of 0.13. From Figure 35, it appears that over the ten year period, 1958 to 1967, the sensible heat flux was gradually increasing. However, the latent heat flux does not show any similar long term trend.

A very pronounced seasonal variation is found in both the sensible and latent heat fluxes (see Figure 36). The largest heat fluxes occur in the fall while the smallest heat fluxes are found in the summer months. A secondary peak in March is found on average, in both the sensible and latent heat fluxes. The monthly latent heat flux is positive for each month (i.e. transfering heat from the ocean into the atmosphere) but the monthly sensible heat flux is generally negative during the months of May through August.

7.3 Climatic Atlas

In order to estimate the effect of the smoothing of data presented in the format of the Marine Climatic Atlas, the data were organized into a similar format and from these data, the turbulent heat fluxes were computed. Marine atlases present the wind data in the form of monthly wind roses (as discussed in Chapter 6) from which the mean monthly wind speed can be accurately determined. These atlases also provide the mean values of the air temperature, sea temperature and wet-bulb temperature
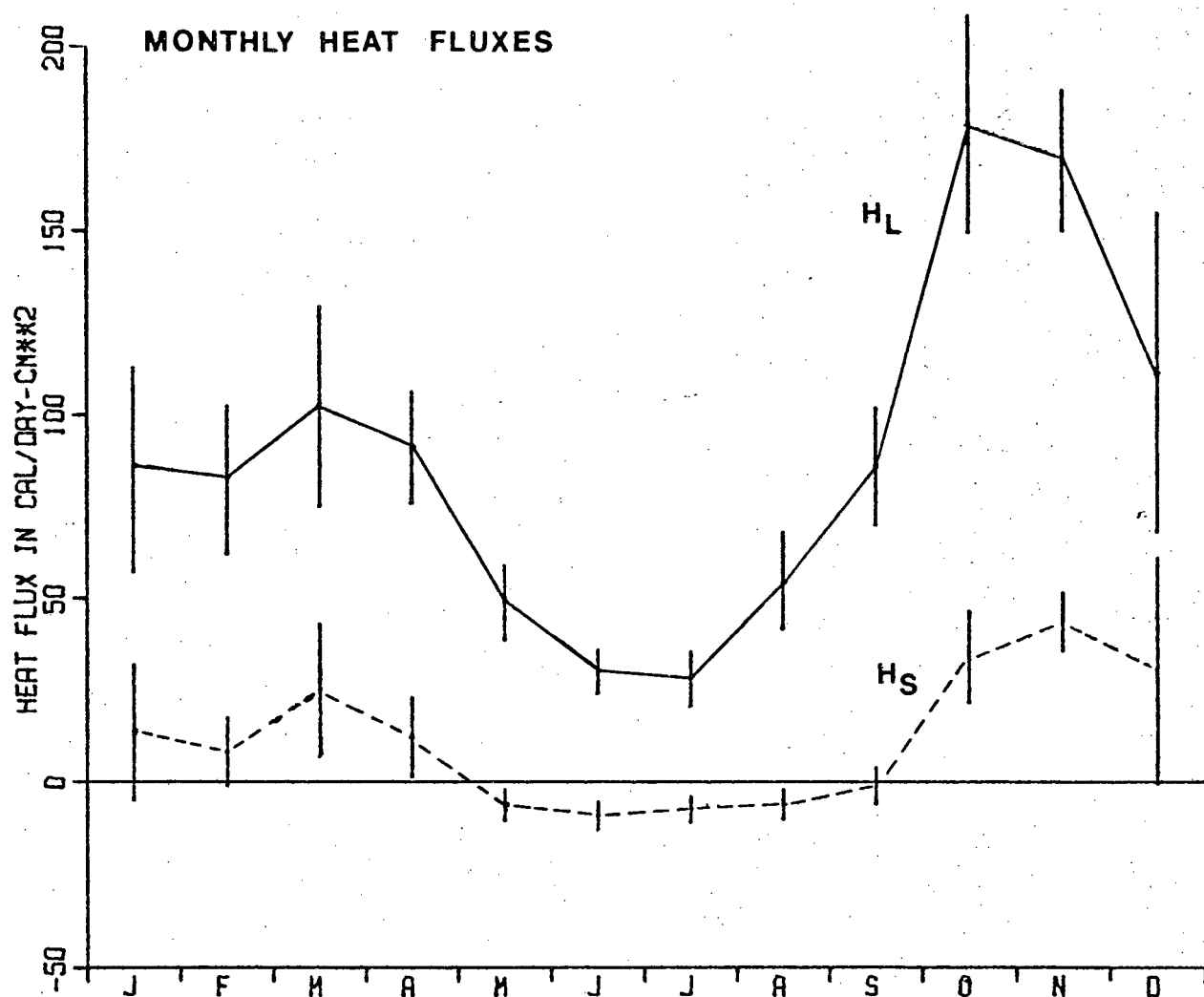
Figure 36: The monthly averaged sensible and latent heat fluxes directly calculated from the 3-hourly data. The vertical error bars represent approximate 95% confidence intervals of the mean computed from the separate monthly averages for each of the ten years.

from which one can determine the mean monthly sea-air temperature difference and sea-air humidity difference.

The data were organized into 120 separate months with each 'month' consisting of 243 readings (as described in section 7.2). In those months with two or more incorrect or missing data values, these values were not included. In mcnths which had only one missing or incorrect value, the bad value was replaced by means of linear interpolation. The data fcr each different month were then grouped together (i.e. data from the ten Januarys, the ten Febuarys and so on, were grcuped tcgether). From the data in these mcnthly groupings, the average wind speed and the average sea-air temperature and humidity differences were computed. These were then used in the bulk parameterization formulae (equations (2) and (3)) to compute the heat fluxes.

The latent heat flux computed from the data in the climatic atlas format shows generally good agreement with the directly calculated heat flux (see Table VII and Figure 37). The average of the monthly absolute percentage difference between the two methods is 5.5%. The agreement is better fcr mcnths of large latent heat fluxes than for months of smaller latent heat fluxes. When the heat fluxes are averaged cver the year, the difference is 2.5%.

The use of the climatic atlas data fcrmat results in greater deviations of sensible heat flux values. The agreement is poor in months of small sensible heat fluxes; in the mcnths of Febuary and May through August ($|H_s| < 12.5$ cal/cm²-day) the absolute percent differences exceeds 25%. However in each month of

TABLE VII

A comparison of the sensible and latent heat fluxes computed from the data organized into the format of the Marine Climatic Atlas ('MCA') with the value computed directly from the 3-hourly data ('Direct'). Both heat fluxes have units of cal/cm²-day.

Sensible Heat Flux

Month	Direct	MCA	%Diff.
Jan.	13.7	14.8	8.0
Feb.	8.41	12.3	46.3
Mar.	25.1	24.5	-2.4
Apr.	12.3	13.2	7.3
May.	-6.09	-3.54	-41.9
June	-9.01	-6.64	-26.3
July	-7.31	-5.06	-30.8
Aug.	-5.79	-3.01	-48.0
Sep.	-0.746	2.61	-450.
Oct.	34.2	34.3	-0.3
Nov.	43.9	45.6	3.9
Dec.	30.5	30.4	-0.3
Year	11.6	13.3	14.5

Latent Heat Flux

Month	Direct	MCA	%Diff.
Jan.	85.2	87.0	2.1
Feb.	82.5	82.9	0.5
Mar.	102.3	102.4	0.1
Apr.	91.3	91.3	0.0
May	49.1	51.8	5.5
June	30.0	36.2	20.7
July	28.3	31.6	11.7
Aug.	54.9	60.4	10.0
Sep.	86.2	94.6	9.7
Oct.	179.3	173.3	-3.3
Nov.	169.5	173.4	2.3
Dec.	111.6	111.3	-0.3
Year	89.2	91.4	2.5
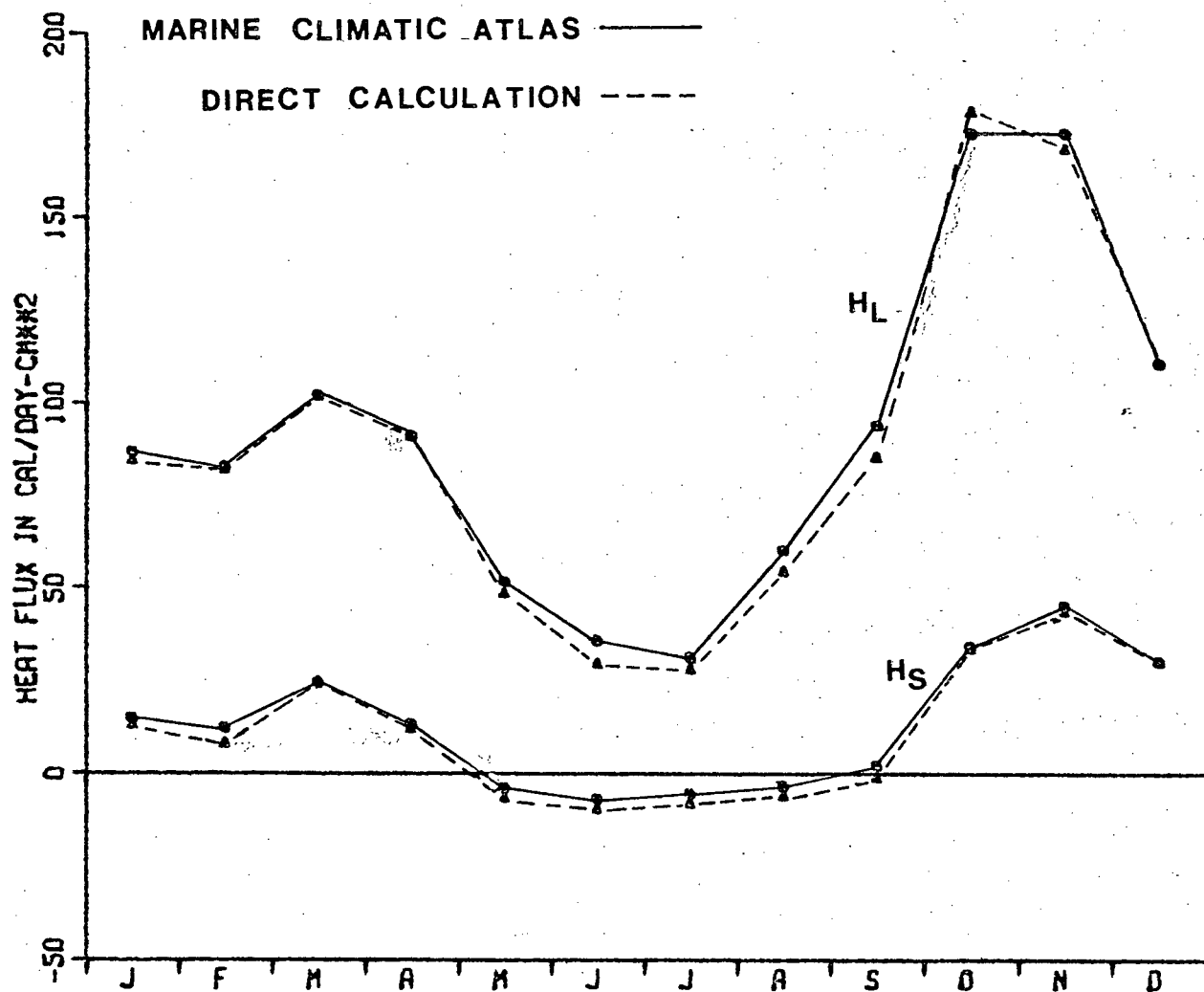
Figure 37: The monthly averaged sensible and latent heat fluxes computed from the data organized into the Marine Climatic Atlases format. For comparison, the corresponding directly calculated values are presented.

larger sensible heat fluxes, ($|H_s| \geq 12.5$ cal/cm²-day) the abso-
lute percent difference is less than 8.0%. Averaged over all
the months, the difference is 14.5%.

For the purposes of computing the turbulent heat exchanges
over the entire year, the data organized in the Marine Climatic
Atlas format can be used with a reasonable degree of accuracy.
However, for the spring and summer months when the heat fluxes
are comparitively small, the difference between the heat fluxes
computed directly and those computed from the marine climatic
format may be unacceptabley high for some purposes.

7.4 Surface Weather Charts

The turbulent heat fluxes may be computed using wind data
derived from surface weather charts. From the isobars provided
on mean surface weather charts, the geostrophic wind may be de-
termined. Knowing the geostrophic wind and correcting for the
effects of surface friction, the surface wind is derived. As
described in section 6.4, the effect of using pressure maps
averaged over long periods, is that of vector averaging the
shorter term wind observations. In order to simulate this
averaging effect, the wind components, vector averaged over
various periods were used to compute the magnitude of the wind.
Often surface weather charts do not provide sufficient informa-
tion to compute the sea-air temperature and humidity dif-
ferences. Therefore, additional sources of data, such as clima-
tic atlases, may be needed to compute the turbulent heat fluxes.

The averaged heat fluxes were computed for each of the five
two-yearly data blocks. As described in section 6.4, two or
more missing or incorrect data readings are replaced by readings

taken from the previous two-yearly data block at the same time of year. For example, the missing data beginning on Dec. 3, 1967 was replaced by data beginning on Dec. 3, 1965. Single incorrect or missing readings are replaced by linearily interpolated values. The effects of the surface weather chart smoothing are displayed in Figure 38. For each heat flux, Figure 38 displays the ratio of the heat flux computed from mean values averaged over a period, T, to the heat flux computed directly from the 3-hourly measurements. The vertical error bars represent the approximate 95% confidence intervals of the mean of the ratio at each period, computed from the five separate data blocks.

The effect of using the surface weather chart data format is to markedly reduce the heat fluxes over averaging periods longer than one day. For example, at a period of one month, the sensible heat flux is reduced to 0.62 of the directly calculated value and the latent heat flux is reduced to 0.53 of the directly calculated value. At periods of approximately one year or more, the ratio between the heat fluxes computed by the two methods appears to become nearly constant.

The reduction of the heat fluxes is less than that found for the magnitude of the wind stress. This difference is due to the wind stress being proportional to the square of the wind while the heat fluxes are proportional to the wind itself. If $C_D = C_T = C_q$ and C_D is a linear function of the wind speed rather than a constant, the effects would be larger as in the case for wind stress although perhaps not so marked. Nevertheless, the reduction in the fluxes is considerable and some correction is
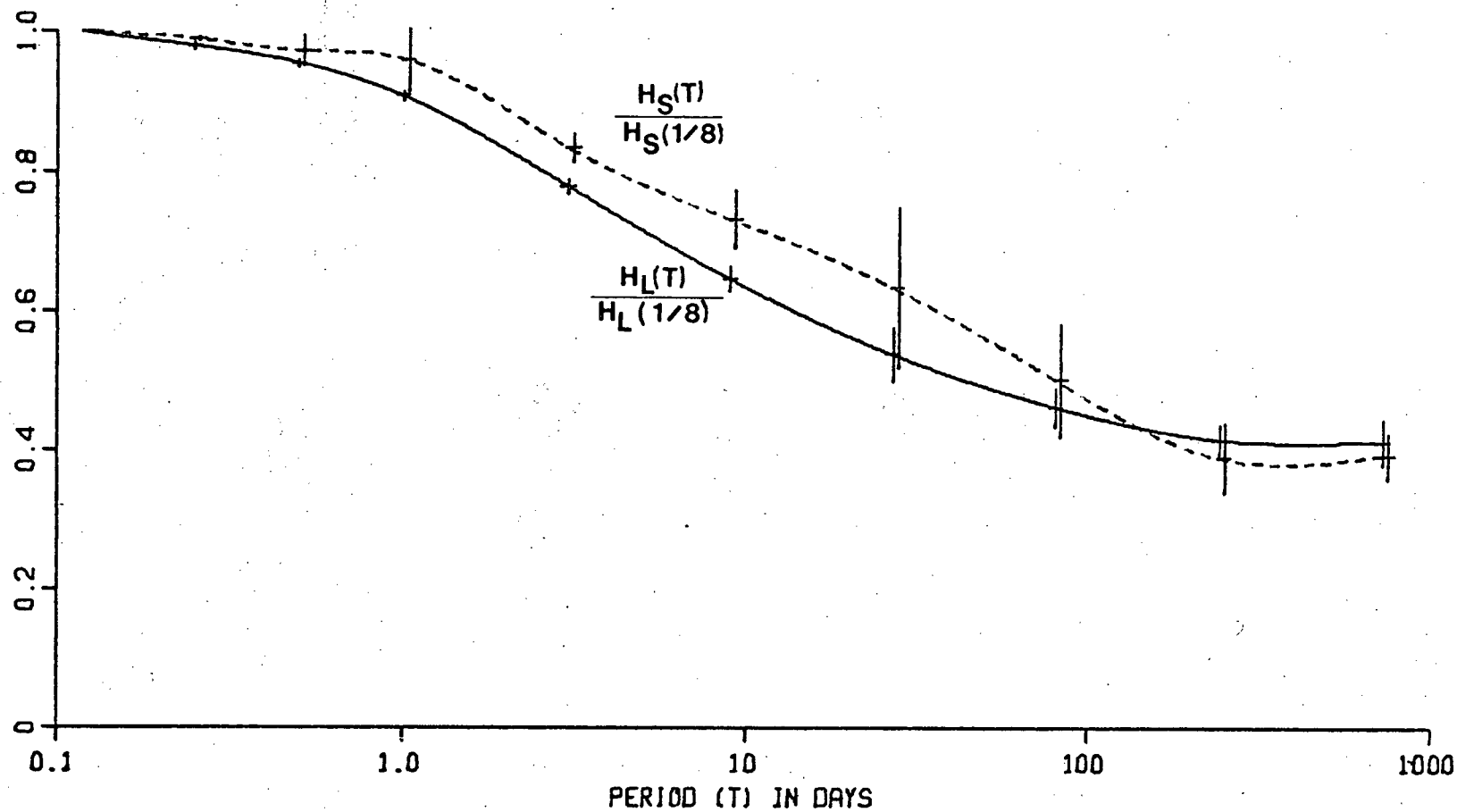
Figure 38: The ratio of the sensible and latent heat fluxes as computed from data that is vector averaged over a period, T to the heat fluxes computed directly from the 3-hourly readings. The vertical error bars represent the approximate 95% confidence intervals of the mean of the ratio's as computed from the five two-yearly data blocks.

needed if surface weather charts of averaging periods of a few days or more are to be used to compute these fluxes.

Chapter 8

SUMMARY

The surface layer of the atmosphere over the open ocean and the interaction between the ocean and the atmosphere were studied by examining a ten year record of 3-hourly surface meteorological quantities at Ocean Weather Station 'Papa' (50N 145W).

To determine the important periodicities of each quantity, the power spectrum was computed from data blocks of two years duration. Separate spectra were computed for each season as well.

The spectrum of the wind speed is dominated by activity of synoptic scales. A peak level in the f•ϕ spectrum of 8.2 (m/sec)^2 occurs at a period of 3 days. The annual peak is prominent while there is no significant diurnal peak. A small but significant amount of activity is present at the semi-diurnal period. Seasonal changes are found in the behavior of the wind speed. The wind speed spectra of the fall and winter feature a larger amplitude synoptic peak centered on shorter periods as compared to the synoptic peak of the spring and summer. A comparison with the wind speed spectra determined by other investigators at various locations, reveals that Ocean Weather Station 'Papa' is characterized by higher levels of activity occurring at generally shorter periods.

An examination of the vector wind was made by computing the rotary power spectrum. Both the clockwise and anti-clockwise part of the spectrum are dominated by a broad synoptic peak at 3 days. The clockwise side has higher synoptic levels, a result of the prevailing pattern of the movement of synoptic distur-

bances to the north of Station 'Papa'. The rotary spectrum shows no significant annual or diurnal activity. A small but significant semi-diurnal peak is found only in the clockwise part of the spectrum. The synoptic peak has a distinct seasonal variation occurring with higher levels and at shorter periods in fall and winter as compared to spring and summer.

The air pressure spectrum is dominated by a broad uneven peak over periods ranging from 3 to 70 days. The spectrum reveals a sizeable annual variation. A much smaller semi-diurnal variation is also present. As with the wind, the spectral levels are largest in the fall and winter, smaller in the spring and smallest in the summer.

The spectra of sea temperature, air temperature and absolute humidity are all dominated by large annual and semi-annual peaks. The average annual range of sea temperature is 7.9 C^o while the range of the semi-annual cycle is 2.2 C^o. The average annual and semi-annual ranges of air temperature are 8.3 C^o and 2.6 C^o, respectively. The average annual and semi-annual ranges of absolute humidity are 4.4 gm/m^3 and 1.7 gm/m^3, respectively.

Both the sea and air temperature have significant diurnal variations. The absolute humidity has a smaller diurnal variation which is only marginally significant. The average diurnal range of the air temperature is 0.64 C^o and that of the sea temperature is 0.13 C^o. Both the sea and air temperature have the largest diurnal variation in spring which includes the period of greatest solar insolation.

From the spectrum of sea surface temperature, it appears that there is very little activity between periods of one day

and one year. However, the air temperature spectrum shows a very broad, uneven peak between periods of 2 days and 60 days. The spectral levels over this range of periods increase in fall and winter and are reduced in spring and summer. The absolute humidity spectrum reveals a broad but well defined synoptic peak (over periods from about 1.5 days to 48 days) with a peak level at 5.5 days. These synoptic spectral levels are largest in the fall and smallest in the spring.

The rotary power spectrum of the time series $(U \cdot U_x, U \cdot U_y)$, proportional through the bulk aerodynamic parameterization to the wind stress, has the same general characteristics as the rotary power spectra of the wind. The spectra of $U \cdot \Delta T$ (representative of sensible heat flux) and $U \cdot \Delta q$ (representative of latent heat flux) each show a strong annual peak and a broad synoptic peak that accounts for most of the quantities' variance. The synoptic peak shows that the largest variations are found between periods of 4 to 7 days. The sensible heat flux has a sizeable diurnal variation with an average daily range of 16.9 cal/cm²-day (as compared to the mean sensible heat flux of 11.7 cal/cm²-day). The latent heat flux has no diurnal cycle. The spectral levels of both the sensible and latent heat fluxes show the greatest variability taking place in the fall and the least in the spring and summer.

A rotary cross-spectral analysis of the relatedness of the vector wind with the scalar quantities of air pressure, air temperature, absolute humidity and sea temperature reveals generally significant coherence levels over synoptic periods. While the coherence is statistically significant, the coherences de-

termined are generally too low to be useful for predictive purposes. In each of the rotary cross-spectra, the synoptic coherence is larger for clockwise wind rotations than those of the anti-clockwise wind.

The cross-spectra between the scalar quantities and the wind speed were also computed. The coherence levels found at synoptic periods were lower than the rotary coherence levels for each scalar quantity except the sea temperature which at periods of 3 days or more showed generally higher coherence. This result suggests that while the wind rotation is important in determining air mass characteristics, it is much less important in the coupling of the wind field to ocean water mass characteristics at a fixed point.

The coherence spectrum between the air temperature and absolute humidity shows high coherence levels (greater than 0.8) from periods of two years to 3 days. At periods shorter than 3 days, the coherence declines rapidly.

The co-spectrum of the east-west wind component with the wind speed and the north-south wind component with the wind speed are representative of contributions to each of the wind stress components over the periods resolved. These values indicate that wind measurements at intervals of 3 days or less are required to accurately estimate the wind stress (within 5%).

The co-spectrum of the wind speed with the sea-air humidity difference, representative of contributions to the latent heat flux, show that contributions from the periods resolved are small. Long-term averages of the wind speed and sea-air humidity difference are adequate to compute the latent heat flux. In

contrast, the co-spectrum of the sea-air temperature difference and the wind speed indicates that measurements at intervals of 3 days or less are required for a reliable estimate (within 5%) of the sensible heat flux.

The effect of data smoothing inherent in the data format of the Marine Climatic Atlas was examined. The wind stress magnitude computed from the data organized into this format, differs by 1 to 14% from the corresponding directly calculated wind stress for each month (taking the drag coefficient, $C_D = 1.5 \times 10^{-3}$) with an average absolute percentage difference of 5.6%. The difference in the stress direction is less than 7 degrees for each month. When a drag coefficient that depends linearily on the wind speed is used ($10^3 C_D = 1.0 + 0.07 \cdot U$, U in m/sec), the differences are slightly larger.

The effect of the data smoothing of the Marine Climatic Atlas on the computation of latent heat flux is also small. The average of the monthly absolute percentage difference between the two methods is 5.5%. For the sensible heat flux, the effect of this data format is larger, exceeding a 25% difference in months of small sensible heat fluxes (less than 12.5 cal/cm^2-day) and averaging just under 8% difference in months of larger sensible heat flux.

An alternative method of computing turbulent fluxes over large oceanic regions is to use averaged surface weather charts. These are equivalent to vector averaging the wind data. The wind stress computed from vector averaged wind data over various periods is displayed in Figure 34. The magnitude of the wind stress, for an averaging period of a month, is reduced to less

than one-half of the directly calculated value for the case of the constant drag coefficient. For the linear drag coefficient, the wind stress magnitude is reduced to less than one-third of the directly calculated value. The effect of vector averaging on the wind stress direction is much smaller, with the methods giving the same results within 3 degrees, for all averaging periods.

The effect of using the surface weather chart data format on the turbulent heat fluxes is also large. For an averaging period of one month, the sensible heat flux is reduced to 0.62 of the directly calculated value while the latent heat flux is reduced to 0.53 of the directly calculated value.

The results of the study of effects of data smoothing on the computation of bulk fluxes, must be regarded as tentative as they are made with data from only one location. Similar studies are needed for other locations.

BIBLIOGRAPHY

Blackman, R.B. and J.W. Tukey (1958). The Measurement of Power Spectra. Dover Publications: New York, N.Y.

Bendat, Julius S. and Allan G. Piersol (1971). Random Data. Wiley-interscience, New York.

Blackadar, A.K. (1959). Periodic wind variations. Mineral Industries, 28(4). College of Mineral Industries, The Pennsylvania State University, pp.1-5.

Burt, W., H. Crew, N. Plutchak and J. Dumon (1974). Diurnal variations of winds over an upwelling region off Oregon. Boundary-Layer Meteorology, 6, pp. 35-45.

Butler, S. (1962). Atmospheric tides. Scientific American, 207(6), pp. 48-59.

Byshev, V.I. and Yu. A. Ivanov (1969). The time spectra of some characteristics of the atmosphere above the ocean. Izvestia, Atmsopheric and Oceanic Physics, 5(1), pp. 17-28.

Cooley, J.W. and J.W. Tukey (1965). An algorithm for the machine calculation of complex Fourier series. Mathematics of Computation, 19, pp. 297-301.

Deacon, E.L. (1969). Physical processes near the surface of the earth. In General Climatology, ed. by H. Flohn, Elsevier, Amsterdam. pp. 39-104.

Deacon, E.L., and E.K. Webb (1962). Small scale interactions. In The Sea Vol. I, ed. by M. Hill, Interscience Publishers, New York. pp. 43-87.

Denman, K. L. (1972). The response of the upper ocean to meteorological forcing. Ph.D. Thesis, Institute of Oceanography, University of British Columbia. 117 pp.

Dorman, C.E. (1974). Analysis of meteorological and oceanographic data from Ocean Station Vessel N (30N 140W). Ph. D. Thesis, Oregon State University. 136 pp.

Fiedler, F. and H.A. Panofsky (1970). Atmospheric scales and spectral gaps. Bulletin of the American Meteorological Society, 51(12), pp. 1114-1119.

Flohn, H. (1969). Climate and weather. McGraw-Hill, New York. 253 pages.

Frye, D.E., S. Pond and W.P. Elliott (1972). Note on the kinetic energy spectrum of coastal winds. Monthly Weather Review, 100(9), pp. 671-672.

Garrett, J. (1970). Field observations of frequency domain statistics and nonlinear effects in wind-generated ocean waves. Ph. D. Thesis, Institute of Cceanography, University of British Columbia. 176 pp.

Gill, A. (1974). Mid-ocean eddies in ocean weather ship records. Mode Hot Line News, No. 49, pp. 3-10.

Gossard, E.E. (1960). Spectra of atmospheric scalars. Journal of Geophysical Research, 65(10), pp. 3339-3351.

Groves, G.W. and E.J. Hannan (1968). Time series regression of sea level on weather. Reviews of Geophysics, 6(2), pp. 129-174.

Hertzman, O., M. Miyake and S. Pond (1974). Ten years of meteorological data at Ocean Station Papa. Manuscript Report No. 29, Institute of Cceanography, University of British Columbia. 46 pp.

Hellerman S., (1965). Computations of wind stress fields over the Atlantic Ocean. Monthly Weather Review, 93(4), pp. 239-244.

Hellerman S., (1967). An updated estimate of the wind stress on the world ocean. Monthly Weather Review, 95(9), pp. 607-626.

Hess, G.D. and R.H. Clarke (1973). Time spectra and cross-spectra of kinetic energy in the planetary boundary layer. Quarterly Journal of the Royal Meteorological Society, 99, pp. 130-153.

Hidaka, K. (1958). Computation of the wind stresses over the oceans. Record of Oceanographic Works of Japan, 4, pp. 77-123.

Jenkins, J.M. and D.G. Watts (1968). Spectral Analysis. Holden-Day, San Francisco. 325 pp.

Kolesnikova, V.N. and A.S. Monin (1965). Spectra of meteorological field fluctuations. Izv., atmospheric and Oceanic Physics, 1, pp. 653-669.

Lea, D.A., and Helvey (1971). Directional bias in wind roses due to mixed compass formats. Journal of Applied Meteorology, 10(5), pp. 1037-1039.

Malkus, J.S. (1962). Large-scale interactions. In The Sea Vol. I ed. By M. Hill, Interscience Publishers, New York, pp. 88-294.

Millard, R.C. (1971). Wind measurements from buoys; a sampling scheme. Journal of Geophysical Research, 76(24), pp. 5819-5828.

Mooers, C.N.K. (1973). A technique for the cross spectrum analysis of pairs of complex-valued time series, with emphasis on properties of polarized components and rotational invarients. Deep-Sea Research, 20, pp. 1129-1141.

Oort, A.H. and A. Taylor (1969). On the kinetic energy spectrum near the ground. Monthly Weather Review, 97(9), pp. 623-636.

Panofsky, H.A. (1969). Spectra of atmospheric variables in the boundary layer. Radio Science, 4(12), pp. 1101-1109.

Pillsbury, R.D. (1972). A description of hydrography, winds and currents during upwelling season near Newport, Oregon. Ph. D. Thesis, Oregon State University. 163 pp.

Polowchak, Van M., and H.A. Panofsky (1968). The spectrum of daily temperatures as a climatic indicator. Monthly Weather Review, 96(9), pp. 595-600.

Pond, S., G.T. Phelps, J.E. Paquin, G. McBean and R.W. Stewart (1971). Measurements of the turbulent fluxes of momentum, moisture and sensible heat over the ocean. Journal of the Atmospheric Sciences, 28, pp. 901-917.

Pond, S., D.B. Fissel and C.A. Paulson (1974). A note on bulk aerodynamic coefficients for sensible heat and moisture fluxes. Boundary-Layer Meteorology, 6, pp. 333-339.

Roden, G.I. (1963). On sea level, temperature, and salinity variations in the Central Tropical Pacific and on Pacific Ocean Islands. Journal of Geophysical Research, 68(2), pp. 455-472.

Roden, G.I. (1965). On atmospheric pressure oscillations along the Pacific coast of North America, 1873-1963. Journal of the Atmospheric Sciences, 22, pp. 280-295.

Roll, H.V. (1965). Physics of the Marine Atmosphere. Academic Press Inc., New York. 426 pp.

Scripps Institute of Oceanography, University of California (1948). The field of mean wind stress over the North Pacific Ocean. Oceanographic Report No. 14.

Scripps Institute of Oceanography, University of California (1951). The mean wind stress over the Atlantic Ocean. Oceanographic Report No. 21.

Singleton, Richard C. (1969). An algorithm for computing the mixed radix Fast Fourier Transform. IEEE Transactions on Audio and Electroacoustics, 17(2), pp. 93-103.

Stewart, R. W. (1974). The air-sea momentum exchange. Boundary-Layer Meteorology, 6(1/2), pp. 151-167.

Sverdrup, H.U. (1947). Wind driven currents in a baroclinic ocean; with application to the equatorial currents of the Eastern Pacific. Proceedings of the National Academy of Sciences. 33(11), pp. 318-326.

Tabata, S. (1961). Temporal changes of salinity, temperature and dissolved oxygen content of the water at Station "P" in the Northeast Pacific Ocean, and some of the determining factors. Journal of the Fisheries Research Board of Canada. 18(6): pp. 1073-1124.

Tabata, Susumu (1965). Variability of oceanographic conditions at Ocean Station 'P' in the Northeast Pacific Ocean. Transactions of the Royal Society of Canada, 3, Series 4, Section 3, pp. 367-418.

U. S. Navy, Chief of Naval Operations (1955 to 1969). Marine climatic atlas of the world. Vol. I to VIII. Washington, D.C. NAVAER 50-1C-528.

Van der Hoven, I. (1957). Power spectrum of horizontal wind speed in the frequency range from .0807 to 900 cycles/hour. Journal of Meteorology, 14, pp. 160-164.

Wunsch, C. (1972). Bermuda sea level in relation to tides, weather and baroclinic fluctuations. Reviews of Geophysics and Space Physics, 10(1), pp. 1-49.

APPENDIX I

INCORRECT DATA

The following table provides a listing of the times of missing (M) or erroneous (E) data samples.

Year	Starting time	Number of readings	θ	U	P	T_a	T_w	T_s
1958	0000 Jan. 1	1			M	M	M	M
	2100 Feb. 19	1			E			
	0900 Oct. 28	1						E
	0900 Nov. 1	1	E	E				
1959	1200 Mar. 25	1	E					
	2100 Sept. 10	1					E	
	0600 Oct. 19	1	E					
	1500 Nov. 14	2	M	M	M	M	M	M
1960	2100 Jan. 30	4						E
	0000 Feb. 7	3						E
	1200 Nov. 15	1						E
	1200 Dec. 18	2	M	M	M	M	M	M
1961	1200 Mar. 3	6	M	M	M	M	M	M
	1500 June 26	2	M	M	M	M	M	M
	0000 July 15	1					E	
	0900 Sept. 15	5	M	M	M	M	M	M
	1200 Dec. 23	2	M	M	M	M	M	M
1962	0900 Jan. 2	2	M	M	M	M	M	M
	0000 Feb. 1	2	M	M	M	M	M	M
	1800 Apr. 13	2	M	M	M	M	M	M
	1200 Oct. 4	1						E
	1500 Oct. 26	1						E
1963	1500 Feb. 27	1					E	
	2100 Nov. 15	1						E
	0300 Nov. 24	1						E
1964	2100 May 6	1						E
	0900 Oct. 6	43	M	M	M	M	M	M
	1500 Oct. 12	1			E			

Year	Starting time	Number of readings	θ	U	P	T_a	T_w	T_s
1965	1200 Jan. 2	52	M	M	M	M	M	M
	0000 Jan. 9	1		M	M			M
	0000 July 226	1			E			
1966	0900 Jan. 29	1						E
	0900 Oct. 15	1	M	M	M	M	M	M
	1200 Oct. 15	1		M	M			M
1967	1500 Jan. 11	61	M	M	M	M	M	M
	0600 Jan. 19	1		M	M			M
	0900 Dec. 3	48	M	M	M	M	M	M
	1200 Dec. 9	1		M	M			M

APPENDIX II

MEANS AND POWER SPECTRAL INTEGRALS

When interpreting power spectral results, it is useful to know the averages of the quantity and the cumulative integral of the spectrum. These values are presented below for the two-yearly spectra and for the seasonal spectra of each quantity.

Quantity	Average				
	Overall	Winter	Spring	Summer	Fall
Wind Speed (m/sec)	10.2	11.5	8.72	8.24	12.3
East-west Wind (m/sec)	4.06	3.38	3.52	3.95	5.34
North-south Wind (m/sec)	1.40	1.54	0.96	1.69	1.41
Air Pressure (mbar)	1012.2	1008.2	1016.6	1017.5	1006.6
Sea Temperature ($^{\circ}$C)	8.46	5.65	7.19	12.5	8.54
Air Temperature ($^{\circ}$C)	8.18	5.25	7.18	12.5	7.78
Absolute Humidity (gm/m^3)	7.35	5.91	6.85	9.82	6.82
$(U \cdot U_x)$ (m/sec)^2	56.4	53.8	42.1	43.5	85.6
$(U \cdot U_y)$ (m/sec)^2	17.5	20.2	9.38	19.1	21.2
Sensible Heat Flux (cal/cm^2-day)	11.7	16.2	-0.93	-4.59	36.3
Latent Heat Flux (cal/cm^2-day)	88.9	89.6	56.8	56.5	153.2

Quantity	Integral				
	Overall	Winter	Spring	Summer	Fall
Wind Speed (m/sec)^2	28.3	28.1	19.4	16.9	31.4
Clockwise U (m/sec)^2	63.0	75.8	43.7	36.7	80.7
Anti-Clockwise U (m/sec)^2	50.5	60.0	34.8	28.2	61.8
Pressure (mbar)	176.	194.	87.1	70.6	175.
Sea Temperature (C^o)^2	8.46	0.106	0.179	0.248	0.172
Air Temperature (C^o)^2	10.7	1.83	0.949	0.837	2.19
Absolute Humidity (gm/m^3)^2	3.94	1.11	0.726	1.28	1.72
Clockwise $U \cdot \vec{U}$ (m/sec)^4	18200	23400	9290	7300	28900
Anti-clockwise $U \cdot \vec{U}$ (m/sec)^4	13200	16900	7130	5060	19500
Sensible Heat Flux (cal/cm^2-day)^2	4130	5020	1500	952	6850
Latent Heat Flux (cal/cm^2-day)^2	14300	12400	5130	6870	22100